Study on CuO-CeO_2 System to develop new Three-Way Catalysts

Nguyen The Luong

Acknowledgements

I would never have been able to finish my dissertation without the guidance of my committee members, help from friends, and support from my family.

First of all, I would like to express sincere gratitude to my supervisor, Professor Keiichi Ishihara, for all his valuable advices, contributive comments and critical guidance from my first days in Japan until now. My profound thanks are to my co-supervisor, Professor Hideyuki Okumura for his kind and many valuable discussions.

I would like to convey my profound appreciation and deep gratitude to Professor Eiji Yamasue, who instructed me about various indispensable techniques and knowledge for research.

Let me give my grateful appreciation to Mr. Shoji Fujimoto, for his kind support and instructions about various experimental techniques helped me a lot.

I would like to express my appreciation to the Global Center of Excellence (GCOE) Program, of Kyoto University for the financial support for my research. My special thanks also go to the Ministry of Education, Cultures, Sports, Science and Technology in Japan (MEXT) for granting me the scholarship to study in Japan.

Finally, I would like to express my heartfelt thanks to all the members belong to Ishihara's laboratory for their helps and friendship during my stay in Japan.

Nguyen The Luong

Abstract

In the traditional three-way catalytic converter for automobile, the honeycomb ceramic support is used as a substrate on which γ-Al_2O_3 is coated with high surface area and thermal stability, which is known as the washcoat layer. Materials with oxygen storage capacity (OSC) such as ceria mixed with zirconia are coated on the washcoat, which is called a catalytic layer. The noble metals (Pt, Pd, Rh) are also coated in order that the catalytic layer acts as active components that help to reduce pollutants like CO, HC and NO_x. Materials with OSC play key role for the performance of the Three-Way Catalyst (TWC). The CeO_2-ZrO_2 composite is well-known as an excellent promoter for OSC, where CeO_2 exhibits oxygen storage/release behavior by redox variation of Ce ions between Ce^{3+} and Ce^{4+}. As legislation becomes tighter, it is required to improve the efficiency of TWCs at low temperatures under an oxygen-rich atmosphere.

In this study, CuO and CeO_2 were considered as materials to improve the OSC, especially at low temperature, based on valence changes of Ce^{4+}/Ce^{3+}, $Cu^{2+}/Cu^{+}/Cu$. Mechanical milling was employed to prepare catalysts CuO-CeO_2. During the milling, structure modifications were observed by X-ray diffraction (XRD) and scanning electron microscope (SEM). The dynamic reduction behavior of CuO-CeO_2 was analyzed by the temperature programmed reduction instrument with Gas Chromatography-Thermal Conductivity Detector (GC-TCD, Varian CP-4900). The total OSC of the CuO-CeO_2 catalysts system was measured by thermogravimetric and differential thermal analysis (TG-DTA). The results show that, the total OSC of the CuO-CeO_2 system was much greater than CeO_2-ZrO_2 traditional catalysts system: at 300^{o}C the OSC of CuO-CeO_2 was 97.5%, which is higher than that of CeO_2-ZrO_2.

In order to apply new catalysts to the TWC system, various characteristics must be considered. The adhesiveness between the developed material and the washcoat is one of these important factors. The adhesion property of $CuO\text{-}CeO_2/\gamma\text{-}Al_2O_3$ on metallic substrate was investigated focusing on the particle size, which secure the durability of $\gamma\text{-}Al_2O_3$ and $CuO\text{-}CeO_2$ on the metallic substrate. The milled samples of $CuO\text{-}CeO_2$ always agglomerated in particles of few micrometers, which exhibit a very poor adhesion property. In the order to improve the adhesion properties of milled $CuO\text{-}CeO_2$, the reduction of the agglomerates was realized by applying further high energy mechanical milling with water and binder up to 72 h. The adhesion property was evaluated by the weight loss under an ultrasonic vibration cleaner: power 100 W, frequency 45 kHz for 20 min. The structure and morphologies of coating layer were observed by XRD and SEM with EDX (Energy dispersive X-ray spectroscopy). The results showed that, when it is coated on $\gamma\text{-}Al_2O_3$ layer, the weight loss reduces from 100% to 25% after 48h wet milling. As the increase of milling time to 72h, the weight loss increases because of re-agglomeration.

Next, for the catalytic performance, an amount of released oxygen from Pd, Pt and Rh coated on a $CuO\text{-}CeO_2/Al_2O_3$/substrate was investigated using the automotive exhaust gas simulator comparing with that of noble metals coated on a $CeO_2\text{-}ZrO_2/Al_2O_3$/substrate and Al_2O_3/substrate. The coated samples were characterized by means of XRD, SEM, Brunauer-Emmett-Teller (BET), X-ray photoelectron spectroscopy (XPS) and GC-TCD. For the cases, $\lambda=1$, the CO conversion ratio for noble metals coated on $CuO\text{-}CeO_2$ was higher at lower temperatures than that of noble metals coated on $CeO_2\text{-}ZrO_2$ and that of noble metals coated on $\gamma\text{-}Al_2O_3$. When $\lambda<1$, CO and C_3H_8 conversion ratios of noble metals coated on $CuO\text{-}CeO_2$ were higher than those of noble metals coated on $CeO_2\text{-}ZrO_2$ and on a $\gamma\text{-}Al_2O_3$ washcoat.

Nowadays, the temperature of TWCs can rise even above 1000^oC, where it is expected that the catalytic performance of Pd, Pt and Rh loaded on $CuO\text{-}CeO_2/Al_2O_3$

quickly reduces. Finally, in order to improve the thermal stability and catalytic performance of Pd, Pt and Rh loaded on $CuO\text{-}CeO_2/Al_2O_3$ at high temperature, the mixture of Al_2O_3 with $CuO\text{-}CeO_2$ was tested. The mixture of $CuO\text{-}CeO_2$ was firstly produced using high energy vibratory ball milling for 18h and then the milled powders of $CuO\text{-}CeO_2$ (40 wt.%) and $\gamma\text{-}Al_2O_3$ (60 wt.%) were further milled with water and a small amount of $Al(NO_3)_3$ as the binder for 24h. Then, the catalytic performance of Pd, Pt and Rh coated on $CuO\text{-}CeO_2\text{-}Al_2O_3$/substrate was evaluated. The microstructure and morphologies showed a good distribution of Al_2O_3 into $CuO\text{-}CeO_2$, rather small particles of $CuO\text{-}CeO_2$ were determined at high temperature. The phase change from $\gamma\text{-}Al_2O_3$ to $\alpha\text{-}Al_2O_3$ at 1000^oC was observed. After being heated at 1000^oC for 20h, the CO, C_3H_8, NO conversion ratio of noble metals coated on $CuO\text{-}CeO_2\text{-}Al_2O_3$ was better than those of ones coated on $CuO\text{-}CeO_2$.

Contents

List of Figures

CHAPTER 1
Introduction

1.1 Research background

In the last 60 years the worldwide annual motor vehicle production increased from about 40 million vehicles to over 700 million [1]. The exhausted emission from automobiles is a main cause of the air pollution, which consists of a complex mixture of gases, whose composition depends on a variety of factors such as: type of engine (two or four-stroke, spark or compression) and driving conditions (urban or extra-urban, vehicle speed, acceleration/deceleration, etc). Table 1-1 reports typical compositions of exhaust gases for some common engine types.

As shown in Table 1-1, the exhaust contains hydrocarbons (HCs), carbon monoxide (CO) and nitrogen oxides (NO_x), mostly NO, in addition to other compounds such as water, hydrogen, nitrogen, oxygen, etc. The CO and some HCs are mainly formed due to

Table 1-1: Example of exhaust for two and four-stroke, diesel and lean-four-stroke engine [2, 3, 4, 5]

Exhaust components and conditions[a]	Diesel engine	Four-stroke spark ignited	Four-stroke lean-burn spark ignited	Two-stroke lean-burn spark ignited
NOx	350-1000ppm	100-4000ppm	≈1200ppm	100-200ppm
HC	50-330ppm C	500-5000ppm C	≈1300ppm C	20000-30000ppm C
CO	300-1200ppm	0.1-6%	≈1300ppm	1-3%
O_2	10-15%	0.2-2%	4-12%	0.2-2%
H_2O	1.4-7%	10-12%	12%	10-12%
CO_2	7%	10-13.5%	11%	10-13%
SO_x	10-100 ppm[b]	15-60ppm	20ppm	≈20ppm
PM	65 mg/m^3			
GHSV (h^{-1})	30000-100000	30000-100000	30000-100000	30000-100000
λ (A/F)[c]	≈1.8 (26)	≈1 (14.7)	≈1.16 (17)	≈1 (14.7)[d]

[a] N_2 is remainder.
[b] For comparison: diesel fuels with 500 ppm of sulphur produce about 20 ppm of SO2 [6].
[c] λ defined as ratio of actual A/F to stoichiometric A/F, $\lambda = 1$ at stoichiometry (A/F = 14.7).
[d] Part of the fuel is employed for scavenging of the exhaust, which does not allow to define a precise definition of the A/F.

incomplete combustion in regions of oxygen deficiency in the engine. There are also HCs emissions due to unburned fuel. CO may be fatal to humans even in low concentrations. NO_x (NO and NO_2) are formed through reactions between N_2 (from the air and fuel-derived N-containing compounds) and O_2 during the combustion. NO_x can react to form photochemical smog containing for instance ozone, which damages forests and plants and also harmful to humans. NO_x also causes acidification. Sulphur oxides (SO_x) such as SO_2 and SO_3 originate from S in fuel and in lubricants, which is oxidized in the engine. SO_x are also a cause of acidification. SO_x are normally not removed by the post-combustion treatments; the only effective way to reduce them is by diminishing the sulphur content in fuel.

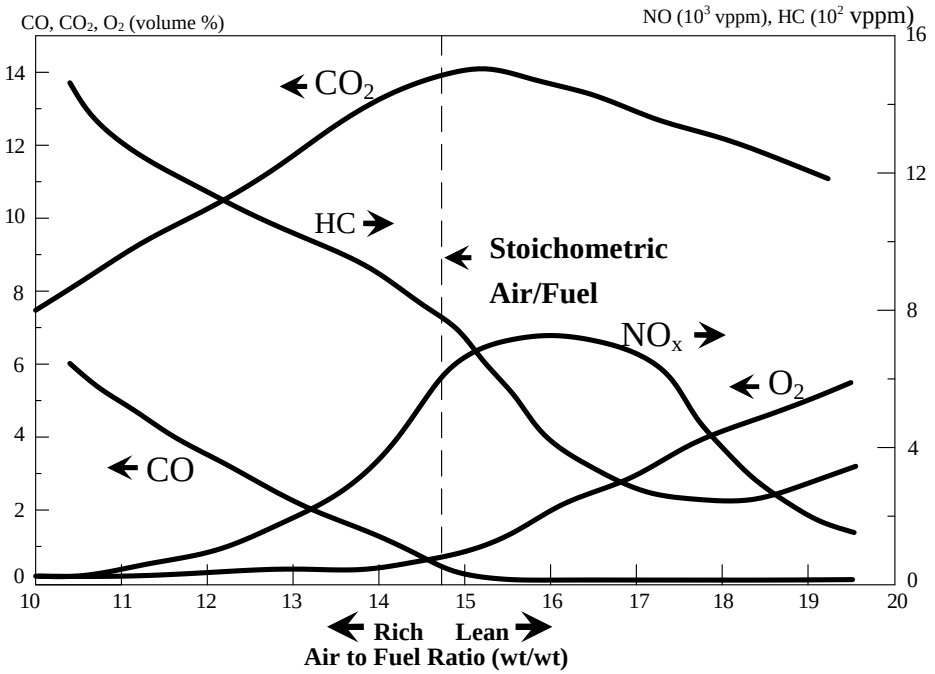

Figure 1-1: Spark-ignited gasoline engine as a function of the air-to-fuel ratio (Kummer 1980)

The quantity of pollutants varies with many of the operating conditions of the engine but it is influenced predominantly by the air-to-fuel ratio in the combustion cylinder. Figure 1-1 shows the engine emissions from a spark–ignited gasoline engine as a function of the air-to-fuel ratio (Kummer 1980) [7]. The term used to describe the air-to-fuel (A/F) weight ratio is the lambda (λ) ratio that is defined as the actual air-to-fuel ratio divided by the air-to-fuel ratio at the stoichiometric point or $\lambda = (A/F)_{actual}/(A/F)_{stoichiometric}$. The stoichiometric point $\lambda = 1$ is the precise amount of air required to oxidize all of the fuel and for gasoline is approximately 14.6 (wt/wt). Thus, $\lambda<1$ denotes a rich A/F (insufficient air), and for $\lambda >1$ a lean A/F (excess air). When the engine operated at a rich stoichiometric point, CO and HC emissions increase, whereas NO_x emissions decrease. This is because the deficiency in O_2 does not allow for a complete combustion of the gasoline. Conversely, the amount of NO_x is reduced because the temperature of the adiabatic flame is reduced. On the lean side of the stoichiometric spectrum, CO and HC are reduced since nearly complete combustion dominates. At lean stoichiometric operation, NO_x reaches their maximum point, given that

the adiabatic flame temperature is highest, On the contrary, at higher stoichiometric points, NOx decrease because less fuel is supplied, the adiabatic flame temperature is reduced.

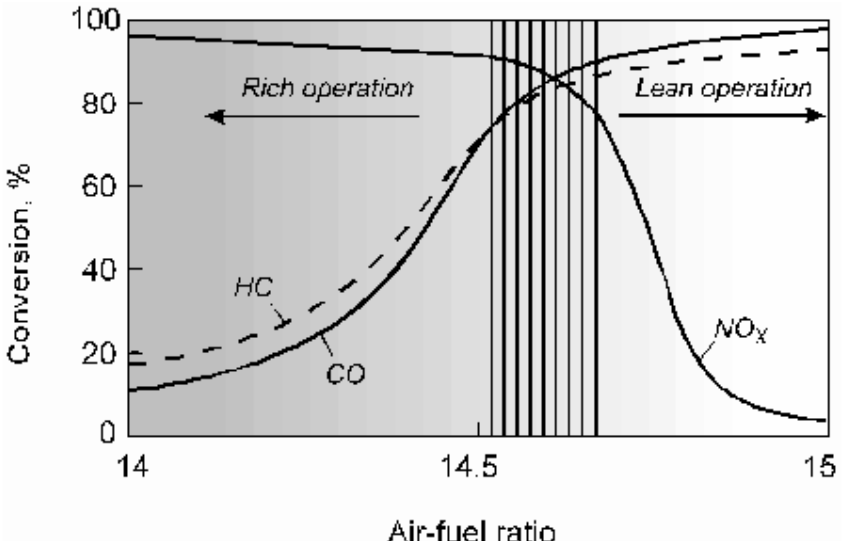

Figure 1-2: The conversion efficiency (%) of a three-way catalyst as a function of A/F-ratio. The lambda window, an A/F-ratio of 14.6 corresponds to stoichiometric operation, λ =1 (cf. Holmgren 1998)

As shown in Figure 1-2, in this narrow window, the high conversions (> 80-90%) of CO, HC and NO_x are achieved simultaneously. If the A/F-ratio is below 14.6, the conversion efficiency of CO, HC decrease rapidly while the conversion efficiency of NO_x does not change. At the A/F-ratio exceeds 14.6, the conversion efficiency of CO, HC increase while the conversion efficiency of NO_x decreases.

It is necessary to simultaneously carry out both reduction and oxidation reactions over the exhaust catalyst, which can occur through a variety of reactions. Some of these are summarized in Table 1-2. It is important to note that, this table only reports the desirable reactions, for many other reactions could occur, for example, the reduction of NO_x to ammonia, the partial oxidation of HC to give aldehydes and other toxic compounds, etc. Given the complexity of the exhaust media, a high selectivity is required in order to promote only the reactions reported in Table 1-2.

1.2 Three way catalyst: Principles and present research

Table 1-2: Reactions occurring on the automotive exhaust catalysts, which may contribute to abatement of exhaust contained pollutants [8]

Oxidation	$2CO + O_2 \rightarrow 2CO_2$
	$HC + O_2 \rightarrow CO_2 + H_2O$[a]
Reduction/three-way	$2CO + 2NO \rightarrow 2CO_2 + N_2$
	$HC + NO \rightarrow CO_2 + H_2O + N_2$
	$2H_2 + 2NO \rightarrow 2H_2O + N_2$
WGS	$CO + H_2O \rightarrow CO_2 + H_2$
Steam reforming	$HC + H_2O \rightarrow CO_2 + H_2$[a]

a Unbalanced reaction

A typical design of a modern three-way catalytic converter (TWCs) is reported in Figure 1-3. Basically, the TWC is a stainless steel container which incorporates a honeycomb monolith made of cordierite ($2MgO.2Al_2O_3.5SiO_2$) or metal [2]. Geometrical characteristics of the honeycomb monolith are key in determining the efficiency of the converter. Nowadays both metal and ceramic monoliths are employed. A major advantage of the metallic substrate is that the wall thickness is limited by the steel rolling mill's capabilities, not by its strength. In a typical automotive 400 cell/in^2, the frontal flow area in a ceramic monolith is 69% open (31% closed), while the metallic version has a 91% open area. This is due to the higher wall thickness of ceramic monoliths (0.007 in; 0.0178 mm) compared to metallic ones (0.002 in; 0.050 mm) [9, 10]. Great technological developments in this field produced high cell densities with a 900 cell/in^2, even higher densities are now commonly available on the market for both types of monoliths [11]. Cordierite monoliths have been employed quite extensively, primarily due to their lower production cost. However, a major advantage of the metal monoliths resides in their high thermal

conductivity and low heat capacity, which allow very fast heating of the close-coupled catalyst (CCCs) during the phase-in of the engine, minimizing the light-off time.

The monolith is mounted in the container with a resilient matting material to ensure vibration resistance [12, 13]. The active catalysts are supported (washcoated) onto the monolith by dipping it into a slurry containing the catalyst precursor. The excess of the deposited material (washcoat) is then blown out with hot air and the honeycomb is calcined to obtain the finished catalyst. In the washcoating process, multiple layer technology or multiple catalyst-bed converters are also employed [12, 14]. The exact method of deposition and catalyst composition varies and often is specific for the every washcoating company. For example, the metallic honeycombs are non-porous, which makes difficult adhesion of the washcoat. To deal with this, a FeCrAl based alloy is employed, which contains up to 5wt.% of aluminum. After an appropriate pre-treatment, this element then acts as an anchoring centre for adhesion of the washcoat [11].

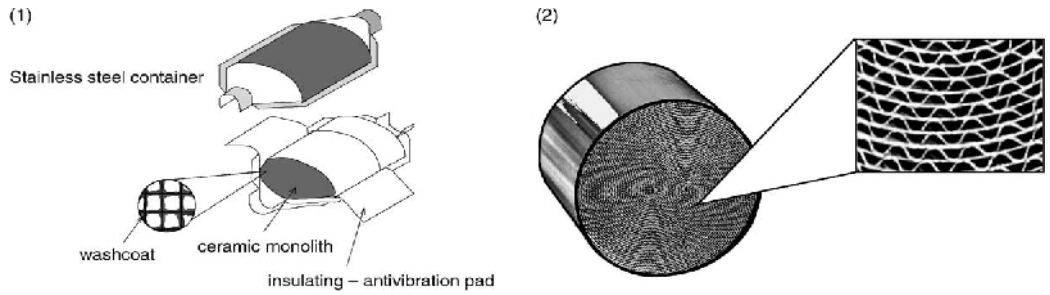

Figure 1-3: Diagram of a typical catalytic converter (1) and a metallic honeycomb (a monolith from Emitec GmbH) (2)

There are some common components which represent the state-of-the-art of in washcoating composition:

- Alumina, which is used as a high surface area support.
- CeO_2-ZrO_2 mixed oxides, principally added to promote OSC.
- Noble metals (NM = Rh, Pt and Pd) as active phases.
- Barium and/or lanthana oxides as stabilizers of the alumina surface area.

1.2.1 Al_2O_3

The choice of the Al_2O_3 as carrier is dictated by the necessity of increasing the surface area of the honeycomb monolith which is typically below 2-4 m^2l^{-1}, where the volume is that of the honeycomb [15]. Alumina has a high surface area and relatively good thermal stability under the hydrothermal conditions of exhausts. Thus, in most studies γ-Al_2O_3 is employed due to its high surface area with respect to other transitional aluminas [16]. However, δ and θ-Al_2O_3 also can be employed for high temperature applications such as in the CCCs because of their high thermal stability compared to γ-Al_2O_3. Given that in the TWCs, temperatures may surpass 1000^{o}C, stabilization of transition aluminas is necessary to prevent their transformation to α-Al_2O_3, which typically features surface areas below 10 m^2 g^{-1}. A number of stabilizing agents have been reported in the literature, being the most investigated lanthanum, barium, strontium, cerium, and more recently zirconium oxides or salts being the most investigated [17–24]. Sometimes, sol–gel techniques are employed to improve the stability of the surface area. The exact mechanism by which this additive stabilizes transitional aluminas strongly depends on the amount of the stabilizing agent and the synthesis conditions. This is illustrated in Figure 1-4, for BaO doped aluminas; BaO and lanthana are the most commonly used and effective stabilizers. The effectiveness of each dopant on the stabilization of alumina is difficult to predict, due to the variability of the factors involved in the synthesis. For example CeO_2 was shown to thermally stabilize Al_2O_3, the maximum stabilization effect being attained at a CeO_2 level of 5% [25]. However, Morterra et al. [26, 27] found that little stabilization of BET areas is attained by adding CeO_2 to γ-Al_2O_3, even though significant modifications of surface properties were detected. A possible rationale may be given by the recent observation that very efficient stabilization of Al_2O_3 by the addition of CeO_2 is achieved due to formation of $CeAlO_3$ [24]. Apparently, the stabilization effect is more pronounced as long as dispersed Ce^{3+} species are present at the Al_2O_3 surface [28, 29]. It is conceivable that CeO_2 stabilizes γ-Al_2O_3 in a similar fashion to La^{3+}, i.e. by the formation of a surface perovskite-type of

oxide $LaAlO_3$ [17]. Under high temperature oxidizing conditions, partial re-oxidation of Ce^{3+} sites may occur, with formation of CeO_2 particles which tends to agglomerate and grow over the Al_2O_3 surface, making stabilization ineffective.

The use of ZrO_2 has also been reported to aid effective stabilization of γ-Al_2O_3 at high temperatures [18]. However, the stabilization of Al_2O_3 seems to be related to the ability of ZrO_2 to spread over the Al_2O_3 rather than to the formation of mixed oxides. Even though the formation of a ZrO_2–Al_2O_3 solid solution has sometimes been claimed, separation into ZrO_2 and Al_2O_3 occurs upon high temperature calcinations, as dictated by the phase diagram [30]. The effectiveness of ZrO_2 in improving the thermal stability of Al_2O_3 surface area seems remarkable; surface areas of as high as $50 m^2 g^{-1}$ have been observed after calcinations at 1200^oC [18]. Interestingly, ZrO_2 appears to be more effective than CeO_2 in stabilizing Al_2O_3. Consistently, ZrO_2-rich CeO_2–ZrO_2 mixed oxides more effectively stabilized Al_2O_3 compared to CeO_2-rich systems [23]. Consequently, for the next generation of TWCs, thermal stability of Al_2O_3 support is not important even for high temperature applications such as in CCCs.

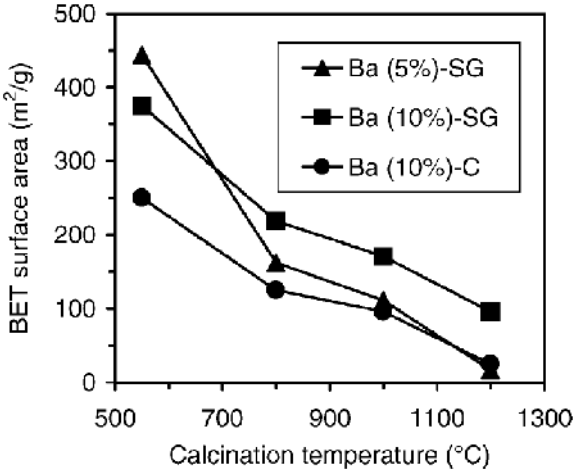

Figure 1-4: Effect of synthesis method and BaO content of the stability of BET areas of Al_2O_3 after calcination at the indicated temperatures for 3 h. SG: sol–gel synthesis method; C: co-precipitated [22].

1.2.2 CeO_2-ZrO_2

The benefits of CeO_2-containing formulations of TWCs performances have been widely recognized [31]. Many different effects have been attributed to this component [8, 32, 33], such as to:

- Promote the noble metal dispersion.

- Increase the thermal stability of the Al_2O_3 support.
- Promote the water gas shift (WGS) and steam reforming reactions.
- Favour catalytic activity at the interfacial metal support sites.
- Promote CO removal trough oxidation employing lattice oxygen.
- Store and release oxygen under lean and rich conditions, respectively.

Among the different roles of CeO_2 in TWCs, the OSC is certainly the most important one, as the unambiguous relationships between the TWCs activity and OSC performance is well established [34].

Since 1995, CeO_2-ZrO_2 mixed oxides have gradually replaced pure CeO_2 as OSC materials in the TWCs [35]. The reason for the introduction of ZrO_2 into CeO_2 lattice is due to the fact that it contributes to their higher thermal stability and to the important improvement of both OSC and BET [36]. CeO_2-rich compositions (around 60-70 mol %) are the most effective OSC promotes for TWCs applications. Further detail of CeO_2-ZrO_2 mixed oxides in the TWCs are described below.

1.2.2.1 Thermal stability of CeO_2-ZrO_2 mixed oxides

Thermal stability has been a major issue in the development of the TWCs, especially due to the higher exhaust temperature observed nowadays (e.g. in the case of CCCs). The relationship between the extent of surface area of CeO_2 and the OSC property, as detected by temperature programmed reduction (TPR) is well established. The released oxygen through the reduction of CeO_2 is widely recognized as an immediate and useful tool to detect the deactivation of the OSC and hence the TWC activity. Accordingly, the main consideration in the development of high temperature OSC materials is the resistance of CeO_2 towards sintering.

There are various way to enhance the thermal stability of the CeO_2-based materials, which can be summarized as follows: (i) design of microstructure/ textural properties by adopting an appropriate synthesis methodology, (ii) appropriate doping of CeO_2, (iii)

dispersing of CeO_2 on a carrier. Recently, CeO_2-ZrO_2-Al_2O_3 system also has been found to promote the thermal stabilization effects of γ-Al_2O_3 [23].

1.2.2.2 OSC of CeO_2-ZrO_2 mixed oxides

The OSC has been established to be a key parameter for the appropriate catalytic performance of commercial TWCs [37‑39]. The OSC allows the storage of the extra oxygen in the catalyst substrate under fuel lean conditions and its release under rich conditions [40]. The released oxygen may participate in the reactions with the reducing agents, thereby increasing the conversion of CO and HC in a rich exhaust gas environment [40]. CeO_2 has been recognized as a key material of the TWCs, since it can release and uptake oxygen owing to the following reversible reaction [41, 42].

$$CeO_2 = CeO_{2-x} + (x/2)O_2 \ (0 \leq x \leq 0.5)$$

An important property of the CeO_2-ZrO_2 mixed oxides compared to CeO_2 is their ability to easily remove bulk oxygen species at mild temperature even in highly sintered samples. This is associated with the ability of ZrO_2 to modify the oxygen sub-lattice in the CeO_2-ZrO_2 mixed oxides, generating defective structures and highly mobile oxygen atoms in the lattice which can be released even at moderate temperature [43, 44]. These early findings suggest that the efficiency of the OSC property may be improved by using CeO_2-ZrO_2 mixed oxides instead of CeO_2. Additionally, it is well recognized that when the OSC property is investigated through the TPR technique, no appreciable distinction between the reduction in the bulk and at the surface can be observed in CeO_2-ZrO_2 mixed oxides. Both, the reduction at the surface and in the bulk proceed with similar energy and occur at mild temperature [45, 46]. Typically, a single peak reduction profile centred around 500^oC is obtained for a single phase CeO_2–ZrO_2 solid solution; thus, the presence of multiple peaks are taken as an indication of the presence of phase impurities [35]. Furthermore, the changes in the TPR behaviour are even more subtle because other factors such as textural properties and even the pre-treatment can affect the TPR profile [47–50].

As indicated above, the TPR technique is commonly applied to investigate the redox properties of the CeO_2–ZrO_2 mixed oxides. It should be noted, however, that under real exhaust conditions, the λ value oscillates between the oxidising and reducing conditions with a frequency of about 1 Hz. In principle, this makes the so-called dynamic-OSC more useful compared to the TPR technique [32, 38], since this technique allows the detection of the oxygen that is available for redox processes on a time scale measured in seconds.

1.2.3 Noble metals

Noble metals (NMs) represent the key component of the TWCs. In principle, the first aspect to be considered is the choice of the NMs and its loading in the washcoat. Rh, Pd and Pt have long been employed in TWCs; Rh is used to promote NO dissociation, thus enhancing the NO removal [51, 52]. Pt and Pd are considered as the most suitable to promote the oxidation reaction, even though Rh also has a good oxidation activity. In particular, besides some initial use in 1975–1976, from the mid-1990s Pd has extensively been added to TWC formulations due to its ability to promote HC oxidation [53]. The increase in the use of Pd for TWCs technology has adversely affected Pd's market price, which is now comparable to that of Pt. In fact, there is a large demand for Pd due to the fact that the straightforward way to increase the efficiency of TWCs at low temperatures is to increase the NMs loading. Pd particularly, which for long time was the cheapest among NMs (Figure 1-5). Consequently, the choice and loading of NMs respond

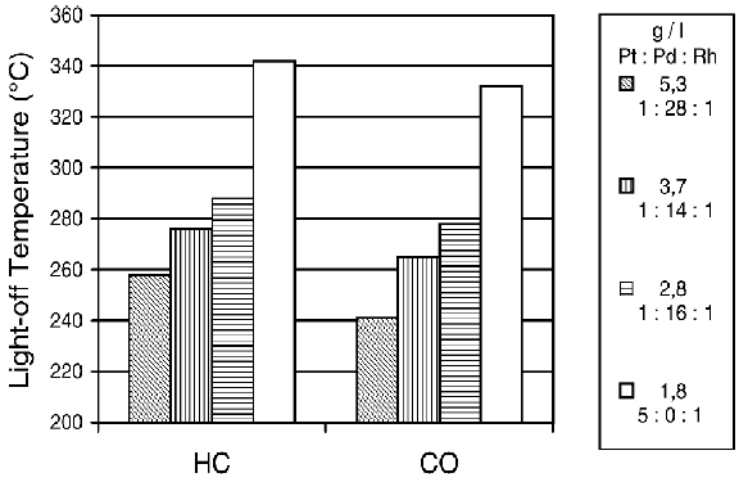

Figure 1-5: Effect of NM loading on the light-off temperature in TWCs

to a combination between the required efficiency of the converter and the market price of NMs.

1.3 The background of CuO-CeO_2

In recent years, the high catalytic activity and selectivity of the CuO-CeO_2 systems form the basis of their rising popular use in various reactions with environmental, commercial and other application. Reactions of environmental importance include complete oxidation of CO [54], oxidation of hydrocarbon [55], oxidation of VOC [56], NO reduction by CO [57], NO reduction by C_3H_6 [58], NO reduction by NH_3 [59], TWCs [60], diesel soot oxidation [61], SO_2 reduction by CO to elemental sulphur [62], ammonia decomposition [63], phenol oxidation [64], etc. Reactions of commercial importance include production of hydrogen by various processes, such as steam reforming of methanol [65], WGS reaction [66] and purification of hydrogen by preferential oxidation of carbon monoxide (CO-PROX) for fuel cells application [67], etc. Reactions of other importance are concerned with the selective oxidation of ammonia to nitrogen [68] and lower hydrocarbon reforming into synthetic gas [69]. Further, Cu/CeO_2 composite catalytic electrodes are used for direct oxidation of various fuels in fuel cells [70]. In addition, these binary oxides are also useful for H_2O_2 decomposition [71] as well as methanol synthesis [72], etc.

CuO-CeO_2 systems have been frequently used as additives to reduce the cost of noble metals in the TWCs [60], for the purification of automotive exhaust gas. CuO-CeO_2 systems has proved to excellent in the oxidation of CO [54], which is significantly higher than that of the commercially precious forms of metal catalysts [73]. Thus, these compounds have been widely studied with the aim to replacing the expensive noble metals.

Many preparation methods for $CuO\text{-}CeO_2$ which depend on the physic-chemical characteristics desired in its final composition. Following methods for the preparation of $CuO\text{-}CeO_2$ catalysts have been reported:

1. Wet impregnation method [54, 74, 75, 76, 77]
2. Co-impregnation method [78, 79]
3. Precipitation deposition method [80, 81]
4. Co-precipitation of Cu and Ce method [82, 83]
5. Urea gelation method [84]
6. Urea nitrate combustion method [56,85]
7. Solution combustion method [86]
8. Citric acid sole-gel method [87]
9. Surfactant assisted method [88]
10. Solvothermal method [89]
11. Leaching method [90]
12. Chelating method [91]
13. Inert gas condensation (IGC) method [92]
14. Electroless method [93]
15. Laser vaporization and controlled condensation [94]
16. Solvated metal atom impregnation method [95]
17. Combinatorial synthesis of mixed metal oxides [96]

1.4 Objective and the structure of the thesis

Table 1-3: EU Emission Standards for Passenger Cars (Gasoline)

Stage	**Date**	**CO**	**HC**	**HC+NOx**	**NOx**	**PM**	**PN**
		g/km					*#/km*
Euro 1†	1992.07	2.72 (3.16)	-	0.97 (1.13)	-	-	-
Euro 2	1996.01	2.2	-	0.5	-	-	-
Euro 3	2000.01	2.30	0.20	-	0.15	-	-
Euro 4	2005.01	1.0	0.10	-	0.08	-	-
Euro 5	2009.09[b]	1.0	0.10[d]	-	0.06	0.005[e,f]	-
Euro 6	2014.09	1.0	0.10[d]	-	0.06	0.005[e,f]	6.0×10^{11} [e,g]

† Values in brackets are conformity of production (COP) limits
a. until 1999.09.30 (after that date DI engines must meet the IDI limits)
b. 2011.01 for all models
c. 2013.01 for all models
d. and NMHC = 0.068 g/km
e. applicable only to vehicles using DI engines
f. 0.0045 g/km using the PMP measurement procedure
g. 6.0×10^{12} 1/km within first three years from Euro 6 effective dates
(Ref: http://www.dieselnet.com/standards/eu/ld.php)

As previously mentioned, OSC is one of the crucial factors for the performance of TWCs. The CeO_2-ZrO_2 composite is well-known as an excellent promoter for OSC, where CeO_2 exhibits oxygen storage/release behavior by redox variation of Ce ions between Ce^{3+} and Ce^{4+}, while the introduction of ZrO_2 into CeO_2 improves the reduction temperature of ceria through structural modification of ceria lattice (shown at section 1.2.2.CeO_2-ZrO_2). Many studies on CeO_2-based materials such as CeO_2-Al_2O_3 [97], CeO_2-SiO_2 [98], CeO_2-La_2O_3 [99], CeO_2-TbO_x [100], and CeO_2-PrO_x [101] have been reported to improve OSC and increase thermal stability; therefore CeO_2 is commonly used as a component in actual TWCs.

Table 1-4: EU Emission Standards for Light Commercial Vehicles (Gasoline)

Category†	Stage	Date	CO	HC	HC+NOx	NOx	PM	PN
			g/km					*#/km*
N_1, Class I ≤1305 kg	Euro 1	1994.10	2.72	-	0.97	-	-	-
	Euro 2	1998.01	2.2	-	0.50	-	-	-
	Euro 3	2000.01	2.3	0.20	-	0.15	-	-
	Euro 4	2005.01	1.0	0.10	-	0.08	-	-
	Euro 5	2009.09[b]	1.0	0.10[g]	-	0.06	0.005[e,f]	-
	Euro 6	2014.09	1.0	0.10[g]	-	0.06	0.005[e,f]	6.0×10^{11} [e,j]
N_1, Class II 1305-1760 kg	Euro 1	1994.10	5.17	-	1.40	-	-	-
	Euro 2	1998.01	4.0	-	0.65	-	-	-
	Euro 3	2001.01	4.17	0.25	-	0.18	-	-
	Euro 4	2006.01	1.81	0.13	-	0.10	-	-
	Euro 5	2010.09[c]	1.81	0.13[h]	-	0.075	0.005[e,f]	-
	Euro 6	2015.09	1.81	0.13[h]	-	0.075	0.005[e,f]	6.0×10^{11} [e,j]
N_1, Class III >1760 kg	Euro 1	1994.10	6.90	-	1.70	-	-	-
	Euro 2	1998.01	5.0	-	0.80	-	-	-
	Euro 3	2001.01	5.22	0.29	-	0.21	-	-
	Euro 4	2006.01	2.27	0.16	-	0.11	-	-
	Euro 5	2010.09[c]	2.27	0.16[i]	-	0.082	0.005[e,f]	-
	Euro 6	2015.09	2.27	0.16[i]	-	0.082	0.005[e,f]	6.0×10^{11} [e,j]
N_2	Euro 5	2010.09[c]	2.27	0.16[i]	-	0.082	0.005[e,f]	-
	Euro 6	2015.09	2.27	0.16[i]	-	0.082	0.005[e,f]	6.0×10^{11} [e,j]

† For Euro 1/2 the Category N_1 reference mass classes were Class I ≤ 1250 kg, Class II 1250-1700 kg, Class III > 1700 kg
a. until 1999.09.30 (after that date DI engines must meet the IDI limits)
b. 2011.01 for all models
c. 2012.01 for all models
d. 2013.01 for all models
e. applicable only to vehicles using DI engines
f. 0.0045 g/km using the PMP measurement procedure
g. and NMHC = 0.068 g/km
h. and NMHC = 0.090 g/km
i. and NMHC = 0.108 g/km
j. 6.0×10^{12} 1/km within first three years from Euro 6 effective dates
(Ref: http://www.dieselnet.com/standards/eu/ld.php)

Tighter legislation on exhaust emission (Table 1-3, 1-4), it is required to improve the efficiency of TWCs at low temperatures under an oxygen-rich atmosphere. Sulfur present in gasoline fuel is one components that deactivates a TWC [1]. As Cu or CuO materials are sensitive to sulfur, the catalytic deactivation of Cu or CuO by sulfur has been reported [102], Cu or CuO material was not used for TWCs. Even more stringent fuel regulation is

Table 1-5: Sulfur Standards for Gasoline and Diesel Fuel

Standard	Gasoline (ppm)	Diesel (ppm)
Euro 1	NA	NA
Euro 2	500	500
Euro 3	150	150
Euro 4	50	50
ppm = parts per million, NA = not applicable		

calling for less sulfur in fuel (Table 1-5); thus, "sulfur-free" diesel and gasoline fuels (≤ 10 ppm S) have become available from 2005, and have become mandatory from 2009. It is reasonable to consider that, Cu or CuO can be used as the new materials for TWCs. Copper/copper oxides as $CuMO_2$ (M=Al, Fe, Mn, Ga) [102] have been found with its oxygen storage/release behavior at low temperatures. Copper (4.7%) and rhodium metals were applied for TWC to investigate the OSC property and CO, C_3H_8, NO conversions ratio [40], the presence of copper promoted CO oxidation at low temperature. In section 1.3 summarized catalytic activities and other preparation methods of the CuO-CeO_2 systems. CeO_2-CuO mixed oxides have been prepared by high-energy mechanical milling, however it's OSC property for TWCs and the effective OSC to catalytic performance in rich stoichiometric operation also has not investigated. CuO-CeO_2 have pinpoint the high mobility of oxygen in CeO_2 crystal structure and the quick reversibility of Cu^{2+}/Cu^{+}, therefore, the CuO-CeO_2 may improve the OSC property at lower temperatures and exhibit high OSC values ascribed to the valence change between Ce^{4+}/Ce^{3+} and $Cu^{2+}/Cu^{+}/Cu$. It is also reasonable to believe that the valence change can be effectively promoted by mechanochemical effects. Thus, the aim of this study is to prepare a CuO-CeO_2 composite by means of mechanical milling and to evaluate its total OSC. The catalytic performance of a new TWCs is investigated and to compare with the traditional TWCs. In order to adapt to high temperature of new TWCs, durability of CuO-CeO_2 also is studied.

This thesis is organized in the following chapters:

Chapter 1 describes an overview of TWCs: Its principles and present research, the background of $CuO\text{-}CeO_2$ and the objectives of this study. **Chapter 2** describes the experimental set up developed in this work and shows details of the experiments undertaken. **Chapter 3** investigates structure and catalytic behavior of $CuO\text{-}CeO_2$ prepared by High-Energy Ball Milling. **Chapter 4** investigates the structure and adhesion properties of $\gamma\text{-}Al_2O_3$ and $CuO\text{-}CeO_2/\gamma\text{-}Al_2O_3$ on metal substrate support for automotive catalytic. **Chapter 5** presents the catalytic performance of Pd, Pt and Rh loaded on $CuO\text{-}CeO_2$ washcoat. **Chapter 6** describes the catalytic performance of Pd, Pt and Rh loaded on $CuO\text{-}CeO_2$ washcoat at high temperature. **Chapter 7** presents the conclusions and recommendations.

REFERENCES

[1] Jan Kaspar, Paolo Fornasero, Neal Hickey, Catal today 77(2003) 419-449.

[2] P. Degobert, Automobiles and Pollution, Society of Automotive Engineers, Inc., Warrendale, PA, 1995.

[3] A. Obuchi, I. Kaneko, J. Oi, A. Ohi, A. Ogata, G.R. Bamwenda, S. Kushiyama, Appl. Catal. B 15 (1998) 37.

[4] M. Iwamoto, H. Yahiro, H.K. Shin, M. Watanabe, J. Guo, M. Konno, T. Chikahisa, T. Murayama, Appl. Catal. B5 (1994) L1.

[5] P. Ciambelli, P. Corbo, M. Gambino, G. Minelli, G. Moretti, P. Porta, Catal. Today 26 (1995) 33.

[6] K.M. Adams, J.V. Cavataio, R.H. Hammerle, Appl. Catal. B 10 (1996) 157.

[7] Catalytic air pollution control commercial technology, Third edition, Ronald M. Heck, Robert J. Farrauto with Suresh T. Gulati, Pushlish by John Wiley & Sons.

[8] K.C. Taylor, Automobile catalytic converters, in: J.R. Anderson, M. Boudart (Eds.), Catalysis-Science and Technology, Springer, Berlin, 1984, Chapter 2, pp. 119-170.

[9] M. Nonnenmann, SAE Paper 850131, 1985.

[10] S.T. Gulati, SAE Paper 850130, 1985.

[11] H. Bode (Ed.), Materials Aspects in Automotive Catalytic Converters, Wiley/VCH, Weinheim, Germany, 2002, pp. 1-281.

[12] R.M. Heck, R.J. Farrauto, Catalytic Air Pollution Control: Commercial Technology, Van Nostrand Reinhold, New York, 1995, 1 pp.

[13] S.T. Gulati, vol. II, Elsevier, Amsterdam, 1991, pp. 481–507.

[14] S. Eto, S. Yamamoto, Japan Patent N. JP-2000/26603 A2 155 9/5/2000.

[15] E.S.J. Lox, B.H. Environmental Catalysis, Wiley/VCH, Weinheim, Germany, 1999, Chapter 1, pp. 1–117.

[16] J.R. Anderson, Structure of Metallic Catalysts, Academic Press, London, 1975.

[17] F. Oudet, P. Courtine, A. Vejun, J. Catal. 114 (1988) 112.

[18] T. Horiuchi, Y. Teshima, T. Osaki, T. Sugiyama, K. Suzuki, T. Mori, Catal. Lett. 62 (1999) 107.

[19] F. Mizukami, K. Maeda, M. Watanabe, K. Masuda, T. Sano, K. Kuno, vol. II, Elsevier, Amsterdam, 1991, pp. 557–568.

[20] L.L. Murrell, S.J. Tauster, vol. II, Elsevier, Amsterdam, 1991, pp. 547–555.

[21] N.A. Koryabkina, R.A. Shkrabina, V.A. Ushakov, M. Lausberg, F. Keptein, Z.R. Ismagilov, Kinet. Catal. 38 (1997) 112.

[22] Z.R. Ismagilov, R.A. Shkrabina, N.A. Koryabkina, D.A. Arendarskii, N.V. Shikina, vol. IV, Elsevier, Amsterdam, 1998, pp. 507–511.

[23] R. Di Monte, P. Fornasiero, J. Kaspar, M. Graziani, J.M. Gatica, S. Bernal, A. Gomez Herrero, Chem. Commun. (2000) 2167.

[24] A. Piras, A. Trovarelli, G. Dolcetti, Appl. Catal. B 28 (2000) L77.

[25] N.A. Koryabkina, R.A. Shkrabina, V.A. Ushakov, E.M. Moroz, M.F. Lansberg, Z.R. Ismagilov, Kinet. Catal. Engl. Transl. 37 (1996) 117.

[26] C. Morterra, G. Magnacca, V. Bolis, G. Cerrato, M. Barricco, A. Giachello, M. Fucale, vol. III, Elsevier, Amsterdam, 1995, pp. 361–373.

[27] C. Morterra, V. Bolis, G. Magnacca, J. Chem. Soc., Faraday Trans. 92 (1996) 1991.

[28] J.Z. Shyu, K. Otto, W.L.H. Watkins, G.W. Graham, R.K. Belitz, H.S. Gandhi, J. Catal. 114 (1988) 23.

[29] J.Z. Shyu, W.H. Weber, H.S. Gandhi, J. Phys. Chem. 92 (1988) 4964.

[30] J.M. Dominguez, J.L. Hernandez, G. Sandoval, Appl. Catal. A 197 (2000) 119.

[31] H.S. Gandhi, A.G. Piken, M. Shelef, R.G. Delosh, SAE Paper 760201, 1976, p. 55.

[32] A. Trovarelli, Catal. Rev.-Sci. Eng. 38 (1996) 439.

[33] J. Kaspar, M. Graziani, P. Fornasiero, The Role of Rare Earths in Catalysis, Elsevier, Amsterdam,2000, Chapter 184, pp. 159–267.

[34] M. Sideris, Methods for Monitoring and Diagnosing the Efficiency of Catalytic Converters: A Patent Oriented Survey, vol. 115, Elsevier, Amsterdam, 1997.

[35] J. Kaspar, P. Fornasiero, M. Graziani, Catal. Today 50 (1999) 285.

[36] J.P. Cuif, G. Blanchard, O. Touret, A. Seigneurin, M. Marczi, E. Quémeré, SAE Paper 970463, 1997.

[37] Duprez D, Descorme C, Birchem T, Rohart E. Top Catal 2001, 16–17(1-4):49-56.

[38] Yao HC, Yu Yao YF. J Catal 1984, 86(2):254-65.

[39] Costa CN, Christou SY, Georgiou G, Efstathiou AM. J Catal 2003, 219(2):259-72.

[40] Gandhi HS, Piken AG, Shelef M, Delosh RG. SAE Trans 1976, 85:201–12.

[41] H. Yao, Y.F. Yu-Yao, J. Catal. 86 (1984) 254.

[42] A. Trovarelli, Catal. Rev. Sci. Eng. 38 (1996) 439.

[43] P. Fornasiero, R. Di Monte, G. Ranga Rao, J. Kaspar, S. Meriani, A. Trovarelli, M. Graziani, J. Catal. 151 (1995) 168.

[44] G. Vlaic, P. Fornasiero, S. Geremia, J. Kaspar, M. Graziani, J. Catal. 168 (1997) 386.

[45] G. Balducci, J. Kaspar, P. Fornasiero, M. Graziani, M.S. Islam, J. Phys. Chem. B 102 (1998) 557.

[46] G. Balducci, M.S. Islam, J. Kaspar, P. Fornasiero, M. Graziani, Chem. Mater. 12 (2000) 677.

[47] G. Balducci, P. Fornasiero, R. Di Monte, J. Kaspar, S. Meriani, M. Graziani, Catal. Lett. 33 (1995) 193.

[48] N. Izu, T. Omata, S. Otsuka-Yao-Matsuo, J. Alloys Comp. 270 (1998) 107.

[49] R.T. Baker, S. Bernal, G. Blanco, A.M. Cordon, J.M. Pintado, J.M. Rodriguez-Izquierdo, F. Fally, V. Perrichon, Chem. Commun. (1999) 149.

[50] P. Fornasiero, J. Kaspar, M. Graziani, Appl. Catal. B 22 (1999) L11.

[51] S.H. Oh, G.B. Fisher, J.E. Carpenter, D.W. Goodman, J. Catal. 100 (1986) 360.

[52] K.C. Taylor, J.C. Schlatter, J. Catal. 63 (1980) 53.

[53] R.M. Heck, R.J. Farrauto, CATTECH 2 (1997) 117.

[54] Luo, M. F. Zhong, Y. J. Yuan, X. X. and Zheng, X. M. Appl. Catal. A. (1997) 162: 121-131.

[55] Terribile, D. Trovarelli, A. de Leitenburg, C. Primavera, A; and Dolcetti, G, Catal. Today (1999) 47: 133-140.

[56] Delimaris, D. and Ioannides, T, Appl Catal B: Env (2009) 89: 295–302.

[57] Bera, P. Aruna, S.T. Patil, K.C. and Hegde, M.S, Journal of Catalysis (1999) 186: 36-44.

[58] Amin, N. A. S. Tan, E. F. and Manan, Z. A, Appl Catal B: Env (2003) 43: 57-69.

[59] Choung, J. W, Nam, I.-S, Appl Catal A: Gen (2006) 312: 165-174.

[60] X. Courtois, V. Perrichon Appl Catal B: Env (2005) 57: 63-72.

[61] Wu, X. Lin, F. Weng, D, Li. J, Catalysis Communications (2008) 9: 2428-2432.

[62] Pantazis, C. C. Petrakis, D. Pomonis, P, J, Appl Catal B: Env (2007) 77: 66-72.

[63] Hung, C.-M, Journal of Hazardous Materials (2008) 150: 53-61.

[64] Lei. Z, Liu. Z, Fuel Processing Technology (2007) 88: 607-615.

[65] Patel. S, Pant. K, Appl Catal A: Gen (2009) 356 189-200.

[66] Gunawardana. P, V. D. S. Lee, H. C.Kim, Int, Journal of Hydrogen Energy (2009) 34: 1336–1341.

[67] Scho¨nbrod. B, Marin˜o. F, Baronetti. G, Laborde. M, Journal of Hydrogen Energy (2009) 34: 4021-4028.

[68] Hung, C.-M, Aerosol Air Qual. Res. (2006) 6: 150-169.

[69] Cha. K.-S, Kim. H.-S, Yoo. B.-K, Lee.Y.-S, Kang. K.-S, Park. C.-S, Kim. Y.-H, Int J of Hydrogen Energy (2009) 34: 1801–1808.

[70] Ye. X.-F, Wang, S.R, Hu. Q, Chen. J.Y, Wen.T.L, Wen. Z.Y, Fuels, Solid State Ionics (2009)180: 276–281.

[71] Deraz, N.M, Applied Surface Science (2009) 255: 3884–3890.

[72] Konstantin A. Pokrovski, Bell, Alexis T, Journal of Catalysis (2006) 241: 276-286.

[73] Kundakovic Lj, Stephanopoulos, M. F, J. Catal. 179 (1998): 203-221.

[74] Jiang, S. P, Mater Sci and Eng A (2006) 418: 199–210.

[75] Zheng, X. Zhang, X. Wang, S.Wu, S, Appied Catal A General (2005) 295: 142-149.

[76] Hu. Yuhai, Dong. L, Wang. J, Ding. W, Chen. Y, Journal of Molecular Catalysis A. Chemical (2000)162:307–316.

[77] Xiaoyuan. J, Liping. L, Yingxu. C, Xiaoming. Z, Journal of Molecular Catalysis A. Chemical (2003) 197:193–205.

[78] Aguila. G, Gracia. F, Araya. P, Appl. Catal. A: Gen (2008) 343: 16–24.

[79] He. H, Vohs. J. M, Gorte. R. J, J. Electrochem. Soc (2003) 150: A1470-A1475.

[80] Zhou. K, Xu. R, Sun. X, Chen. H, Tian. Q, Shen. D, Lia. Y, Catal Letters (2005) 101: 169-173.

[81] Hermans, L. A. M.; and Geus, J. W, Elsevier, Amsterdam, (1979) p. 113.

[82] Liu, Y.; Hayakawa, T.; Suzuki, K.; Hamakawa, S.; Tsunoda, T.; Ishii, T.; and Kumagai, M, Appl Catal A: Gen, (2002) 223:137–145.

[83] Djinovic´. P, Batista. J, Pintar. A, Applied Catalysis A (2008) General 347: 23-33.

[84] Liu. Y, Fu. Q, Stephanopoulos. M. F, Catal. Today (2004) 93–95: 241-246.

[85] Tao. H, Jian. Y, Jun. Z, Danjun. W, Huanling. S, Lingjun. C, Chinese Journal of Catalysis 28 (2007): 844-846.

[86] Bera. P, Aruna. S.T, Patil. K.C, Hegde. M.S, Journal of Catalysis 186 (1999): 36-44.

[87] Liang. Q, Wu. X, Weng. D. Lu, Catalysis Communications 9 (2008): 202-206.

[88] Cao.J-L, Wang, Y.Zhang, T-Y.Wu, S-H.Yuan, Appl. Catal. B 78 (2008):120-128.

[89] Zheng, X. Wang, S. Wang, S. Zhang, S. Huang, W. Wu, Catalysis Communications 5 (2004): 729-732.

[90] Zhu.J, Gao. Q, Chen. Zhi, Appl Catal B. Environmental 81 (2008) 236–243.

[91] Liu. Z, Zhou. R, Zheng. X, Journal of Natural Gas Chemistry (2007) 167-172.

[92] Skårman. B, Nakayama. T, Grandjean. D, Benfield. R. E, Olsson. E, Niihara. K, Wallenberg. L. R, Chem. Mater. 24 (2002): 3686-3699.

[93] Shiau. C, Ma. M, Chuang. C, Appl. Catal. A (2006) 301: 89-95.

[94] Sundar. R. S, Deevi. S, Journal of Nanoparticle Research 8 (2006) : 497-509.

[95] Zhang. S-M. Huang. W-P, Qiu. X-H, Li. B-Q, Zheng. X-C, Wu. S-H, Catal. Letters 80 (2002) : 41-46.

[96] Wilhelm F. M, Saalfrank. J, Chemical Engineering Science 59 (2004): 4673-4678.

[97] R.K. Usmen, G.W. Graham, W.L.H. Watkins, R.W. McCabe, Catal. Lett. 30 (1995) 53.

[98] A. Bensalem, F. Bozon-Verduraz, M. Delamar, G. Bugli, App Catal. A 121 (1995) 81.

[99] M. Ozawa, M. Kimura, H. Sobukawa, K.Yokota, Toyota Tech. Rev. 27 (1992) 43.

[100] F. Zamar, A. Trovarelli, C. de Leitenburg, G. Dolcetti, Stud. Surf. Sci. Catal. 101 (1996) 1283.

[101] M.Y. Sinev, G.W. Graham, L.P. Haach, M. Shelef, J. Mater. Res. 11 (1996) 1960.

[102] R. Prasad, Gaurav Rattan, Bulletin of Chemical Reaction Engineering & Catalysis, 5 (1), 2010, 7- 30.

[103] Sumio Kato, Ryu Fujimaki, Masataka Ogasawara, Takashi Wakabayashi, Yuunosuke Nakahara, Shinichi Nakata, Appl. Catal B 89(2009) 183-188.

CHAPTER 2
Experimental methods

2.1 Materials

As starting materials, CuO, ZrO_2 (Nilaco Corporation, 99.999%, < 250 μm, 99.8%, < 200 μm) and CeO_2 (Kojundo Chemical, 99.99%, <180 μm) powders were used to prepare CuO-CeO_2 or CeO_2-ZrO_2. CuO and ZrO_2 powder adopt a monoclinic structure in which each Cu and Zr atom is bonded to four and six oxygen atoms (Figure 2-1). CeO_2 powders have cubic structures in which the cations bond to eight oxygen neighbors, respectively (Figure 2-1).

γ-Al_2O_3 powder (Nilaco Corporation, 99.99%, < 45μm) and FeCrAl alloy (Cr 17~21%, Al 2-4%, C<1%, Fe Balance, Nilaco Corporation) were used for preparation the binder and washcoat layer.

Pd (Nilaco Corporation, 99.9%), $Pt(NO_3)_2$ powder (Wako Pure Chemical Industries, Ltd, 99.9%) and $Rh(NO_3)$ solution (Wako Pure Chemical Industries, Ltd, 1.2 g/ml) were

used to investigate the catalytic performance of noble metals (Pt, Rh, Pd) were coated on CuO-CeO_2 layer support for TWCs.

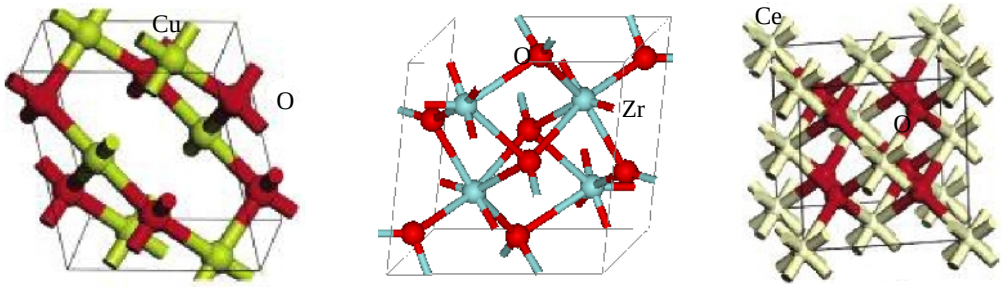

Figure 2-1: Crystal structures of CuO, ZrO_2 and CeO_2

2.2 Prepared CuO-CeO_2 by High-Energy Ball Milling

In the preparation of CuO-CeO_2, the molar ratio of CuO was changed to be 0, 20, 30, 50, 80 and 100 %. A high energy vibratory ball milling (Super Misuni, Nissin Giken Co. Ltd.) was employed, with a rotational speed of milling machine of 710 rpm. The powders and zirconia balls (ϕ10 mm) were charged in a stainless-steel vial (ϕ100 mm), where the ball to powder weight ratio was 18:1 (18g balls per 1g powders) [1] and the milling time was changed from 0 to 30h.

Similar milling conditions were used for the evaluation of OSC of CeO_2-ZrO_2 (50 and 80 molar % of CeO_2) prepared by high energy vibratory ball milling, with the only difference being the milling time, which was 14h.

2.3 Prepared coating layer

2.3.1 Substrate

The FeCrAl sheet was used as a metal substrate. In order to achieve good adhesiveness between the substrate and washcoat layer, the surface of substrate was chemically treated through the following procedure [2, 3]: The substrate was first immersed in HCl solution (69 wt. %) for 2-3 min to improve superficial roughness, followed by immersion in HNO_3 solution at 80^oC for 5 min to clean superficial oxides. Then the

substrate was heated at 900°C for 10h, resulting in the formation of a γ-Al_2O_3 layer on the substrate surface, which is expected to contribute to good contact with a γ-Al_2O_3 washcoat layer. Finally the treated substrate was rinsed with acetone.

2.3.2 Washcoat and Catalysts layer

A hybrid method of suspension and sol-gel method was employed [4, 5]. In this method, slurry which was composed of binder and sample powders is appropriately prepared. Then a substrate was dip-coated. After dip-coated, the samples were dried at room temperature for 30 min and then heated at 250°C for 2h, followed by a sintering at 650°C for 2.5 h [4].

A Binder is an agent that binds together a meal substrate surface with aluminum oxide particles as well as between CuO-CeO_2 particles or the CeO_2-ZrO_2 particles in the coating. The slurry which is a mixture of a binder, water and metal oxide powder was agitated or milled until a refractory metal oxide powder was completely suspended.

In this study, a dip-coating method was employed to deposit γ-Al_2O_3 washcoat layer on the treated substrate and CuO-CeO_2 layer or CeO_2-ZrO_2 layer on the washcoat layer. The slurry for dip-coating was made in the following manner [4]; The binder solution as the matrix of slurry was first prepared by mixing 4 wt. % of γ-Al_2O_3, 16 wt. % of concentrated nitric acid (15N) and 80% of distilled water. After agitating the mixture at 80°C for 8 h, $Al(NO_3)_3$ solution with pH ranges from 2.95 to 3.1 was obtained. Then the slurry for washcoat (or CuO-CeO_2 or CeO_2-ZrO_2) was made by mixing 23 wt. % of the binder prepared above, 23 wt. % of γ-Al_2O_3 powder (or 23 wt. % of milled CuO-CeO_2 powder or 23 wt. % of milled CeO_2-ZrO_2 powder) and 54 wt. % of distilled water. The slurry was agitated for 8h at room temperature after the mixing. In order to reduce the particle size, a high-energy ball milling process was also introduced instead of the agitation process. The milling time was changed up to 72h for CuO-CeO_2 and 80h for CeO_2-ZrO_2. In the dip-coating process, withdrawal velocity and the water content in slurries were changed as

parameters. The coated layer was dried at room temperature for 30 min and then heated at 250^{o}C for 2h, followed by sintering at 650^{o}C for 2.5h.

2.3.3 Noble metal layer

Firstly, the salt solution of $Pd(NO_3)_2$ was prepared from Pd powder through the following reactions [6]:

$$Pd + 2HNO_3 + 2HCl = PdCl_2 + 2H_2O + 2NO_2$$

$$PdCl_2 + 2NH_4OH = Pd(OH)_2 + 2NH_4Cl$$

$$Pd(OH)_2 + 2HNO_3 = Pd(NO_3)_2 + 2H_2O$$

The Pd powder was dissolved in mixed HNO_3 (70%) and HCl (37%) to form a $PdCl_2$ solution and then an ammonia solution (28%) was added dropwise to form $Pd(OH)_2$ (until a PH of about 10). The precipitate was filtered out and washed with a dilute ammonia solution to reduce Cl^- ions. The precipitate was dissolved in dilute HNO_3 at 60^{o}C in strong string in 2h for $Pd(NO_3)_2$. Following, the porous washcoat and catalysts layer is impregnated with the mixed solution of $Pt(NO_3)_2$, $Pd(NO_3)_2$ and $Rh(NO_3)_3$ to be the ratio of Pt : Pd : Rh = 1:14:1 (total 3.7 gram/L) [7]. The total loading amount of NMs was wt. 4% in overall sample and kept at the same weight level in case coated on CuO-CeO_2, ZrO_2-CeO_2, and Al_2O_3 respectively.

2.4 Properties of mixed oxide and coating layer

2.4.1 Microstructure

2.4.1.1 X-ray diffraction (XRD)

The crystal structure of CuO-CeO_2, CeO_2-ZrO_2 and those of the coating layer were evaluated by X-Ray diffraction (XRD) with Cu Kα radiation at 40 kV and 30mA working at the θ-2θ mode (Rint 2100, Rigaku). XRD is a powerfull non-destructive method that is used to measure structural properties, such as residual stress, grain size, epitaxial relations,

texture, defect structural and crystal structure. The X-rays have wavelengths in the order of few angstroms, the same as typical interatomic distances in crystalline solids. When certain geometric requirements are met, X-ray scattered from a crystalline solid can constructively interfere, producing a diffracted beam. The condition for constructive interference is given by the Bragg's law: $n\lambda=2d\sin\theta$, where n is an integer, λ is the wavelength, d is the interatomic spacing, and θ is the diffraction angle. The diffracted beam intensity will depend on several factors such as the chemical composition of materials and the local arrangement of the atoms. The step size and the time per step were 0.05^{o} and 5 sec respectively. The silver crystal was used as a calibration standard.

2.4.1.2 Scanning electron microscopy (SEM)

A scanning electron microscopy (SEM) was used for microstructural analysis (JSM-5800, JEOL). SEM is a versatile and widely used tool as it allows the study of both morphology and composition of materials. A monochromatic electron beam is focused onto a fine probe that is scanned over a rectangular area of the sample. As the electrons collide with the surface, a number of interactions occur resulting in the emission of electron and photons from surface. The intensity of the secondary electrons is point to point mapped onto a screen. The electron beam in the cathode ray tube illuminating the screen is synchronized with the electron beam scanning sample. High-resolution images of the morphology or topography of specimen at very high magnifications can be obtained. Characterization in terms of size, shape and distribution as well as statistical analyses is performed.

2.4.2 Surface properties

2.4.2.1 Surface area (BET)

BET device (Micromeritics, flowsorb III) was used in surface area measurements of powder or batch samples. The device determined the needed quantity of nitrogen gas to cover the sample surface with a molecular layer and calculated the surface area according to the Brunauer, Emmett and Teller (BET) theory. For the CuO-CeO_2 and CeO_2-ZrO_2 powders, the surface area was evaluated in m^2/g units with the chemical absorption technique. For the surface area of coating layer, the samples were evaluated in m^2/m^2 of substrate. The minimum measureable surface area was 0.05 m^2/g when nitrogen was used.

2.4.2.2 X-ray photoelectron spectroscopy

Chemical bonding states of NMs were analyzed by X-ray photoelectron spectroscopy (XPS) using monochromatic Mg Kα radiation (10 mA, 10 kV). X-ray photoelectron spectroscopy is a widely used technique for the structural study of solid surface. XPS can be described as a technique for the measurement of the kinetic energy of the inner or valence electron by an incident X-ray photon of known energy (hv). Knowing these values it is possible to calculate the binding energy (E_b), which is characteristic of the chemical bonds in a compound. Electron binding energies are also affected by the chemical environment of the ion, making XPS useful to identify not only the ion, but also its oxidation state. The spatial resolution (ejected electron) of diameter and thick is < 1-5 nm and 100-150 μm. XPS can be considered as a surface analysis technique, and depth profiling analysis (measure of the elemental composition as a function of depth) of a material is also feasible by ion beam etching.

2.4.3 Evaluation of the coated samples

In order to evaluate the coating layers of γ-Al_2O_3 washcoat, CuO-CeO_2 and CeO_2-ZrO_2, the coating load and the thickness after the sintering were measured. The former was determined by weighing the coating layer per unit substrate area (mg/cm^2) and the latter by SEM. Adhesive properties after the sintering process were evaluated by measuring weight loss (Mettler Toledo AG245 analytical balance) by an ultrasonic vibration cleaner with 100 W of power and 45 kHz of frequency; the coated sample was immersed in ethanol inside a glass beaker, which is subjected to an ultrasonic process for 20 min. The thickness of coating layer was observed by SEM, the particle size was estimated by Zeta potential analyzer (ZetaPlus Model, Serial No 21455).

2.5 Measurement and analysis

2.5.1 OSC and TPR (temperature programmed reduction) measurement

The milled sample was subjected to the total OSC measurement according to the method of Tanabe et al [8] and Morikawa [9]. The weight change of the milled sample was measured by TG-DTA (RIGAKU TG-8120) in the following procedure; The milled sample (about 20 mg) in an alumina container was completely oxidized at 500^oC in a N_2-20%O_2 mixed gas flow (500 ml/min) for 60 min, followed by cooling to 300^oC. Then, the gas atmosphere was switched to an Ar-5%H_2 flow (500 ml/min) and the weight decrease due to reduction was monitored until no weight change was observed. Afterward, the gas atmosphere was again switched to air and the weight increase due to oxidation was monitored until no weight change was observed. This process was repeated twice. The dynamic reduction behavior was measured by temperature-programmed reduction (TPR), where the milled sample (about 50 mg) was put in a quartz reactor and heated at 400^oC for 1 hour under a N_2-20%O_2 gas flow (30 ml/min) and cooled to room temperature. The gas was then changed to Ar-5%H_2 (25 ml/min) and heated with 15^oC/min in the temperature range of 35^oC-1000^oC, where the H_2 consumption was measured by GC-TCD.

2.5.2 Catalytic performance measurement

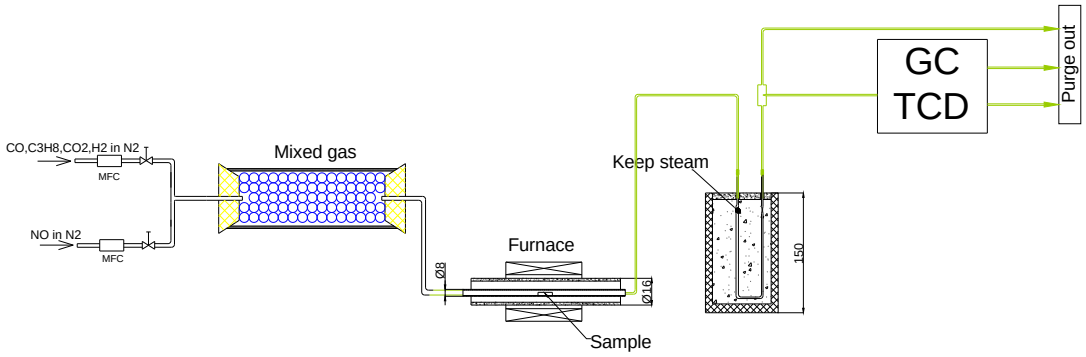

Figure 2-2: Schematic apparatus for catalytic performance measurement in case λ=1

The simulant exhaust gas containing O_2, CO (1.5%), H_2 (0.5%), CO_2 (12%), C_3H_8 (0.1%), NO (0.05%) and N_2 (balance) [10] was prepared; where the λ value as oxidants/reductions factor was defined to be $\lambda = (2O_2+NO)/(CO+H_2+10C_3H_8)$. The λ was adjusted by controlling the concentration of oxygen. The catalyst activity (CO, C_3H_8, NO) was analyzed by GC-TCD. The sample was put in a reaction tube (i.d = 8mm) made from quartz (Figure 2-2). In the case of a λ=1 (the concentration of O_2 was 1.5%), the reaction temperature was varied from 30 to 540^{o}C at the heating rate of 3 ^{o}C/min with the gas flow of 20 ml/min, the catalytic performance was measured with the increase of temperature.

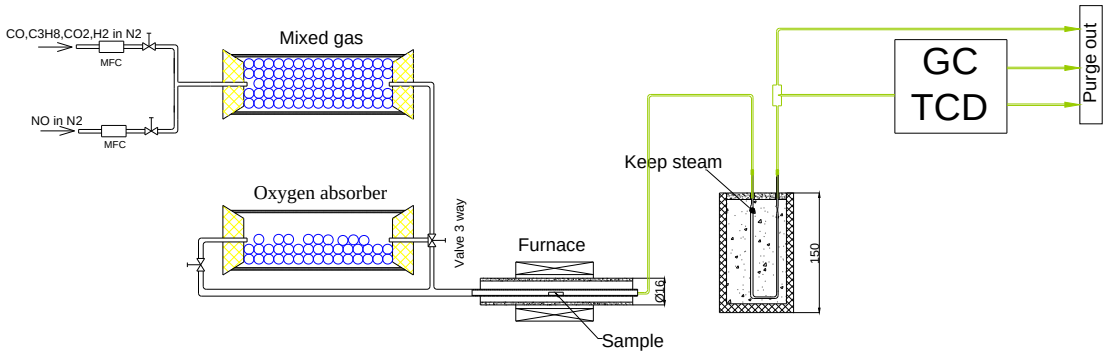

Figure 2-3: Schematic apparatus for catalytic performance measurement in case λ<1

In the case of λ<1, the concentration of oxygen was controlled from 1.5% (λ=1) to 0.42% (λ=0.3) by amount of oxygen absorber (ageless, 227 gram) and absorber time about for 15 minutes, the reaction temperature was kept constant at 500^{o}C, and the catalytic activities were measured with the λ value change from 1-0.3 (Figure 2-3). Finally, in case of λ>1, pure oxygen gas was mixed with the simulant exhaust gas above; the flow of feed stream was controlled with the increasing O_2 concentration from 1.5% (λ=1) to 2.1% (λ=1.4), the reaction temperature was also kept at 500^{o}C and the catalytic activities were measured with the changing λ value from 1-1.4.

2.5.3 Conversion rate calculation

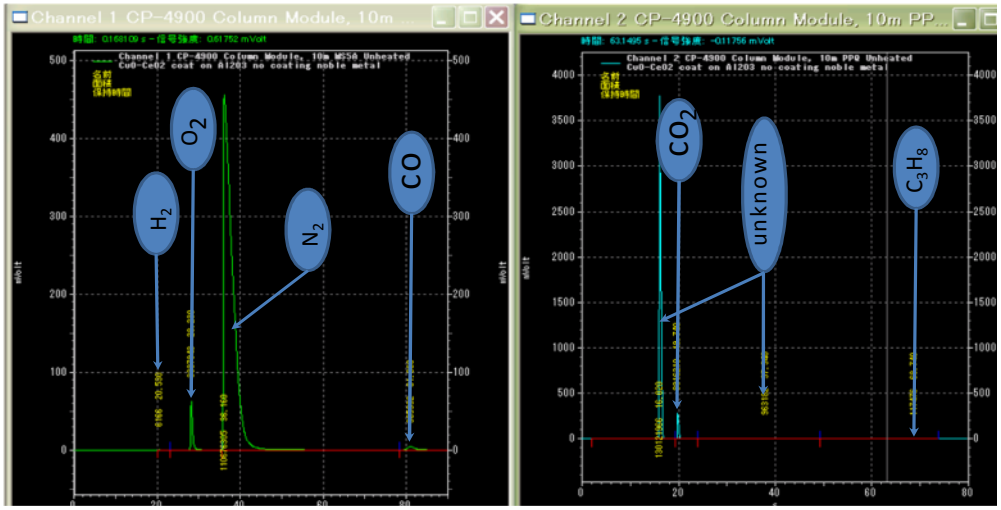

Figure 2-4: Schematic for determined CO, C_3H_8, N_2, O_2 by GC-TCD

GC-TCD was used for the CO, CO_2, C_3H_8, N_2, O_2 analysis (Figure 2-4). The NO was not detected by Varian CP-4900, the NO was calculated from N_2 by the reduction reactions of NO to N_2 as shown in Table 1-2.

The CO conversion rate was calculated based on the CO consumption as follows:

$$\%\,\text{of conversion of CO} = \frac{[CO]_{in} - [CO]_{out}}{[CO]_{in}} \times 100$$

The C_3H_8 conversion rate was calculated based on the C_3H_8 consumption as follows:

$$\%\,\text{of conversion of } C_3H_8 = \frac{[C_3H_8]_{in} - [C_3H_8]_{out}}{[C_3H_8]_{in}} \times 100$$

The NO conversion rate was calculated based on the N_2 consumption. At first, the N_2 (99.95%) was determined, and then the gas was change to N_2 (100%). The N_2 (0.05%) was calculated as follows:

$$N_2\ (0.05\%) = N_2\ (100\%) - N_2\ (99.95\%)$$

Finally, the NO conversion rate was calculated as follows:

$$\%\,\text{of conversion of NO} = \frac{[N_2]_{out} - [N_2]_{in}}{N_2(0.05\%)} \times 100$$

REFERENCES

[1] Alessandro Trovarelli, Francesca Zamar, Jordi Llorca, Carla de Leitenburg, Giuliano Dolcetti, and Janos T. Kissz, Journal of catalysis 169, 490–502 (1997).

[2] Michela Valentini, Gianpiero Groppi, Cinzia Cristiani, Marinella Levi, Enrico Tronconi, Pio Forzatti, Catalysis Today 69 (2001) 307–314.

[3] Su Zhao, Jizhong Zhang, Duan Weng, Xiaodong Wu, Surface and Coatings Technology 167 (2003) 97–105.

[4] Di-jia Liu, Daniei R. Winstead, Norman Van Den Bussche, US Patent No.6,540,843 B1 (Apr. 1, 2003).

[5] Valerie Meille, Review on methods to deposit catalysts on structured surfaces. Applied Catalysis A: General 315 (2006) 1-17.

[6] H. He, H.X. Dai, L.H. Ng, K.W. Wong, C.T. Au, . Journal of catalysis 206 (2002), 1-13.

[7] Jan Kaspar, Paolo Fornasero, Neal Hickey, Catal today 77(2003) 419-449.

[8] T. Tanabe, A. Suda, C. Desorme, D. Duprez, H. Shinjyoh, M. Sugiura, Stud. Sci. Catal. 138 (2001) 135.

[9] Akira Morikawa, Tadashi Suzuki, Takaaki Kanazawa, Koichi Kikuta, Akihiko Suda, Hirofumi Shinjo, Appl, Catal, B 78 (2008).

[10] Xiaodong Wu, Luhua Xu, Duan Weng, Applied surface science 221 (2004) 375-383

CHAPTER 3

Improved OSC of TWCs using CuO-CeO_2 prepared by High-Energy Ball Milling

3.1 Introduction

Nowadays, more than 95% of the vehicles produced are equipped with a catalytic converter. The TWCs, used for the gasoline-fuelled engine, are capable of simultaneously converting CO, HC and NOx, into harmless CO_2, H_2O and N_2 respectively; with a stoichiometric air-to-fuel ratio (A/F=14.6) [1]. OSC is one of the crucial factors for the performance of TWCs. The CeO_2-ZrO_2 composite is well-known as an excellent promoter for OSC, where CeO_2 exhibits the oxygen storage/release behavior by redox variation of Ce ions between Ce^{3+} and Ce^{4+}, while an introduction of ZrO_2 into CeO_2 improves the reduction temperature of ceria through structural modification of the ceria lattice [2], although the OSCs at low temperatures are still not high [1]. Many studies on CeO_2-based

materials have been reported, such as CeO_2-Al_2O_3 [3], CeO_2-SiO_2 [4], CeO_2-La_2O_3 [3,5,6], CeO_2-TbO_x [7], and CeO_2-PrO_x [8], to improve the OSC and increase the thermal stability.

As legislation becomes tighter, it is required to improve the efficiency of TWCs at low temperatures under an oxygen-rich atmosphere. Copper/copper oxides have been found with its oxygen storage/release behavior at low temperatures, though it causes fragmentation due to the large volume change [9]. Then, various metal oxides without large volume change, such as $CuMO_2$ (M=Al, Fe, Mn, Ga), have been investigated to reduce fragmentation [9], where the reduction of Cu^{2+} to Cu is studied by the H_2-TPR (temperature-programmed reduction) and the OSC is improved at lower temperatures.

Recently, $CuO\text{-}CeO_2$ mixed oxides have found to exhibit high activity for oxidation of carbon monoxide and hydrocarbon [10-12], SO_2 reduction by CO [13-15], NO reduction [16, 17] and phenol oxidation [18, 19]. It also has been shown that, redox properties and catalytic performance strongly depend on the preparation method, such as sol-gel [20], hydrothermal routes [21, 22], precipitation method [23, 24], reverse micelle [25], sonochemical [26], chemical vapor deposition (CVD) [27], flux method [28], micro-wave heating [29] and surfactant-assisted [30]. The preparation conditions and mixed oxide composition influence the form and distribution of copper species on ceria. The enhanced catalyst activity results from interactions between the copper-cerium oxide phases.

The mechanical milling has long been used to prepare non-equilibrium materials, solid solutions and other metastable phases, and also to drive mechanochemical reactions. It has been shown that, since the enhanced reaction rate can be achieved and dynamically maintained during milling as a result of microstructural refinement and mixing processes accompanying repeated fracture, deformation and welding of particles during collision events [31], several treatments employing mills could be applied for various preparation stages of mixed oxides to enhance catalytic activity or selectivity [32–34]. Recently, the

mixed oxides containing CeO_2 and other dopants such as TbO_x, HfO_2 and ZrO_2, have been prepared by mechanical milling [7, 35-36] with a strong enhancement of the OSC properties of CeO_2. In addition, Castricum et.al. reports that the milling process of the mixed Cu, Cu_2O or CuO and ZnO in a synthetic air results in oxidation of Cu precursors, while results in reduction under vacuum, and that the mechanochemical reactions are promoted by mechanical milling in presence of ZnO [37].

However, the OSC property of CuO-CeO_2 support for TWCs has not been reported. Since, it is also reasonable to consider that the valence change of Ce^{4+}/Ce^{3+} and/or $Cu^{2+}/Cu^{+}/Cu$ can improve the OSC property at lower temperatures. The aim of this chapter is to characterize the properties of CuO-CeO_2 mixed oxides prepared high-energy mechanical milling. The OSC properties of milled CuO-CeO_2 samples are investigated to compare with that of CeO_2-ZrO_2 traditional catalysts prepared by the same experimental condition.

3.2 Results and discussion

3.2.1 Structural characterization

The XRD patterns of milled samples having a composition of 50 %mol CuO and 50 %mol CeO_2 are shown in Figure 3-1. The reflection peak intensities of the CuO phase are largely reduced with peak broadening after 2h milling, while no appearance of other phases is detected. Some CuO phase may exist as nanostructured or amorphous state. After 7h milling the CuO peaks are almost eliminated and replaced instead by an appearance of the faint reflections from Cu_2O phase and the clear peaks of fcc Cu. The coexistence of both phases lasts until the milling duration of around 14h. The Cu_2O reflections become weaker with milling, while the Cu peaks become more distinguished with milling, where the tendency continues up to 30h milling. On the other hand, there is no change in the observed phase of CeO_2 up to 30h milling, though the peak broadening with milling is

significant, particularly during the early milling stages regarding the change of the peak shape.

From the XRD results the reductive valence change of CuO, i.e. $Cu^{2+} \rightarrow Cu^{1+} \rightarrow Cu$, or $Cu^{2+} \rightarrow Cu$, is evidenced to occur during milling. This is consistent with a report [10] claiming that there are three ways for reduction of Cu^{2+} to Cu: (i) $CuO \rightarrow Cu_4O_3 \rightarrow Cu_2O \rightarrow Cu$, (ii) $CuO \rightarrow Cu_2O \rightarrow Cu$, or (iii) $CuO \rightarrow Cu$. The presence of Cu is also confirmed by nuclear magnetic resonance (NMR) spectroscopy in the 7h- and 18h-milled samples (Appendix D). When the CeO_2 and CuO powder phases are forced to contact at the bounding interphase interface during milling the cations of Ce^{4+} (or Ce^{3+} for nonstoichiometric sites especially near the surface) could be interchanged with Cu^{2+} cations through the vacancy mechanism. According to [38], the CeO_2 powder, the surface volume in particular, exhibits non-stoichiometric compositions with various defects, which can be formed upon the introduction of metal cations with higher or lower valences into CeO_2. It is

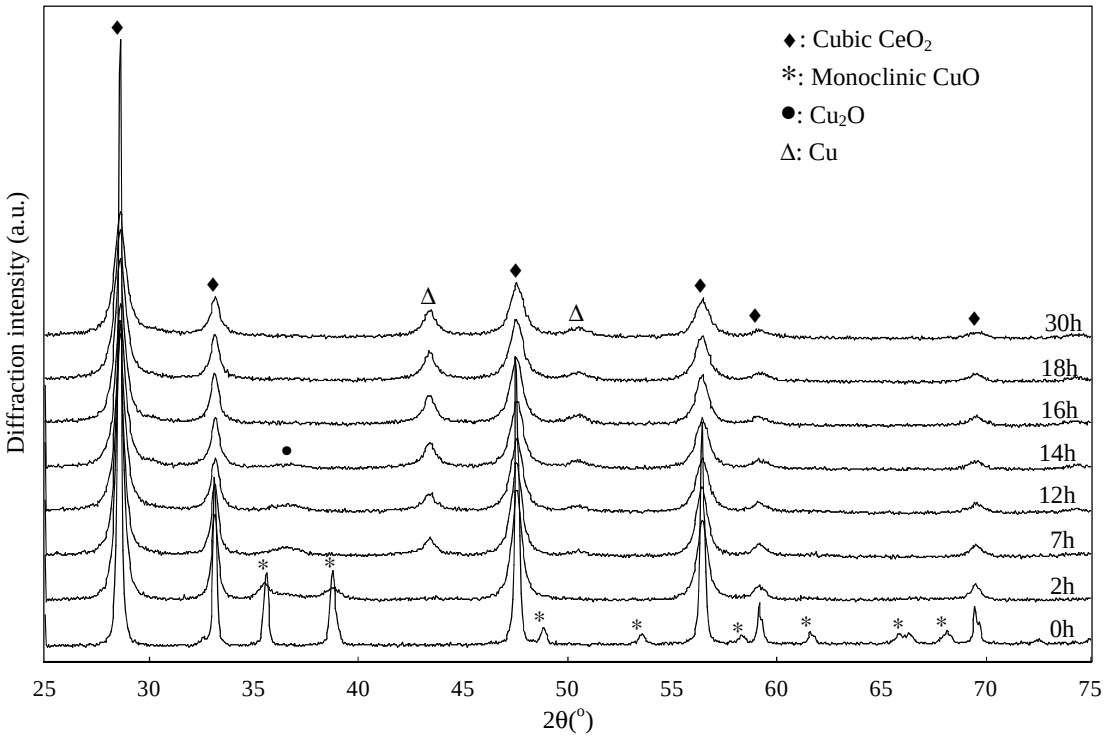

Figure 3-1: XRD patterns of $(CuO)_{0.5}(CeO_2)_{0.5}$ powder (CuO: monoclinic, CeO_2: cubic) with milling

also known that the mechanical milling of powders induces fracture and deformation through high-energy collisions between balls and particles [39], leading to a modification of crystal structure as well as high lattice strain. In this study, the Cu cations can be introduced in the lattice of CeO_2 replacing the Ce cations, as well as producing the extra oxygen vacancies in the CeO_2 lattice.

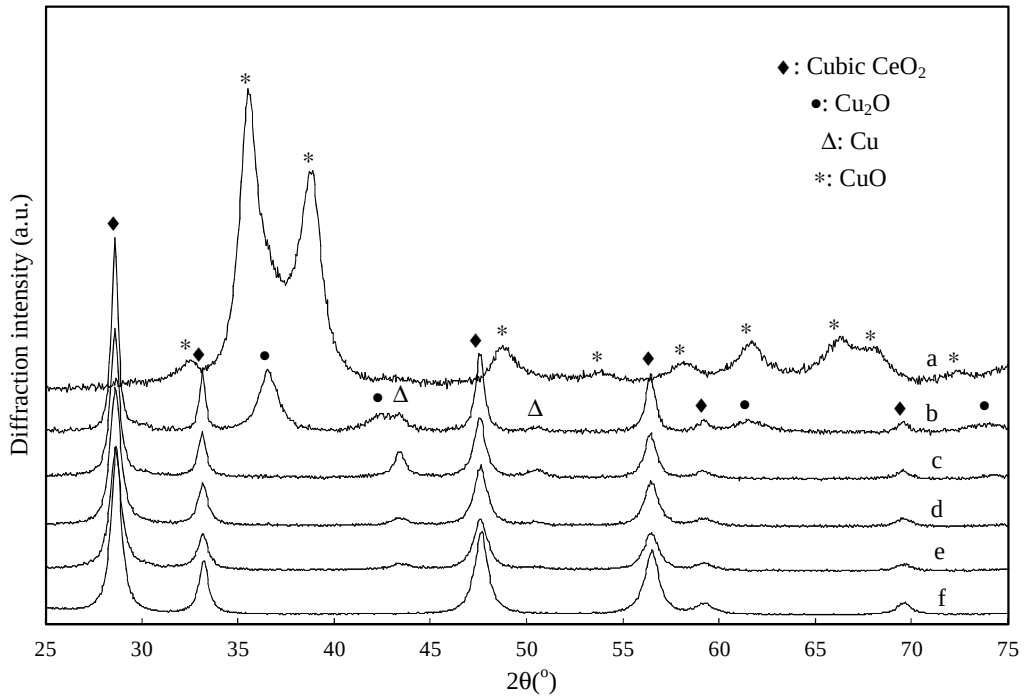

Figure 3-2: XRD patterns $(CuO)_x(CeO_2)_{1-x}$ powder after 18h milling (x=: (a) 1, (b) 0.8, (c) 0.7, (d) 0.5, (e) 0.2, (f) 0)

Figure 3-2 shows XRD patterns of 18h-milled-samples with various CuO-CeO_2 content ratios. For pure CuO, i.e. the highest CuO content (Figure 3-2a), no phase change of CuO is observed after 18h of milling. On the other hand, with the 80 mol% CuO composite (Figure 3-2b) the coexistence of both Cu and Cu_2O phases is observed replacing the CuO, besides the existence of the cubic CeO_2. With 70 mol% CuO (Figure 3-2c) the observable Cu-related phase after 18h milling, besides the cubic CeO_2, an fcc Cu phase only. With further reducing the CuO content (Figure 3-2c and Figure 3-2f) for each after

18h milling; the emergence intensity of the Cu phase is gradually lowered, without a major change in the CeO_2 reflections.

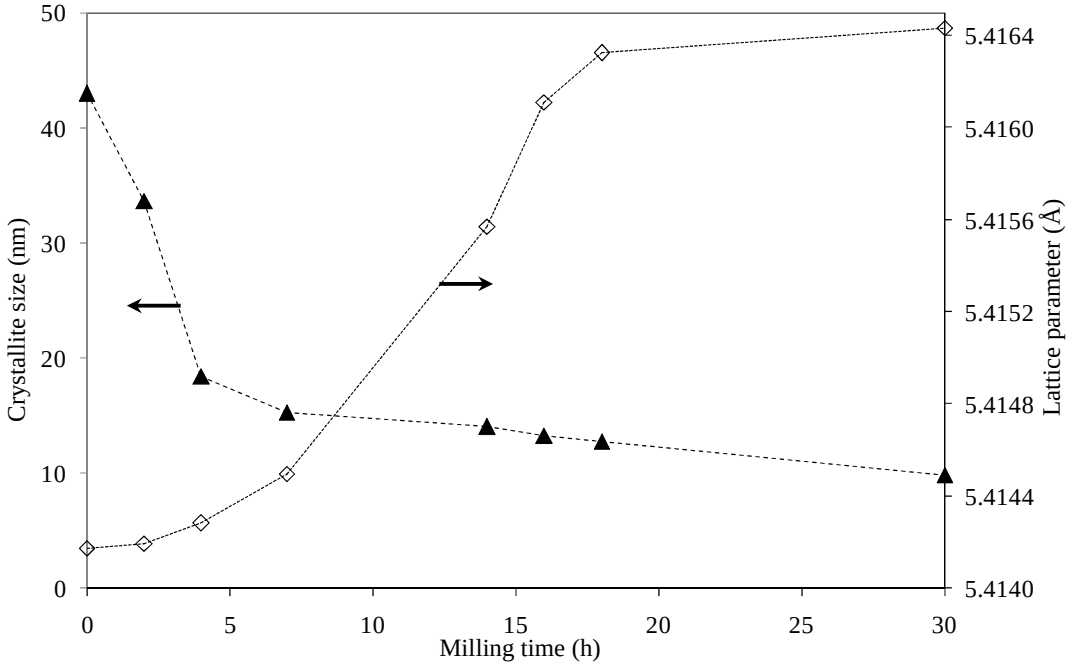

Figure 3-3: Crystallite size and lattice parameter of CeO_2 in $(CuO)_{0.5}(CeO_2)_{0.5}$ composite powder as a function of milling time

The lattice parameter and the estimated crystallite size of the cubic CeO_2 phase in the $(CuO)_{0.5}(CeO_2)_{0.5}$ composite as a function of milling time are shown in Figure 3-3. The crystallite size is rapidly decreased during an early stage of milling periods, less than ~5h, followed by a gradual decrease up to 30h milling. On the other hand, the lattice parameter is only gradually increased during an early stage of milling less than ~5h, followed by a rather rapid increase with increasing the milling time up to ~18h, and then the variation becomes small till 30h milling. This indicates that, although the change of the crystallite size is not directly related to the lattice parameter variation, the latter is activated only after the former event. This is consistent with that the appearance of Cu and Cu_2O phases is clearly observed when the milling duration is longer than 7h, as shown in Figure 3-1, since the so-called kneading effect during milling is in general only expected after atomic-order

mixing of the powders. It is also suggested that a steady state of the structural variation of CeO_2 is attained after ~18h of milling. The decrease of crystallite size and the increase of lattice parameter of CeO_2 by the increase of milling time is reported in [40-44].

Table 3-1: Lattice parameter, crystallite size, BET surface area of cubic CeO_2 for various $(CuO)_x(CeO_2)_{1-x}$ samples after 18h milling

Sample	Lattice parameter	Crystallite size (nm)	S_A (BET)
	(Å)	d[220]	m^2g^{-1}
$(CuO)_{0.8}(CeO_2)_{0.2}$	5.4168(6)	11.3	17-19
$(CuO)_{0.5}(CeO_2)_{0.5}$	5.4163(2)	12.8	18-21
$(CuO)_{0.3}(CeO_2)_{0.7}$	5.4160(0)	13.6	19-22
$(CuO)_{0.2}(CeO_2)_{0.8}$	5.4158(9)	14.4	21-23
CeO_2	5.4152(4)	15.6	23-25

The lattice parameters, crystallite sizes and specific surface areas (BET) of 18h-milled-samples with various CuO contents are listed in Table 3-1. With an increase of mol% CuO contents the lattice parameter of CeO_2 increases, the crystallite size decreases, and the BET surface area of CuO-CeO_2 powder composite decreases. Since the smaller crystallite size may cause an elongation of the cubic lattice in the nano-sized CeO_2 phase [44], which is ascribed to the lattice strain from the formation of the Ce^{3+} cations and the corresponding vacancies, the observed tendency is consistent. The slight decrease of the BET area with the CuO ratio is probably due to the formation of the soft Cu phase during 18h milling (Figure 3-2), which may cause agglomeration of powders.

3.2.2 Morphological features

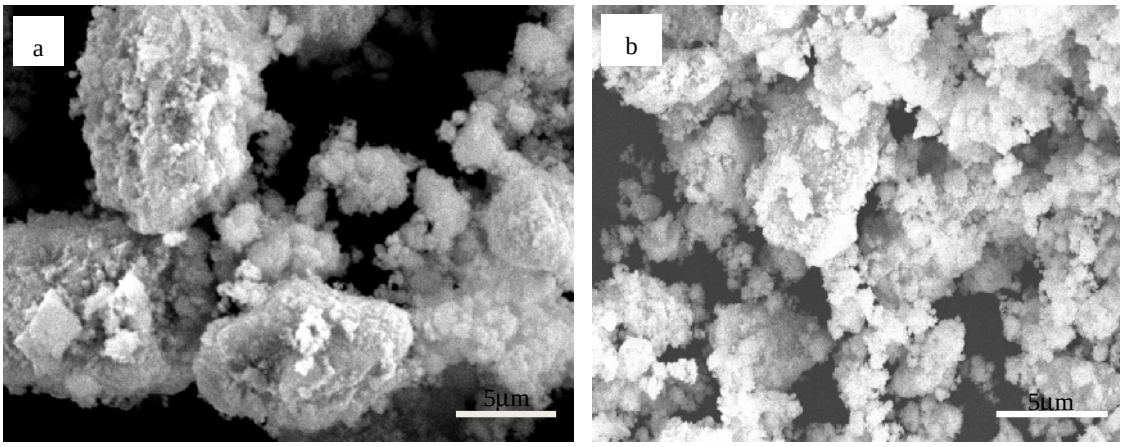

Figure 3-5: SEM micrograph of 18h-milled powders; (a) $(CuO)_{0.8}(CeO_2)_{0.2}$ and (b)

The morphological features and the compositional homogeneity were studied by SEM and EDX. Similar morphology is observed in all the milled samples, where there exist aggregations of packed particles from a few hundred nanometers to micrometers in size, as showed in Figure 3-4. Some reports show that the CuO is incorporated and evenly

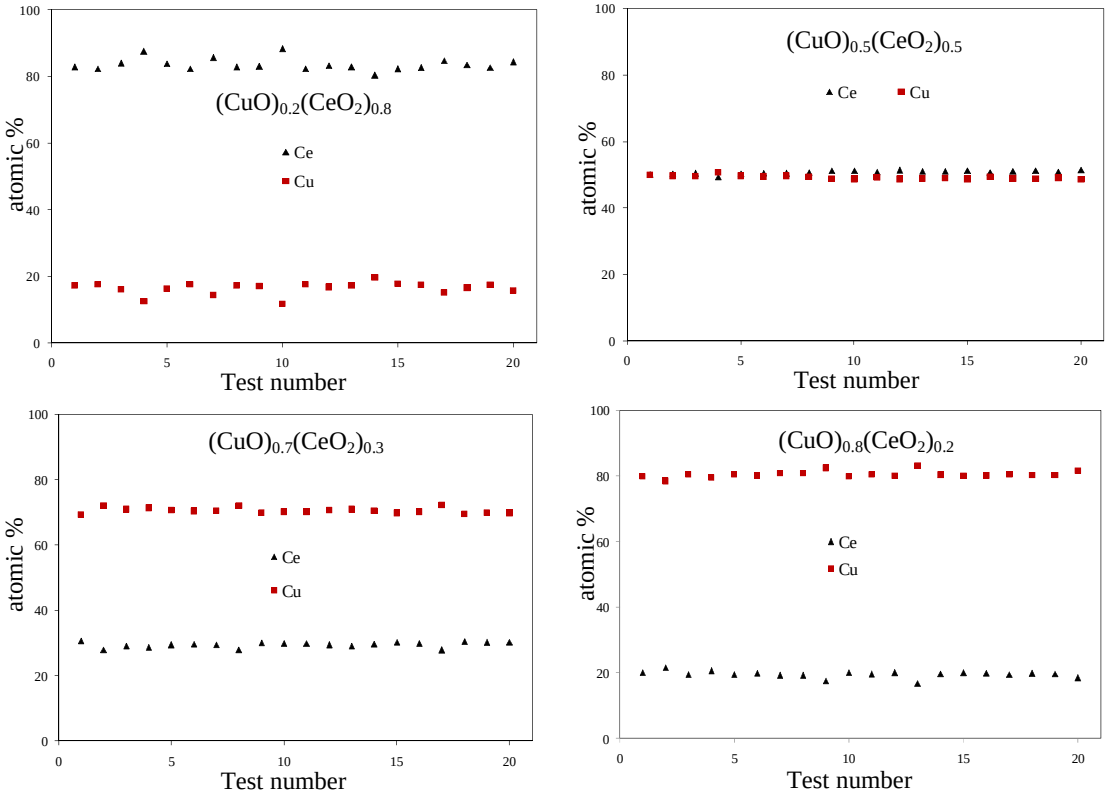

Figure 3-4: EDX analysis on various $(CuO)_x(CeO_2)_{1-x}$ samples after 18h milling

distributed into the CeO_2 structure [45, 46]. As shown in Figure 3-5, with use of each beam size adjusted 10 μm the areal average concentrations of each 18h-milled sample with a different overall composition (20, 50, 70 and 80 mol% CuO) exhibit high homogeneity in terms of Ce and Cu contents, judging from the EDX analyses at twenty randomly-selected squares. The magnification of SEM is fixed at 220 times. This strongly suggests that the dimensional size of the Cu or Cu_2O phase as observed in Figure 3-2 is much smaller than 10 μm. The homogeneity of the milled samples is better than those by the microemulsion method [47]. The contaminations from the milled media (ZrO_2 balls and a steel vial) were also examined by EDX, and the maximal contamination level was found to be less than 1 wt% for Fe while no contamination was detectable for Cr, ZrO_2, and so on, after 18h milling.

3.2.3 Reduction behavior by TPR

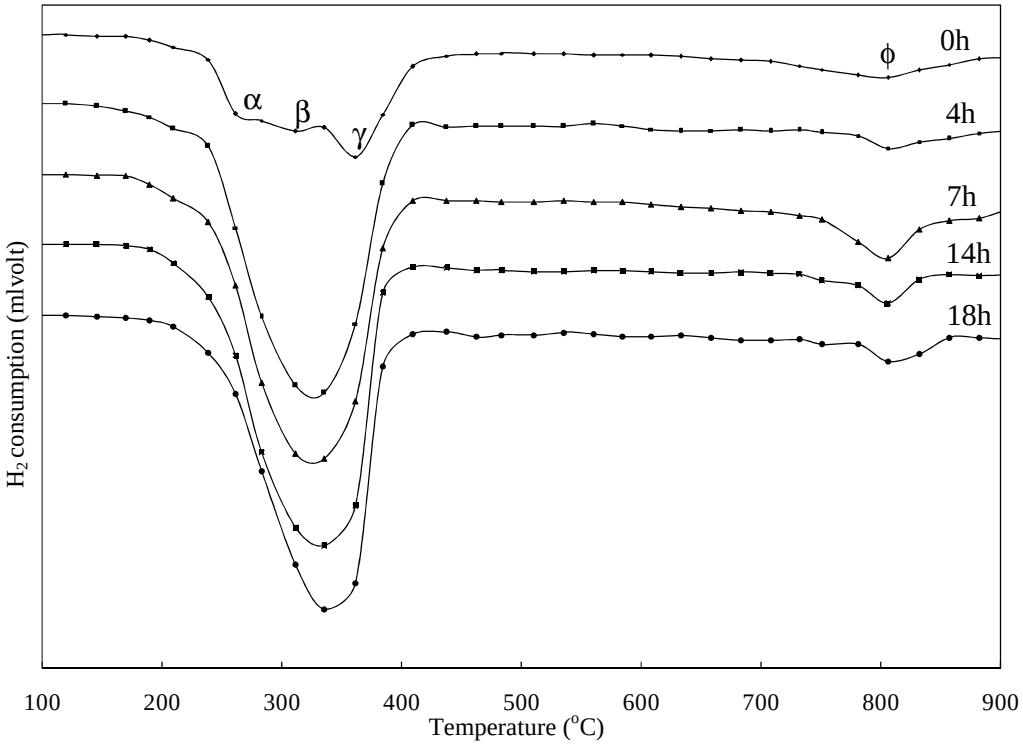

Figure 3-6: TPR of $(CuO)_{0.5}(CeO_2)_{0.5}$ composite powder with milling time

The H_2-TPR profiles of the $(CuO)_{0.5}$-$(CeO_2)_{0.5}$ samples milled for 0, 4, 7, 14 and 18h are shown in Figure 3-6. For 0h milling, the reduction of $(CuO)_{0.5}$-$(CeO_2)_{0.5}$ is characterized by three peaks (α, β, and γ) and ϕ in the range of 200°C-410°C for the former peaks and 780°C-870°C for the latter. After 4h milling, the three peaks (α, β and γ) merge into one peak around 316°C, and the intensities of the peaks become higher after 7h, 14h and 18h milling (Figure 3-6).

It has been reported that, ceria promotes the reduction of highly dispersed copper oxide surface species [48-55] and the smaller size of supported CuO particles was easier to reduce [56]. W. Liu et al [49] reported the reduction peaks; one at low temperature attributed to the reduction of copper oxide clusters strongly interacting with ceria and one at higher temperature attributed to the reduction of larger CuO particle, non-associated with ceria. Similar results of H_2-TPR profile were also reported by Xiaoyuan at el [52] and Luo et al [51]. While X. Tang et al [57] reported that low temperature reduction peak assigned to the reduction of amorphous CuO clusters closely interacting with the CeO_2. In addition, Meng-Fei Luo et al [45] also showed that the low temperature reduction peak is due to the reduction of Cu^{2+} ions in $Cu_xCe_{1-x}O_{2-\delta}$ solid solution.

Consequently, the α peak should be attributed to the reduction of amorphous CuO clusters closely interacting with the CeO_2, the β peak may be due to the reduction of Cu^{2+} ions in CeO_2, the γ peak can be attributed to the reduction of larger CuO particle or bulk CuO, non-associated with ceria, and the reduction of ϕ peak suggests to reduction of bulk oxygen ions in CeO_2 interacting with CuO [58, 59]. With the increase of milling time, the particles of CuO highly disperse and incorporate in to CeO_2, so the intensity of β peaks rapidly increase, whereby only a single β peak is observed.

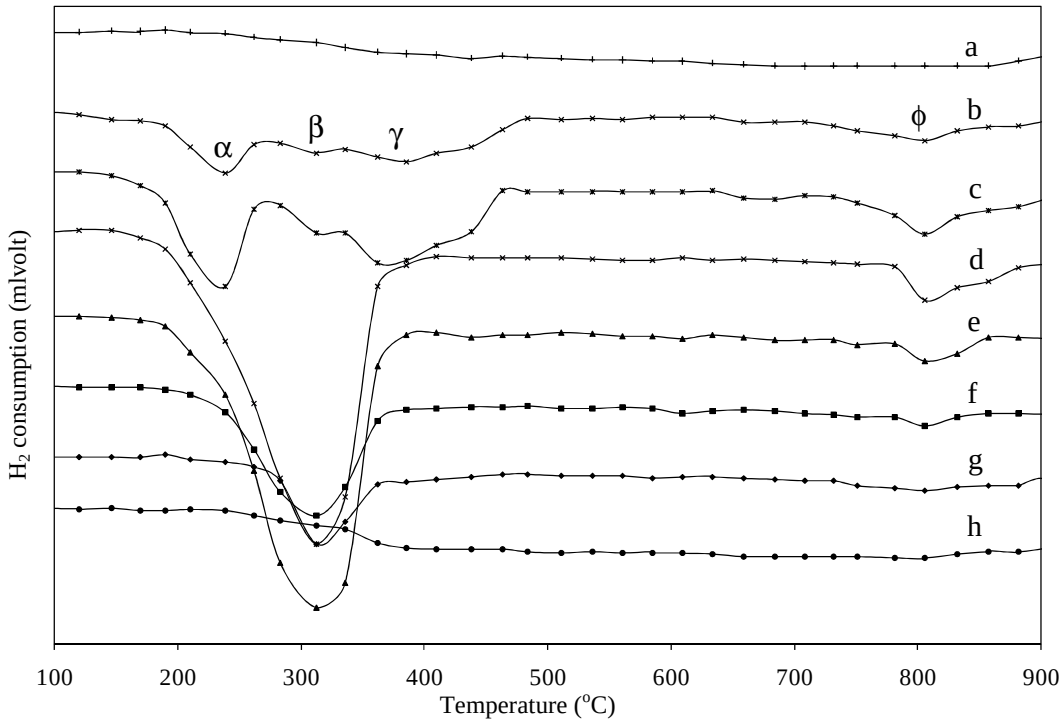

Figure 3-7: TPR of (a) CeO_2, (b) CuO powder for 0h milling and $(CuO)_x(CeO_2)_{1-x}$ powder after 18h milling (x= (c) 1, (d) 0.8, (e) 0.5, (f) 0.3, (g) 0.2, (h) 0)

Figure 3-7 shows the H_2-TPR profiles CeO_2 and CuO powder for 0h milling and various $(CuO)_x$-$(CeO_2)_{1-x}$ powders (x=1, 0.8, 0.5, 0.3, 0.2, 0) after 18h milling. For pure CuO (x=1) the reduction is also characterized by three peaks (α, β, and γ) and ϕ in the range of 200°C-410°C for the former peaks and 780°C-870°C for the latter (Figure 3-7b, 3-7c). On the other hand, only two peaks are observed for smaller CuO contents (Figure 3-7d-7g), and the intensity of both peaks is reduced with decreasing the CuO content. For pure CeO_2 (Figure 3-7a and x=0 of Figure 3-7h) there is no distinguished H_2-TPR peaks observed in the range of the temperatures, while the consumption of H_2 steadily exists above 370°C up to ~900°C for CeO_2 reduction to Ce_2O_3. It has been reported that, the H_2-TPR profile of CuO depends on particle size and surface area of CuO [60]. For the reduction of pure CuO for 0h milling (Figure 3-7b) and after 18h milling (Figure 3-7c), the α peak suggests to the reduction of amorphous CuO clusters, the β peak assigns to the

reduction of larger CuO particle, the γ peak may be attributed to the reduction of CuO bulk, the ϕ peak can be due to volume defects by the recrystallization of Cu in the interaction of SiO_2 of quartz reactor [61]. For the reduction of pure CeO_2 for 0h milling (Figure 3-7a) and after 18h milling (Figure 3-7h), the first is due to the surface defects [58-59] followed by reduction of Ce_xO_{2-x} to Ce_2O_3, where the CeO_2 is completely transformed into Ce_2O_3.

In order to examine the reduction process of milled samples, pure CuO and 80 mol% CuO after 18h milling are chosen to check XRD patterns after TPR stopped at 400°C, 600°C and 900°C. The results showed that, CuO and CeO_2 are reduced to Cu and Ce_2O_3 respectively, no intermediate phase was observed during checked XRD.

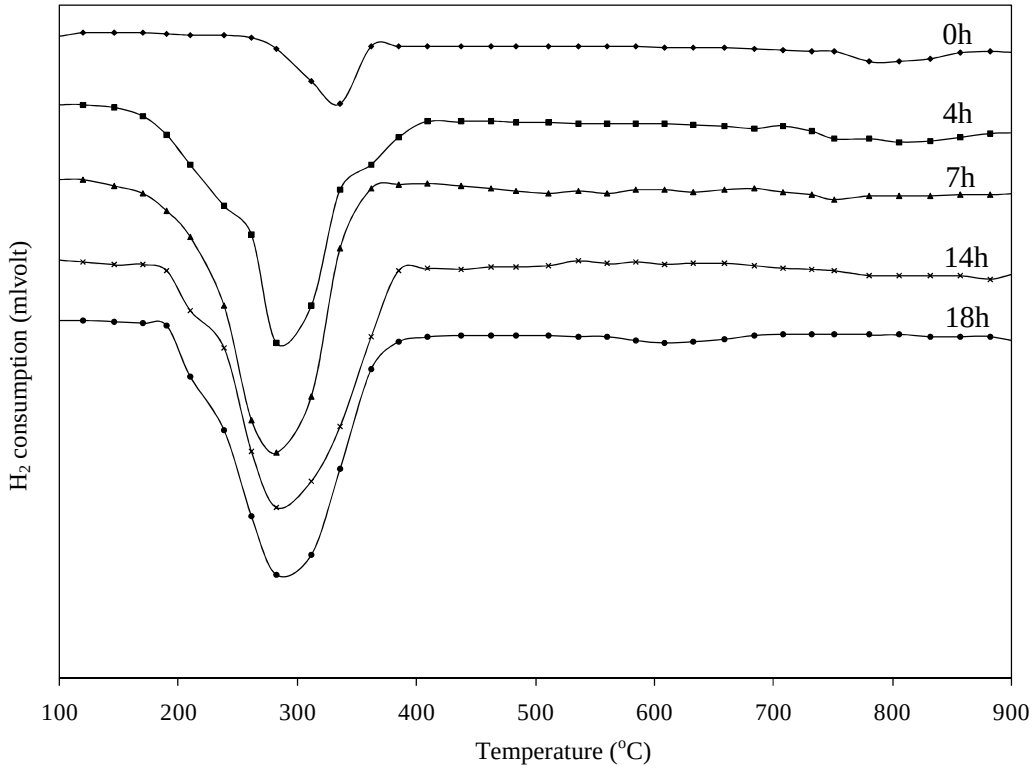

Figure 3-8: TPR of $(CuO)_{0.5}(CeO_2)_{0.5}$ powder with milling time after the first TPR cycle

Figure 3-8 shows the repeated H_2-TPR cycles of milled samples (50 mol% CuO milled for 0, 4, 8, 14 and 18 h) in Figure 3-6, each after the first TPR. The intensity of peak for the 0h milled sample is largely decreased; suggesting agglomeration/recrystallization of

CuO that produces bulk CuO after heating to 1000°C. When increasing the milling time the particles of CeO are finely distributed into the CuO particles, which prevent the recrystallization of CuO, leading to the observed slow decrease in the peak intensity.

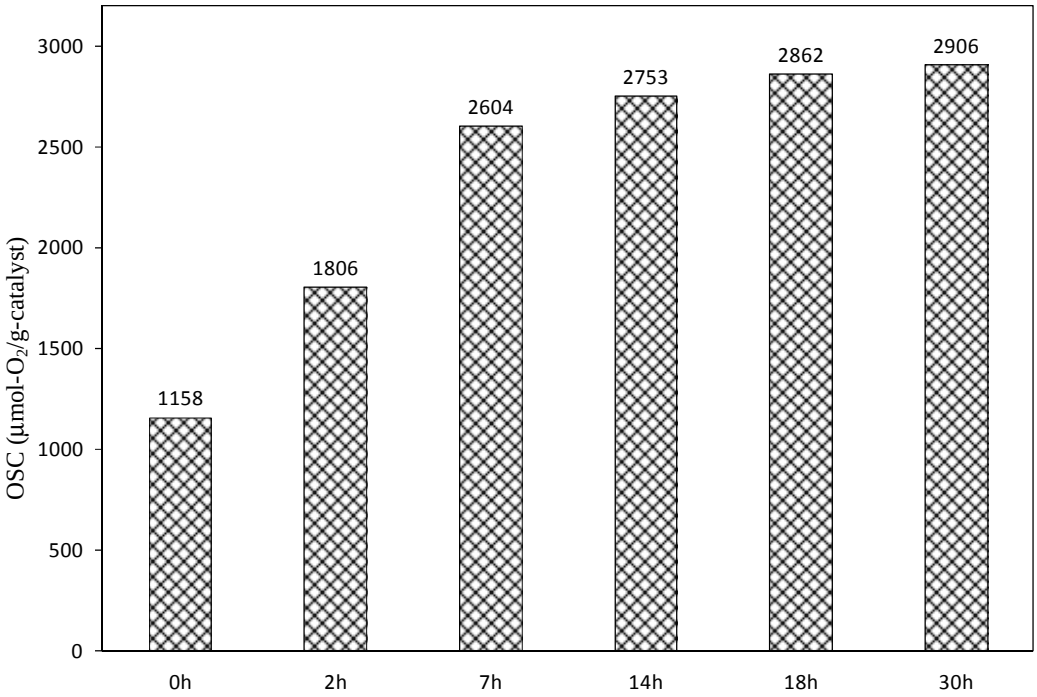

Figure 3-9: Total OSC at 300°C of $(CuO)_{0.5}(CeO_2)_{0.5}$ powder with milling time

Figure 3-9 shows the total OSC at 300°C of various milled samples (50 mol% of CuO) after 0, 4, 7, 14, 18 and 30h milling. The total OSC is increased with milling time, with a rapid increase from 0 to 8h milling followed by the gradual increase from 8h to 30h. The reason for this improvement may be that the CuO introduced into CeO_2 lattice enhances the oxygen storage/transport, since the valence change of $Cu^{2+}/Cu^{+}/Cu$ becomes easier and the number of the available oxygen vacancy is copious with the large powder surface area.

The total OSC at 300°C for the samples milled for 18h increases from 0 to 7094 µmol-O_2/g-catalyst with the increase of CuO content from 0 to 80 mol% but then decreases to 3919 µmol-O_2/g-catalyst for pure CuO (BET surface area was 15-16 $m^2.g^{-1}$). After

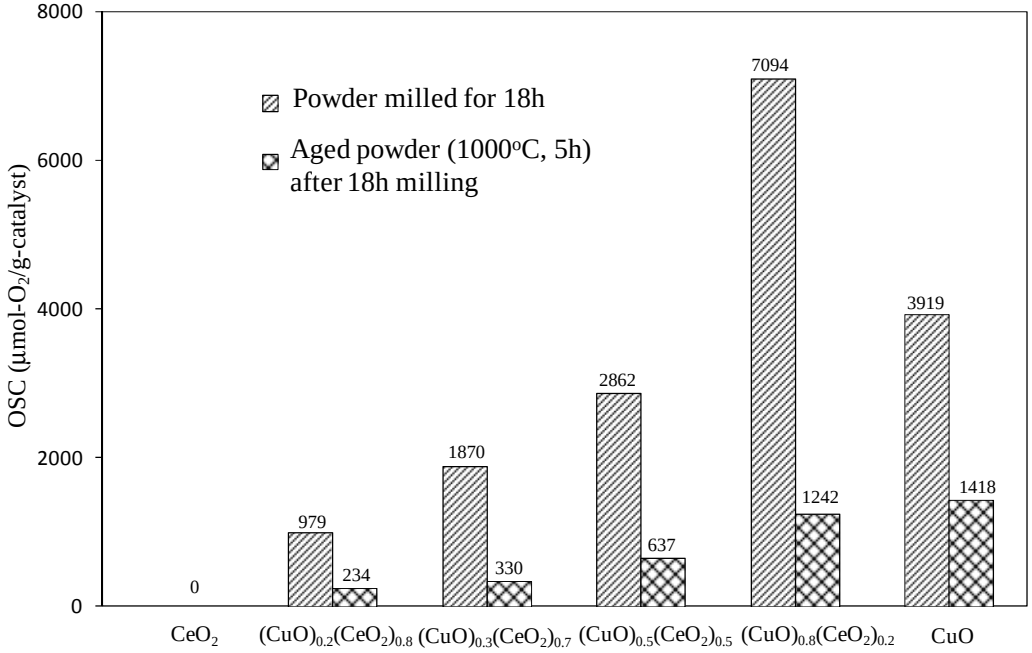

Figure 3-10: Total OSC at 300°C of milled samples for 18h and after aging at 1000°C for 5h

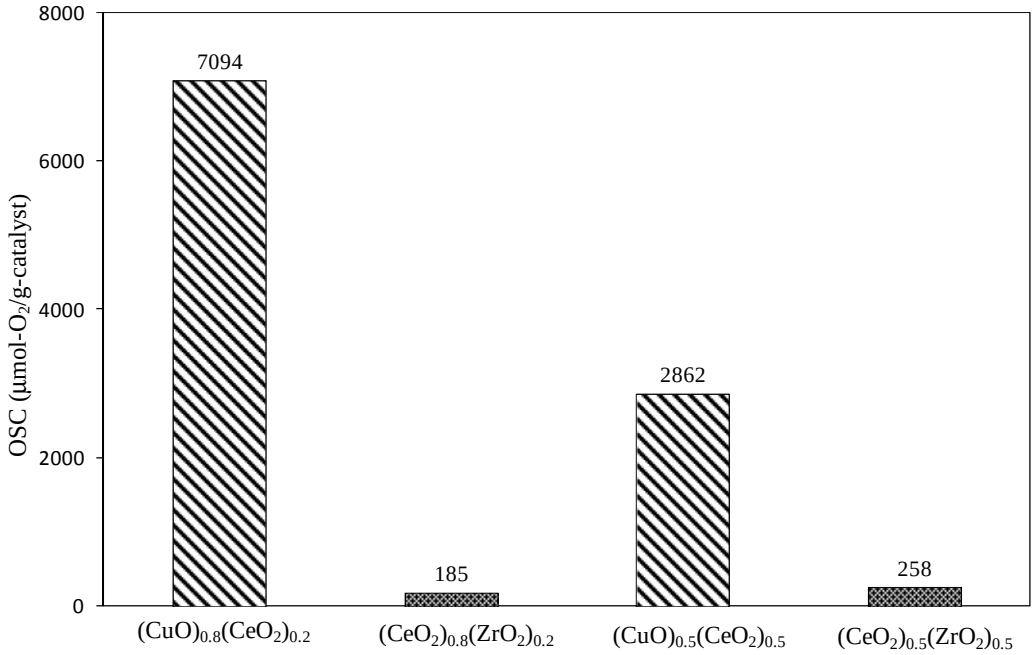

Figure 3-11: Comparison on total OSC at 300 °C of CuO-CeO_2 and CeO_2-ZrO_2 milled powder

ambient aging at 1000°C for 5h, on the other hand, the total OSCs at 300°C significantly reduced (Figure 3-10), probably ascribed to the agglomeration/recrystallization of fine particles.

As shown in Figure 3-11, the total OSCs of the CeO_2-20%ZrO_2 and the CeO_2-50%ZrO_2 at 300°C are 185 and 258 μmol-O_2/g-catalysts, respectively; while that of the $CuO\text{-}CeO_2$ catalyst system prepared in the same way is one order greater. This clearly shows that the mechanically driven $CuO\text{-}CeO_2$ system exhibits the high OSC property, and this should contribute improving the characteristics performance of TWCs at lower temperatures.

3.3 Conclusions

Mechanical milling was applied to the $CuO\text{-}CeO_2$ system to produce mixed-oxide catalysts. The milled sample was characterized by XRD, SEM, TG-DTA, GC-TCD. Milling of mixtures of CuO and CeO_2 showed the reduction of CuO when milling was processed in air. The redox property of milled $CuO\text{-}CeO_2$ sample was investigated by mean of H_2-TPR. Three reduction peaks were observed for 0h milling and only one β-peak for various milling times; the valence change of Cu ions in CuO enhanced the redox activity. The higher OSC of $CuO\text{-}CeO_2$ was observed with the increase of milling time; the total OSC of $CuO\text{-}CeO_2$ catalyst was much higher than the CeO_2-ZrO_2 traditional catalyst system at low temperature.

REFERENCES

[1] Jan Kaspar, Paolo Fornasero, Neal Hickey, Catal today 77(2003) 419-449.

[2] Toshiyuki Masui, Tetsuya Ozaki, Ken-ichi Machida, Gin-ya Adachi, Journal of Alloys and Compounds 303-304 (2000) 49-55.

[3] R.K. Usmen, G.W. Graham, W.L.H. Watkins, R.W. McCabe, Catal. Lett. 30 (1995) 53.

[4] A. Bensalem, F. Bozon-Verduraz, M. Delamar, G. Bugli, App Catal. A 121 (1995) 81.

[5] M. Ozawa, M. Kimura, H. Sobukawa, K.Yokota, Toyota Tech. Rev. 27 (1992) 43.

[6] S. Matsumoto, N. Miyoshi, T. Kanazawa, M. Kimura, M. Ozawa. Catal. Sci. Technol. 1 (1991) 335.

[7] F. Zamar, A. Trovarelli, C. de Leitenburg, G. Dolcetti, Stud. Surf. Sci. Catal. 101 (1996) 1283.

[8] M.Y. Sinev, G.W. Graham, L.P. Haach, M. Shelef, J. Mater. Res. 11 (1996) 1960.

[9] Sumio Kato, Ryu Fujimaki, Masataka Ogasawara, Takashi Wakabayashi, Yuunosuke Nakahara, Shinichi Nakata, Appl. Catal B 89(2009) 183-188.

[10] Liu.W, Flytzani-Stephanopoulos, *J. Catal. (*1995) 153: 304-316.

[11] Luo. M, F. Zhong, Y. J. Yuan, X. Zheng, *Appl. Catal. A.* (1997) 162: 121-131.

[12] Luo. J, Y. Meng, M. Yao, S. Li, X.G. Zha, Y.Q. Wang, X. Zhang, *Catal B:* (2009) *Env*. 87: 92-103.

[13] W. Liu, A.F. Sarofim, M. Flytzani-Stephanopoulos, Appl. Catal. B 4 (1994) 167.

[14] A. Tschope, W. Liu, M. Flytzani-Stephanopoulos, J.Y. Ying, J. Catal. 157 (1995) 42.

[15] T. Zhu, Lj. Kudakovic, A. Dreher, M. Flytzani-Stephanopoulos, Catal. Today 50 (1999) 381.

[16] M. Fernandez-Garcia, E. Gomez Rebollo, A. Guerrero Ruiz, J.C. Conesa, J. Soria, J. Catal. 172 (1997) 146.

[17] P. Bera, S.T. Aruna, K.C. Patil, M.S. Hegde, J. Catal. 186 (1999) 36.

[18] S. Hocevar, J. Batista, J. Levec, J.Catal. 184 (1999) 39.

[19] S. Hocevar, U. Opara Krasovec, B. Orel, A.S. Arico, H. Kim, Appl. Catal. B 28 (2000) 113.

[20] Laberty Robert C, Long JW, Lucas EM, Pettigrew KA, Stroud RM, Doescher MS, Rolison DR (2006) Chem Mater 18:50.

[21] Mai HX, Sun LD, Zhang YW, Si R, Feng W, Zhang HP, Liu HC, Yan CH, J. Physchem B (2005) 109 - 24380.

[22] Zhou KB, Yang ZQ, Yang S, Chem Mater (2007) 19 1215.

[23] Chang HY, Chen HI, J Cryst Growth 283-457.

[24] Scholes FH, Hughes AE, Hardin SG, Lynch P, Miller PR, Chem Mater 19 2321.

[25] Gu FB, Wang ZH, Han DM, Shi C, Guo GS, Mater Sci Eng B 139 62.

[26] Zhang DS, Fu HX, Shi LY, Pan CS, Li Q, Chu YL, Yu WJ, Inorg Chem 46 2446.

[27] Barreca D, Gasparotto A, Maccato C, Maragno C, Tondello E, Langmuir 22 8639.

[28] Bondioli F, Bonamartini Corradi A, Leonelli C, Manfredini T, Mater Res Bull 34 2159.

[29] Yang HM, Huang CH, Tang AD, Zhang XC, Yang WC, Mater Res Bull 40 1690.

[30] Zhou F, Zhao XM, Xu H, Yuan CG J Phys Chem C 111 1651.

[31] G. B. Schaffer and P. G. McCormick, Metall. Trans. 23A, 1285 (1992)

[32] Zazhigalov.V. A, Haber. J, Stoch. J, Bogutskaya.L.V, and Bacherikova.I.V, Appl. Catal. A: Gen. 135-155 (1996).

[33] Mori. S, Xu.W.C, Ishidzuki.T, Ogasawara.N, Imai.J, and Kobayashi.K, Appl. Catal. A: Gen. 137- 255 (1996).

[34] Trovarelli.A, Matteazzi, P. Dolcetti, G.Lutman. A, and Miani. F, Appl. Catal. A: Gen. 95, L9 (1993).

[35] Alessandro Trovarelli, Francesca Zamar, Jordi Llorca, y Carla de Leitenburg, Giuliano Dolcetti, and Janos T. Kiss, journal of catalysis 169, 490-502 (1997).

[36] S. Enzo and F. Delogu, J.Mater. Res, Vol 15 No. 7 (2000).

[37] Hessel L. Castricum, Hans Bakker, Eduard K. Poels, Materials Science and Engineering A304-306 (2001) 418-423.

[38] B.K. Cho, Catal., 1991, vol. 131, P.74.

[39] C.C. Koch and .J.D.Whiittenberger, Intermetallics 4 339 (1996).

[40] T.P. Yadav, O.N.Srivastava, Ceramics International 38 (2012) 5783–5789.

[41] Slavica Zec, Snezana Boskovic, Branka Kaluderovic, Zarko Bogdanov, Nada Popovic, Ceramics International 35 (2009) 195-198.

[42] S.Zec, S. Boskovic, journal of materials science 39 (2004) 5283-5286.

[43] Sameer Deshpande, Swanand Patil, Satyanarayana VNT Kuchibhatla, Sudipta Seal, Appl. Phys. Lett. 87, 133113 (2005).

[44] Feng Zhang, Siu-Wai Chan, Jonathan E. Spanier, Ebru Apak, Qiang Jin, Appl. Phys. Lett. 80, 127 (2002).

[45] Meng-Fei Luo, Jing-Meng Ma, Ji-Qing Lu, Yu-Peng Song, Yue-Juan Wang, Journal of catalysis 246 (2007) 52-59.

[46] Xianqin Wang, José A. Rodriguez, Jonathan C. Hanson, Daniel Gamarra, Arturo Martínez-Arias, Marcos Fernández-García, J. Phys. Chem. B 2005, 109, 19595-19603.

[47] D. Gamarra, G. Munuera, A. B. Hungrı´a, M. Ferna´ndez-Garcı´a, J. C. Conesa, P. A. Midgley, X. Q. Wang, J. C. Hanson, J. A. Rodrı´guez, A. Martı´nez-Arias, J. Phys. Chem. C 2007, 111, 11026-11038

[48] Y. Li, Q. Fu, M. Flytzani-Stephanopoulos, Appl. Catal. B Environ. 27 (2000) 179.

[49] W. Liu, M. Flytzani-Stephanopoulos, Chem. Eng. J. 64 (1996) 283.

[50] L. Kundakovic, M. Flytzani-Stephanopoulos, Appl. Catal. A Gen. 171 (1998) 13.

[51] M. Luo, Y. Zhong, X. Yuan, X. Zheng, Appl. Catal. A Gen. 162 (1997).

[52] J. Xiaoyuan, L. Guanglie, Z. Renxian, M. Jianxin, C. Yu, Z. Xiaoming, Appl. Surf. Sci. 173 (2001) 208.

[53] P. Bera, K.R. Priolkar, P.R. Sarode, M.S. Hegde, S. Emura, R. Kumashiro, N.P. Lalla, Chem. Mater. 14 (2002) 3591.

[54] J. Wang, D. Tsai, T. Huang, J. Catal. 208 (2002) 370.

[55] G. Wrobel, C. Lamonier, A. Bennani, A. D'Huysser, A. Aboukais, J. Chem. Soc., Faraday Trans. 92 (1996) 2001.

[56] S. Zhang, W. Huang, X. Qiu, B. Li, X.Zheng, S. Wu, Catal. Lett. 80 (2002) 41.

[57] X. Tang, Baocai Zhang, Yong Li, Yide Xu, Qin Xin, Wenjie Shen, Appl Catal. A Gen 288 (2005) 116-125.

[58] A. Pintar, J. Batista, S.Hocevar, Journal of Colloid and Interface Science 285 (2005) 218-231.

[59] J.Z. Shyu, W.H. Weber, H.S. Gandhi, J. Phys. Chem 92 (1988) 17.

[60] G. Fierro, M. Lo Jacono, M. Inversi, P. Porta, R. Lavecchia, F. Cioci, Journal of Catalysis 148 (1994), 709-721.

[61] Xinyan Yan, Y.A. Chang, Journal of Alloys and Compounds 308 (2000) 221–229

CHAPTER 4

Structure and adhesion properties of $CuO\text{-}CeO_2/\gamma\text{-}Al_2O_3$ on metallic substrate for automotive catalytic converter

4.1 Introduction

TWCs converters have been used in vehicles to control gas emission to be innoxious. The TWCs consist of a honeycomb ceramic support or recently a metal sheet as a substrate, a $\gamma\text{-}Al_2O_3$ washcoat layer on the substrate with high surface area and thermal stability and oxygen storage layer with NMs on the washcoat layer. Since a TWCs functions only when an engine is operating under a narrow region of air-fuel ratios near stoichiometry, the oxygen storage layer plays an important role to keep appropriate oxygen level; thus, the OSC is generally used as an indicator of TWCs.

It was found in 1980s that a zirconia-ceria ($ZrO\text{-}CeO_2$) compound shows remarkably high OSC. However, to cope with increasingly strict exhaust emission regulation, it is required to further improve the efficiency of TWCs. That is, to achieve even higher OSC at low temperatures and/or under oxygen-rich environment. Reuse et al have focused on CuO-based catalysts coated on Fe-Cr-Al substrate by a suspension method [9]. Bravo et al. have

used $CuO/ZnO\text{-}Al_2O_3$ coated on silica substrate [10]. And recently, copper-ceria oxide compound ($CuO\text{-}CeO_2$) treated by means of high energy mechanical milling has been found to promote OSC by authors [8].

Besides OSC, other important characteristics must be considered when developing a new material for TWCs; for example, the adhesiveness between the developed material and the washcoat is one of important factors. In this sense, many preparation methods such as sol-gel and suspension methods have been investigated [1, 2]. However, besides Agragiols et al. whom reported the effect of particle sizes on the adhesion with alumina, zirconia and titania washcoats deposited on the honeycomb ceramic [3-7], only a few studies overcame the problem of adhesion between the washcoat and the substrate or between the oxygen storage layer and the washcoat.

In this study, thus far, we introduced a hybrid preparation method between the suspension and the sol-gel method [1, 11] incorporating with a mechanical milling, and it showed good properties for TWCs preparation. However, it is not evaluated yet what parameters play important role for TWCs preparation. Thus, in this chapter we investigate the optimum way to prepare a $\gamma\text{-}Al_2O_3$ washcoat layer on a metallic substrate and a $CuO\text{-}CeO_2$ layer on the $\gamma\text{-}Al_2O_3$ coated metallic substrate.

$CeO_2\text{-}ZrO_2$ layer on the $\gamma\text{-}Al_2O_3$ coated metallic substrate was also prepared through a hybrid method, in order to compare its catalytic performance with NMs coated on $CuO\text{-}CeO_2$ and NMs coated on $\gamma\text{-}Al_2O_3$.

4.2 Results and discussion

4.2.1 $\gamma\text{-}Al_2O_3$ washcoat

4.2.1.1 Coating load

Figure 4-1 show the effect of withdrawal speed on the coating load, where the water content in the slurry, H_2O/Al_2O_3 (w/w), is 1.4 (g/g). The coating load rapidly increases with increasing the withdrawal velocity up to 0.5 mm/sec, and followed by near-plateau. Figure

4-2 shows the relationship between the coating load after sintering and the water content (H_2O/Al_2O_3), where the withdrawal speed is 0.8 mm/sec. It is found that the coating load increases with decreasing the water content, and they fall into decline at lower water contents than about 0.8 g/g of H_2O/Al_2O_3 (Figure 4-2). The maximum value may be ascribed to the decrease in strength due to cracks and the increase in binding strength, which occur at lower water contents.

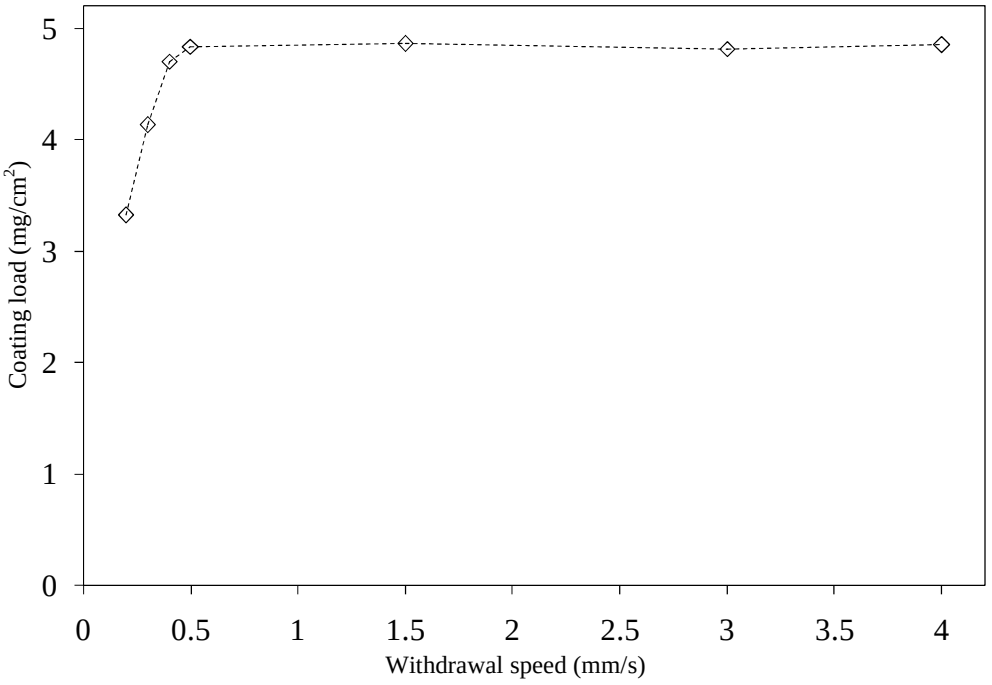

Figure 4-1: Effect of withdrawal speed on the coating load of $\gamma\text{-}Al_2O_3$/substrate, the Al_2O_3 slurry was stirring for 8h, H_2O/Al_2O_3 (w/w) = 1.4 g/g

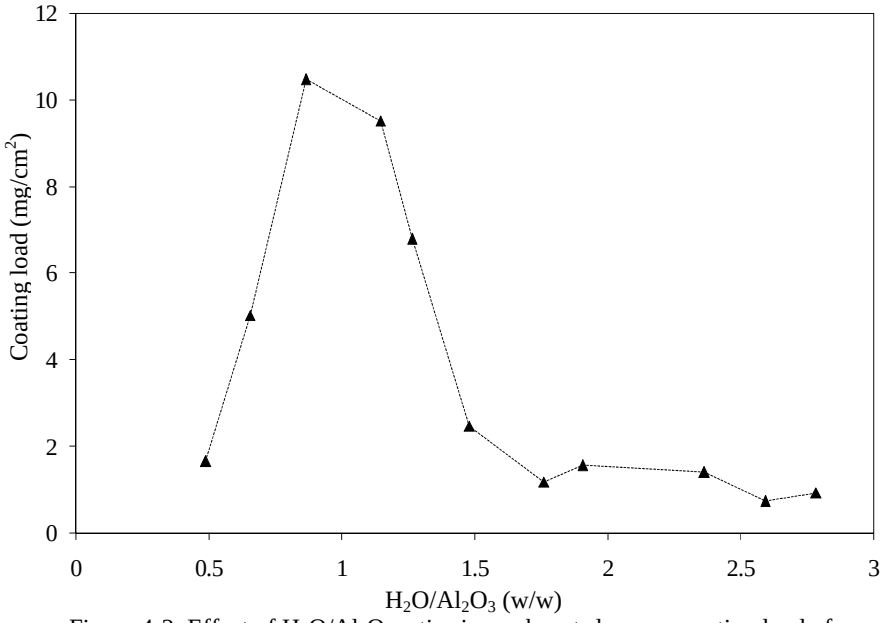

Figure 4-2: Effect of H_2O/Al_2O_3 ratios in washcoat slurry on coating load of γ-Al_2O_3/substrate, the Al_2O_3 slurry was stirring for 8h

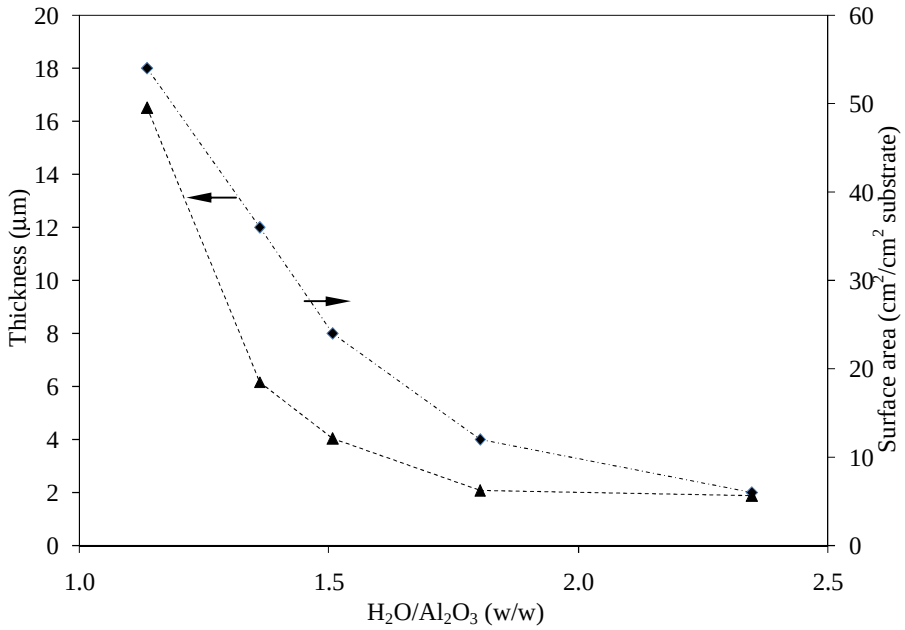

Figure 4-3: Effect of H_2O/Al_2O_3 ratios in washcoat slurry on surface area and thickness of γ-Al_2O_3/substrate, the Al_2O_3 slurry was stirring for 8h

4.2.1.2 Thickness and surface area

Figure 4-3 shows the thickness and surface area of γ-Al_2O_3 washcoat layer after the sintering process as a function of H_2O/Al_2O_3 ratio. The thickness and surface area of γ-Al_2O_3 washcoat increased with decrease of H_2O/Al_2O_3 ratios from 2.3 to 1.2 (g/g). It has been reported that, γ-Al_2O_3 is a materials which have high porous structure [1], so the acceleration of surface area of γ-Al_2O_3 was observed, this is a more evidence for surface area improvement supported by γ-Al_2O_3.

4.2.1.3 Adhesion properties

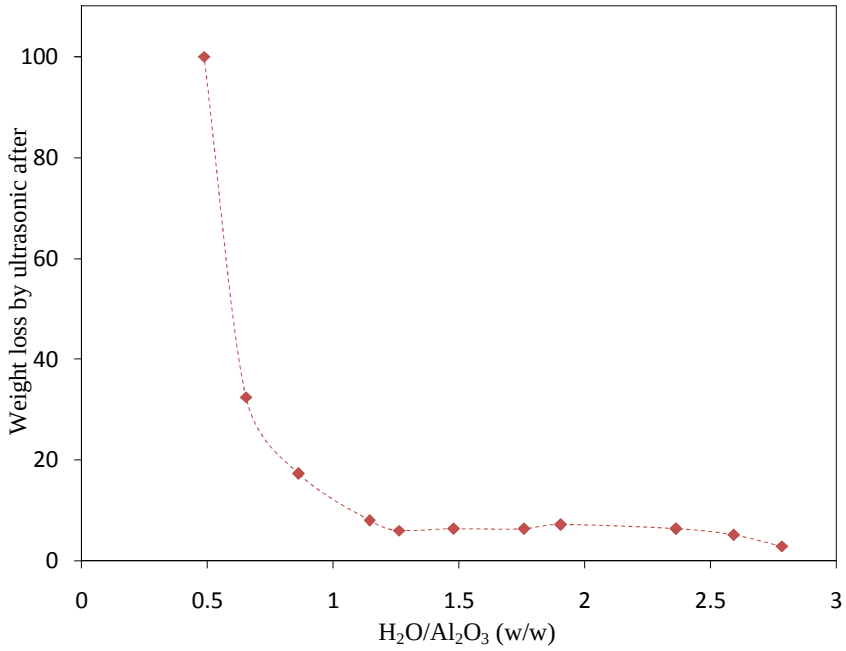

Figure 4-4: Effect of H_2O/Al_2O_3 ratios in washcoat slurry on weight loss of γ-Al_2O_3/substrate, the Al_2O_3 slurry was stirring for 8h

Figure 4-4 shows the effect of the H_2O/Al_2O_3 ratio on the weight loss by the ultrasonic treatment. When the H_2O/Al_2O_3 ratio is 0.5 g/g, almost the entire washcoat layer is removed. With increasing H_2O/Al_2O_3 ratios, however, the weight loss drastically decreases. The reason for this is that, at a high H_2O/Al_2O_3 ratio, the coating load is small, and the binder promoted the adhesion of γ-Al_2O_3 powders together and of γ-Al_2O_3 powders

to surface of FeCrAl substrate, so the good adhesion of γ-Al_2O_3 washcoat was observed. On the other hand, smaller H_2O/Al_2O_3 ratios lead to the increase of coating load; however when the increase of coating load over the limit of binding force between γ-Al_2O_3 powders and binder together, so the sample layer is cracked and broken as soon as the samples are dried so the cracks is also main reason for poor adhesion.

4.2.1.4 Structure and morphological

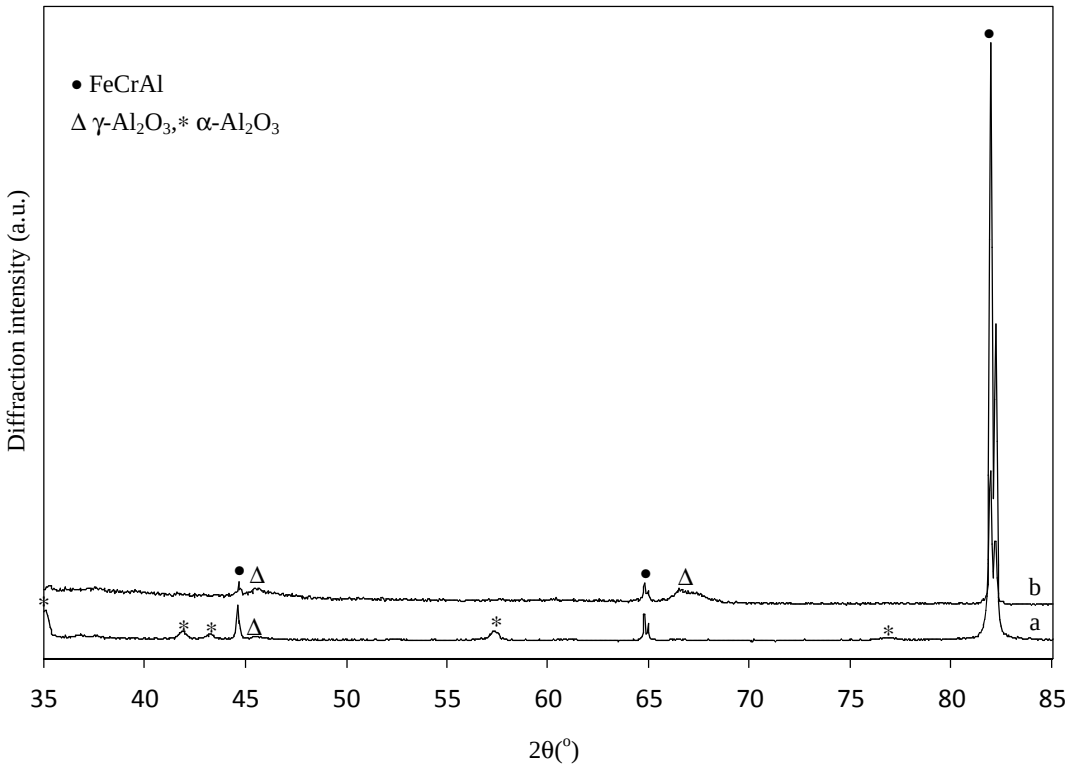

Figure 4-5: XRD patterns of (a) FeCrAlloy after pre-oxidation at 900°C for 10h; (b) γ-Al_2O_3 coated on FeCrAlloy substrate

XRD patterns of the substrate and γ-Al_2O_3 washcoat after the sintering were shown in Figures 4-5a, and 4-5b, respectively. It is found that γ-Al_2O_3 and α-Al_2O_3 (Figure 4-5a) are formed on the substrate, which may support the good contact with γ-Al_2O_3 washcoat layer. SEM photographs of the initial state of γ-Al_2O_3 powder are shown in Figure 4-6a. It can be seen that, the powder is in a form of agglomerate with the size of about ten micrometers. The mixture of initial γ-Al_2O_3 powders, binder and water were stirred for 8h, the result

showed that the agglomerate particles of γ-Al_2O_3 in the slurry broke down with the dimension in the range from 47 nm to 49 nm (checked by Zeta potential analyzer). After dip-coating and sintering, the finer batcher of the particles of γ-Al_2O_3 on washcoat can be seen (Figure 4-6b). Compared with the initial γ-Al_2O_3 powder, the agglomerate particles of γ-Al_2O_3 washcoat are more regular with dimensions of about 1μm (Figure 4-6b).

4.2.2 $CuO\text{-}CeO_2$ coating layer

The results of preliminary experiments for the preparation of a γ-Al_2O_3 washcoat layer, the coating load does not changes when the withdrawal speed ranges from 0.5 to 4 mm/sec (H_2O/Al_2O_3 (w/w) is 1.4 g/g), the speed was set as 0.8 mm/sec in this study. Under these experimental conditions, the coating load, thickness and surface area of the layer were measured to be 5 mg/cm^2, 10 μm and 11-13 cm^2/cm^2 substrates. Also good adhesion between the γ-Al_2O_3 washcoat layer and the treated metallic substrate was observed. Finally, in this study, the $CuO\text{-}CeO_2$ layer will be coated on the γ-Al_2O_3 washcoat layer.

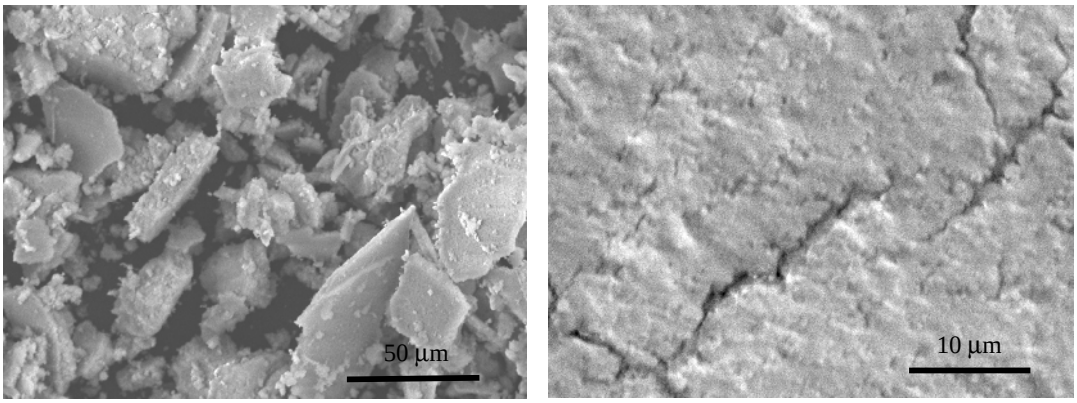

(a) (b)

Figure 4-6: SEM photographs of (a) commercial γ-Al_2O_3 powder; (b) γ-Al_2O_3 washcoat layer after sintering

4.2.2.1 Results

Coating load

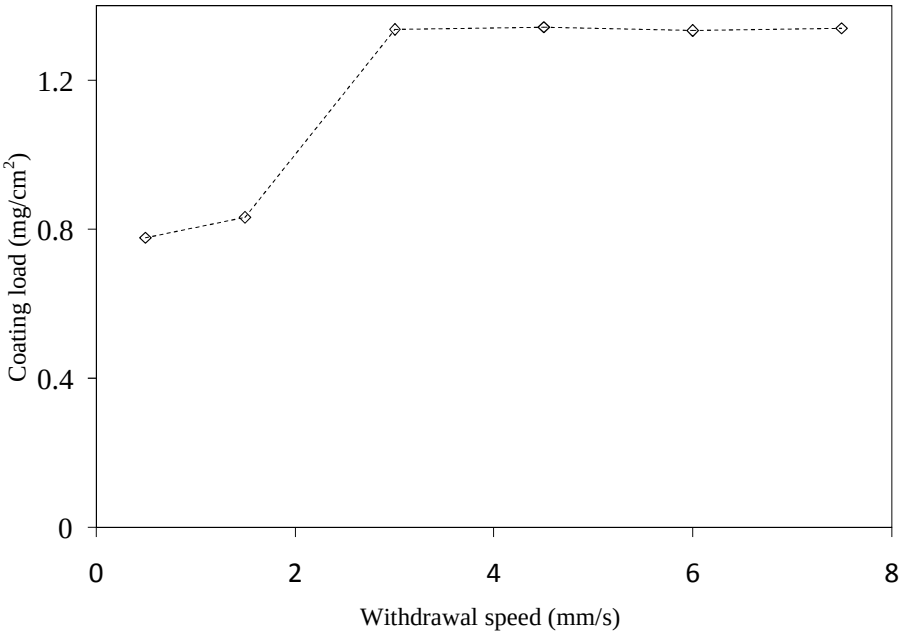

Figure 4-8: Effect of withdrawal speed on the coating load, where $CuO\text{-}CeO_2$ slurry is vigorously stirred for 8h at $H_2O/CuO\text{-}CeO_2$ (w/w) = 2.7 g/g

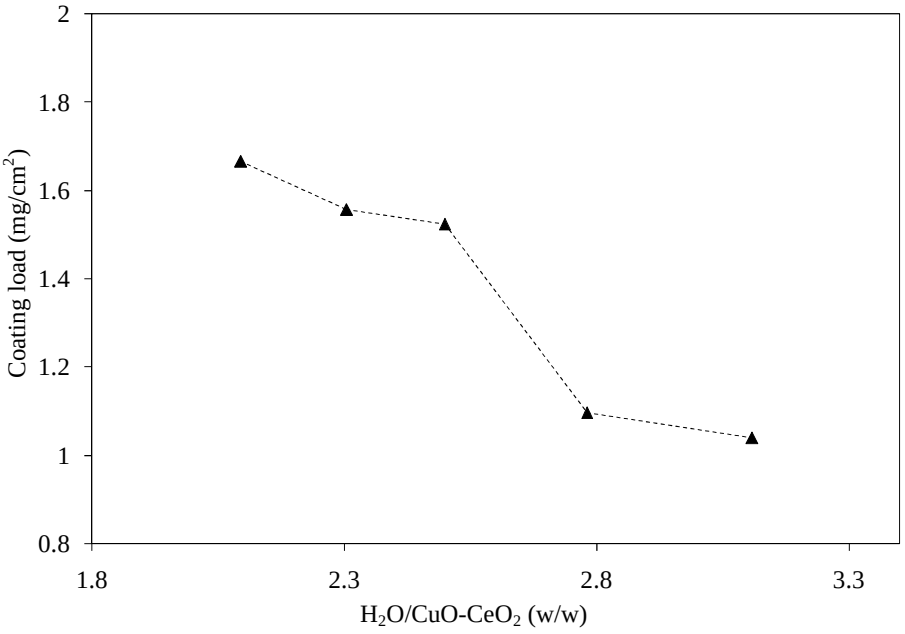

Figure 4-7: Effect of H_2O content in the $CuO\text{-}CeO_2$ slurry on the coating loads, where the $CuO\text{-}CeO_2$ slurry is vigorously stirred for 8h

Figure 4-7 shows the effect of withdrawal speed on the coating load of $CuO\text{-}CeO_2$

layer, where $H_2O/CuO\text{-}CeO_2$ (w/w) ratio is fixed to be 2.7 (g/g). The coating load increases with increasing the withdrawal speed up to 3 mm/sec, followed by near-plateau. Thus, hereafter the withdrawal speed is set to be 6.5 mm/sec. As for the effect of water content, the coating load monotonously increases with decreasing the water content as shown in Figure 4-8. This is due to $H_2O/CuO\text{-}CeO_2$ ratios from 2.1 to 3.1 (g/g).

Thickness and surface area

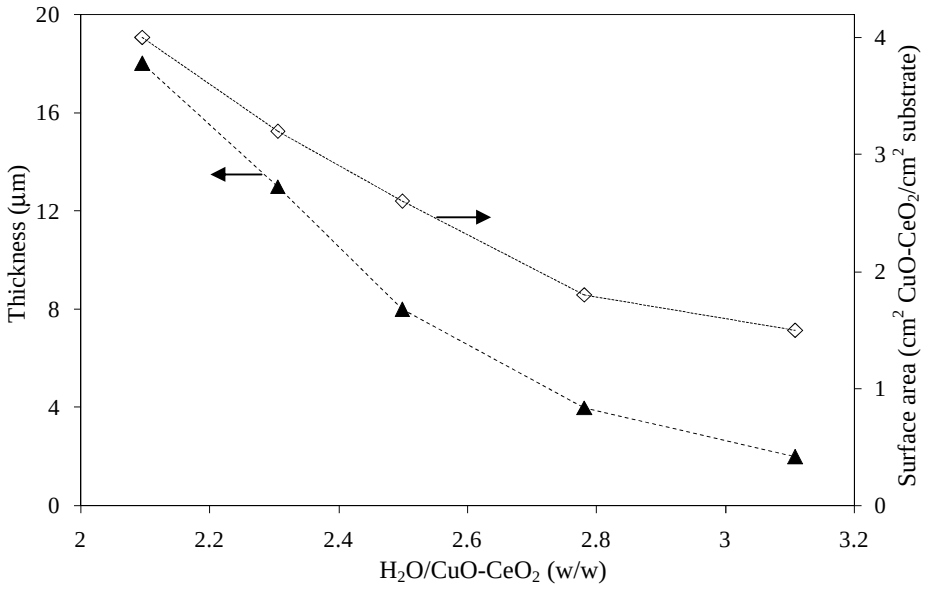

Figure 4-9: Effect of H_2O content in the $CuO\text{-}CeO_2$ slurry on the thickness and surface area, where the $CuO\text{-}CeO_2$ slurry is vigorously stirred for 8h

The surface area and thickness of the $CuO\text{-}CeO_2$ layer after the sintering decrease with the increase of the $H_2O/CuO\text{-}CeO_2$ ratio from 2.1 to 3.1 (g/g) as shown in Figure 4-9. This result indicates that the $CuO\text{-}CeO_2$ layer is porous. If the layer is not porous, the surface area must be constant regardless of the thickness.

Adhesion property

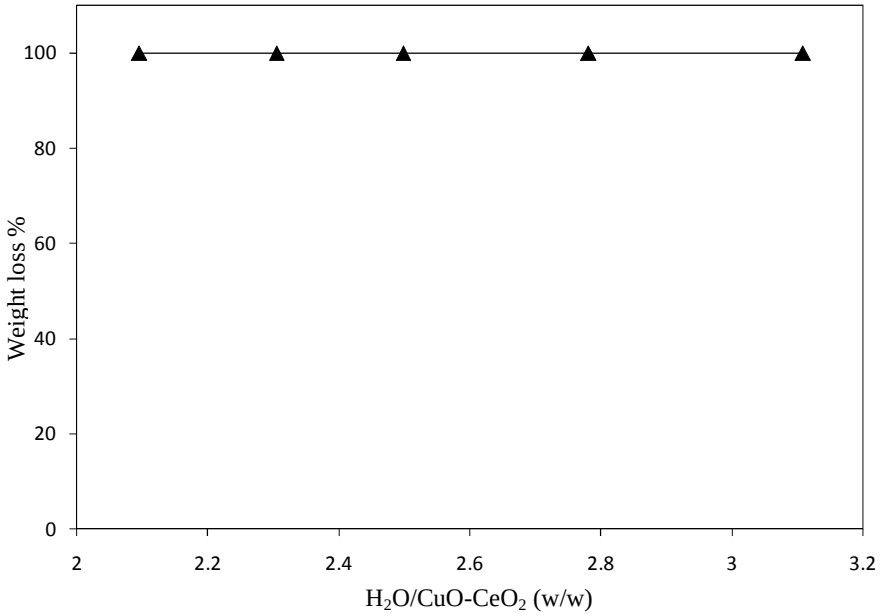

Figure 4-10: Effect of H_2O content in the $CuO\text{-}CeO_2$ slurry on adhesion, the $CuO\text{-}CeO_2$ slurry was stirring for 8h

The adhesiveness of the $CuO\text{-}CeO_2$ layer without slurry-milling is quite poor (Figure 4-10) in the range of $H_2O/CuO\text{-}CeO_2$ ratios from 2.1 to 3.1 (g/g). Even at a higher sintering temperature (900^{o}C for 5 h or 10 h), it is not improved, which appears inconsistent with the reported results [2, 12]. However, when the mechanical milling of slurry (with a $H_2O/CuO\text{-}CeO_2$ ratio of 2.7 and a 23-wt% binder) is performed instead of stirring, the adhesiveness considerably improved, shown in Figure 4-11. Figure 4-12 shows the relationship between the weight loss and the water content in the slurry milled for 48h. Three is a clear transition from poor adhesion to good adhesion at around 2.5 of the $H_2O/CuO\text{-}CeO_2$ ratio. That is, the adhesive property is quite poor (weight loss of 100%) at lower water contents, however, it is drastically improved when the water content is over ~2.5 w/w.

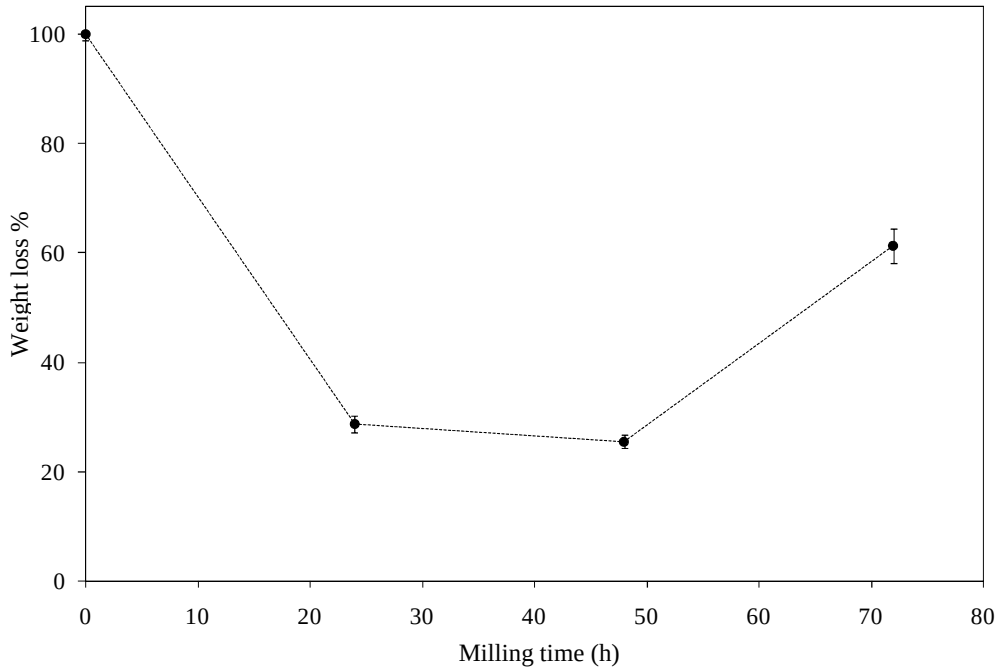

Figure 4-12: Relation between the weight loss and the milling times of CuO-CeO_2 slurry. The samples are dip-coated in the milled CuO-CeO_2 slurry, followed by sintering at 650°C for 2.5 h, where the H_2O/CuO-CeO_2 (w/w) ratio = 2.7 g/g

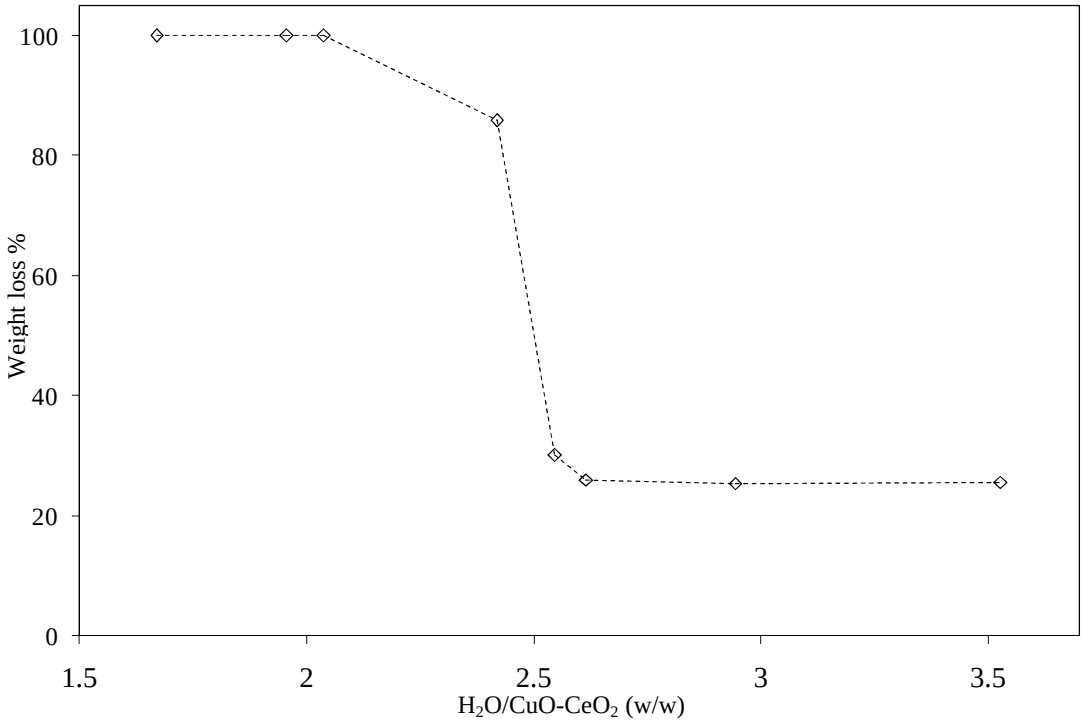

Figure 4-11: Effect of H_2O content in the CuO-CeO_2 slurry on adhesiveness. The slurry was milled for 48 h, and the sintering was at 650°C for 2.5 h

4.2.2.2 Discussions

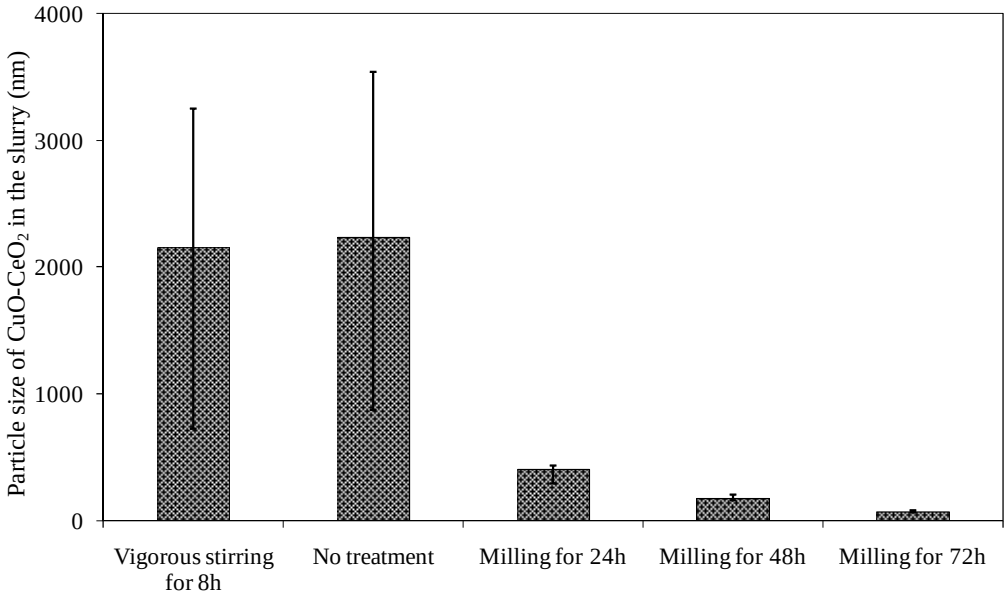

Figure 4-13: Particle size of $CuO\text{-}CeO_2$ in the slurry after vigorous stirring for 8h, no treatment, slurry milling for 24, 48 or 72 h

In this section, the effect of mechanical milling of slurry on the properties of adhesion will be discussed. Figure 4-13 shows the particle size in the $CuO\text{-}CeO_2$ slurry for various mixing conditions. It is found that the particle size is significantly reduced with the slurry milling, and that the longer the milling time is the smaller the particle size becomes, exhibiting rather homogeneous distributions. The stirring process hardly contributes to the reduction in particle size. Figure 4-14 shows cross-sectional SEM images of the layered catalyst samples after sintering at 650^{o}C for 2.5h, where the slurry milling was performed with various milling times. When no milling is given to the slurry (Figure 4-14a), the particles appear often agglomerated with irregular morphology, where the coarser particles of agglomerates (of size between 5 and 10 μm) are spread on the $\gamma\text{-}Al_2O_3$ washcoat surface, leading to poor adhesion between the two layers (0 h milling time in Figure 4-11). With increasing the milling time, however, the particles become finer with homogeneous size distributions (Figure 4-14b and 4-14c), where they appear interlocked with each other

exhibiting tighter packing. The fine particles are densely spread on the γ-Al_2O_3 washcoat surface, which should lead to better adhesion between two layers (Figure 4-11). This is consistent with the report by Agrafiotis and Tsetsekou [8] in that the adhesion depends both on the extent of mechanical anchorage as well as on the attractive forces exerted among the particles in each layer. It is also reasonable that the reduction in the particle size would have accelerated the sintering process even at the relatively low temperature (650^{o}C).

It is also quite interesting that the so-called "over-milling" effect is found even in our hybrid slurry-milling system. Although the delamination weight loss is improved up to 48 h of milling time, it becomes worse after 72 h of milling (Figure 4-11), despite the fine

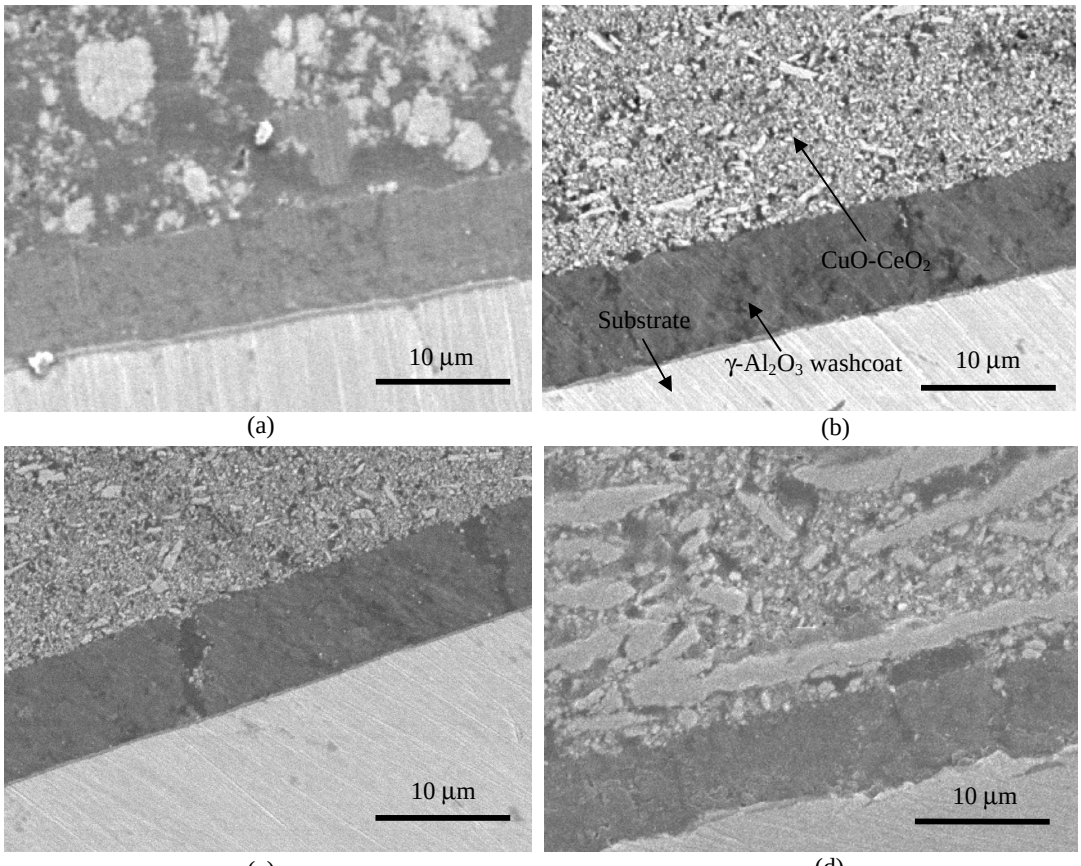

Figure 4-14: SEM images of three-layered structure consisting of CuO-CeO_2/γ-Al_2O_3 washcoat/FeCrAl substrate sintered at 650^{o}C for 2.5 h, for various milling periods of CuO-CeO_2 slurry ((a) 0 h, (b) 24 h, (c) 48 h, (d) 72 h)

particle size (60-80 nm, Figure 4-13). The large surface area and the densely populated defects involving the large strains stored are the natural driving force for necking the particles and increasing the particle sizes, respectively, during the sintering process. As shown in Figure 4-14d, the sintered $CuO\text{-}CeO_2$ layer milled for 72h is clearly different from those milled for shorter periods. The elongated powder morphology strongly suggests that such a longer time of milling is excessive and causes re-agglomeration of the small particles, followed by their rearrangement, necking and growth during sintering, leading to the appearance of the "over-milling" phenomenon.

Even employing the mechanical milling for the slurry, the adhesion property is not improved for the lower water contents, as shown in Figure 4-12. In order to avoid delamination during sintering the homogeneous particle size distribution as well as the homogeneous dispersion in the binder are required, and the polarity of water molecules plays a significant role on both. The sharp transition of the adhesion property (i.e. drastic change of weight loss) strongly suggests that even a small inhomogeneity in the layer is disastrous during sintering, where the inhomogeneous local strain would cause the local delamination around a singular point, propagating toward the entire coated layer during sintering. The delaminated layer with fine cracks at the smaller $H_2O/CuO\text{-}CeO_2$ ratios is observed with SEM as soon as the samples are dried, and the cracks around the inhomogeneity are thus the possible main reason for the poor adhesion.

The contaminations from the milled media (ZrO_2 balls and a steel vial) are also examined by EDX. The Fe and ZrO_2 contaminations in the $CuO\text{-}CeO_2$ samples are 1.2 wt% and 0.2 wt%, respectively, as the maximum value with the milling time of 72h.

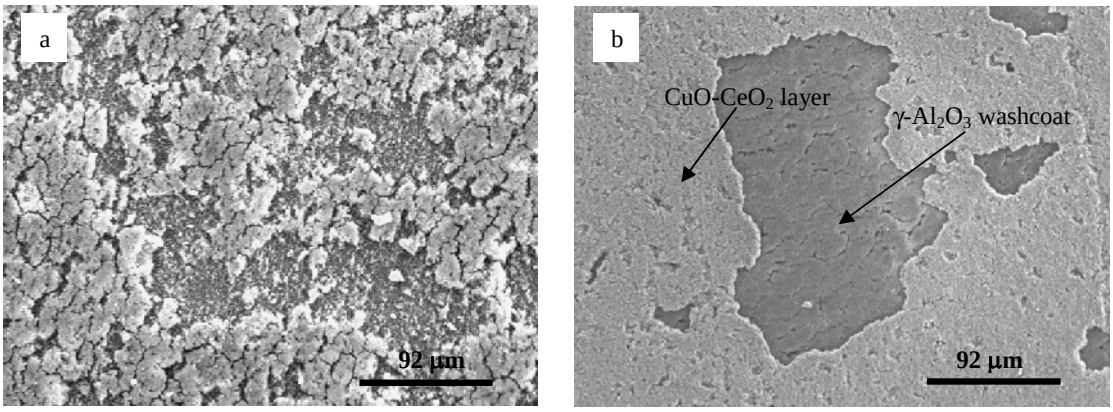

Figure 4-15: The surface morphology of $CuO\text{-}CeO_2$ layer coated on Al_2O_3 washcoat sintered at 650°C for 2.5 h after adhesion testing in ultrasonic vibration, where the $CuO\text{-}CeO_2$ slurry was milled for (a) 48h and (b) 72h.

Figure 4-15 shows, with use of SEM, the rather macroscopic surface morphology of the $CuO\text{-}CeO_2$ layer coated on Al_2O_3 washcoat after adhesion testing of ultrasonic vibration. When the $CuO\text{-}CeO_2$ slurry is milled for 48h (Figure. 4-15a), there appear smaller particles or some aggregates of smaller particles of $CuO\text{-}CeO_2$ falling off from the surface after adhesion testing, while rather large patches of densely sintered $CuO\text{-}CeO_2$ layer fall off when milled for 72h (Figure. 4-15b), *i.e. "overmilling"*. This is consistent with the above discussion in that the accumulated strains on the layer can be easily accommodated by losing smaller aggregates when the $CuO\text{-}CeO_2$ particles are small (the former case), while the densely sintered layer containing some elongated particles cannot accommodate the mismatch strain induced during sintering between the substrate Al_2O_3 washcoat layer and the $CuO\text{-}CeO_2$ catalytic layer. Such a "distinguished" layered structure cannot endure the vigorous adhesion testing of ultrasonic vibration, providing large momentum on the larger particles, which should result in the observed "over-milling" weight loss.

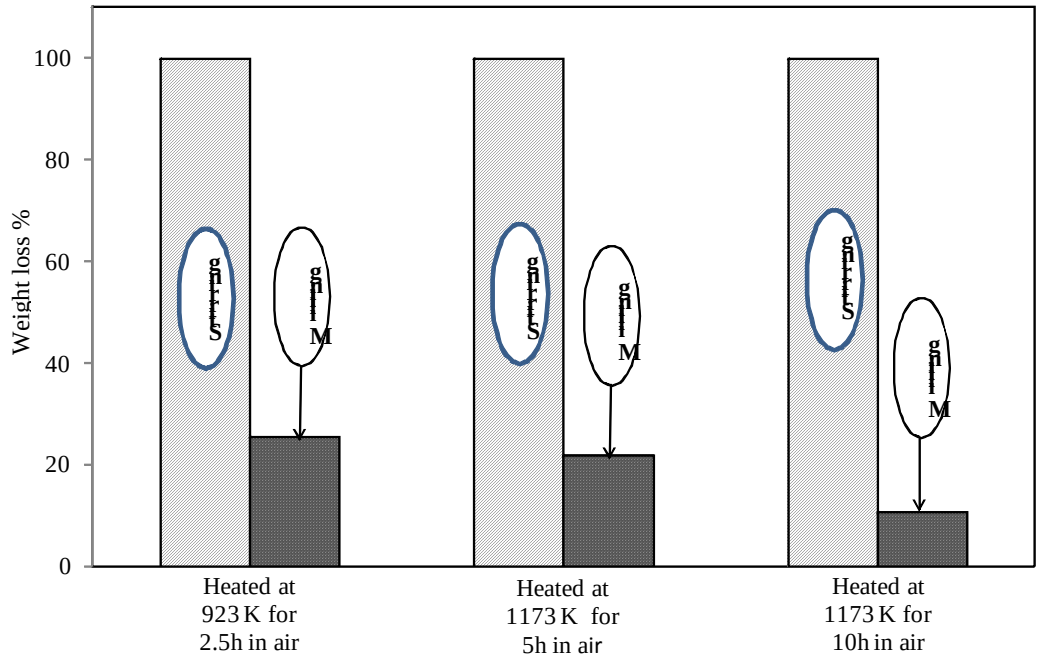

Figure 4-16: Adhesiveness evaluation of CuO-CeO_2 layer on Al_2O_3 washcoat for various heat treatment conditions, where the CuO-CeO_2 slurry was vigorously stirred for 8 h and milled for 48 h

It should be noted that, when the sintering temperature is increased from 650°C to 900°C (both treated for 5h), the adhesive property is slightly improved, and when the sintering duration is increased from 5 h to 10 h (both treated at 900°C) the property is nearly twice improved, only for the milled samples (Figure 4-16). The improvement is not observed for the samples without milling of slurry. The possible reason is that, since the mechanical milling contributes the reduction in particle size and thus the increase the contact area during sintering among particles, the thermal energy of sintering drives the particle growth to reduce the high surface energy of small particles, homogeneously covering the substrate. The existence of "over-milling" and elongated particles evidences such a mechanism, though it appears there is an epitaxial growth of the sintered layer inherent from the strain or the texture of the substrate. Thus, the slurry milling is highly effective for the adhesion property of the CuO-CeO_2 layer on the Al_2O_3 washcoat layer.

The good adhesion is also reported by S.H. Zeng et al [13] for the CuO-CeO_2/Al_2O_3/FeCrAl system prepared by a sol-pyrolysis method.

4.3 Conclusion

Adhesion properties of CuO-CeO_2/γ-Al_2O_3 layers on FeCrAl metallic substrate were investigated, where the hybrid preparation method between suspension and sol-gel is further combined with a mechanical milling process of the slurry. Poor coating adhesion was observed when the slurry is vigorously stirred, where the milled powders are agglomerated and the stirring process hardly reduces the particle size. The combined method is found to significantly improve the adhesion property between the milled CuO-CeO_2 catalytic layer and the γ-Al_2O_3 washcoat, compared with the vigorous stirring of the slurry. The so-called “over-milling” phenomenon is also exhibited, where the elongated large particles are observed after sintering of the longer-milled powders, leading to the lowered adhesion quality.

REFERENCES

[1] T. Masui, T. Ozaki, K. Machida, G. Adachi, Preparation of ceria–zirconia sub-catalysts for automotive exhaust cleaning Adachi, Journal of Alloys and Compounds 303-304 (2000) 49-55J.

[2] P. Reuse, P. Tribolet, L. Kiwi-Minsker, A. Renken, in: M.E. Baselt, Microreaction Technology. IMRET 5: Proceedings, Springer, 2001, pp. 322–331.

[3] J. Bravo, A. Karim, T. Conant, G.P. Lopez, A. Datye, Wall coating of a CuO/ZnO/Al2O3 methanol steam reforming catalyst for micro-channel reformers, Chem. Eng. J. 101 (2004) 113–121.

[4] Nguyen The Luong, Eiji Yamasue, Hideyuki Okumura and Keiichi N. Ishihara, Structure and catalytic behavior of CuO-CeO2 prepared by High-Energy Ball Milling, Catalysis Letters (under review).

[5] V. Meille, Review on methods to deposit catalysts on structured surfaces, Applied Catalysis A: General 315 (2006) 1-17.

[6] M. Valentini, G. Groppi, C. Cristiani, M. Levi, E. Tronconi, P. Forzatti, The deposition of γ-Al2O3 layers on ceramic and metallic supports for the preparation of structured catalysts, Catalysis Today 69 (2001) 307–314.

[7] C. Agrafiotis, A. Tsetsekou, A. Ekonomakou, The effect of particle size on the adhesion properties of oxide washcoats on cordierite honeycombs, J. Mater. Sci. Lett. 18 (1999) 1421..

[8] C. Agrafiotis, A. Tsetsekou, The effect of powder characteristics on washcoat quality. Part I: Alumina washcoats, J. Eur. Ceram. Soc. 20 (2000) 815-824.

[9] C. Agrafiotis, A. Tsetsekou, The effect of powder characteristics on washcoat quality. Part II: Zirconia, titania washcoats: multilayered structures, J. Eur. Ceram. Soc. 20 (2000) 825-834.

[10] C. Agrafiotis, A. Tsetsekou, I. Leon, Effect of Slurry Rheological Properties on the Coating of Ceramic Honeycombs with Yttria-Stabilized-Zirconia Washcoats, J. Am. Ceram. Soc. 83 (2000) 1033-1038.

[11] C Agrafiotis, A Tsetsekou, The effect of processing parameters on the properties of γ-alumina washcoats deposited on ceramic honeycombs, Journal of materials science 35 (2000) 951-960.

[12] S. Zhao, J. Zhang, D. Weng, X. Wu, A method to form well-adhered γ-Al2O3 layers on FeCrAl metallic supports, Surface and Coatings Technology 167 (2003) 97–105.

[13] S. H. Zeng, Y. Liu, Y.Q.Wang. CuO-CeO2/Al2O3/FeCrAl monolithic catalysts prepared by sol-pyrolysis method for preferential oxidation of carbon monoxide, Catalysis letter (2007) Vol. 117, Nos. 3-4.

CHAPTER 5

Investigation on Catalytic Performance of Pt, Pd and Rh/CuO-CeO_2 /Al_2O_3 on Metallic Substrate for Three-Way Catalysts

5.1 Introduction

TWCs are capable of simultaneously converting CO, HC and nitrogen oxides (NOx) into harmless CO_2, H_2O and N_2. In TWCs, NMs act as the active components. Since the TWCs function occurs only when an engine is operating under a narrow range of air-fuel ratios near stoichiometry, the oxygen storage layer plays an important role to keep an appropriate oxygen level. Thus, being the OSC is generally used as an indicator of TWCs.

In 1980s, a zirconia-ceria (ZrO-CeO_2) compound was found to show remarkably high OSC, where CeO_2 exhibits oxygen storage/release behavior by redox variation of Ce ions between Ce^{3+} and Ce^{4+} [1], while the introduction of ZrO_2 into CeO_2 improved the reduction temperature of ceria through structural modification of ceria lattice [2]. It is required, however, to further improve the efficiency of TWCs in order to abide by severe regulations regarding the exhaust emission. That is, to achieve a higher OSC at low

temperatures and/or under an oxygen-rich environment. Among many studies on CeO_2 base materials such as CeO_2-Al_2O_3 [3], CeO_2-SiO_2 [4], CeO_2-La_2O_3 [5-6], CeO_2-TbO_x [7], and CeO_2-PrO_x [8] have been reported to improve OSC and increase the thermal stability. Recently, copper-ceria oxide compound (CuO-CeO_2) prepared by high energy mechanical milling has been found, by authors, to significantly promote the OSC [9].

Nonetheless, in order to determine whether a newly developed material suitable for a TWCs, it is important to consider other characteristics. For example, the catalytic performance of the new material for the conversion of CO, C_3H_8 and NO is fundamental aspect. There are many reports on the traditional catalyst system for conversion performance of CO, C_3H_8 and NO was shown [10, 11, 12]. For example, H. He et al reported the performance and redox properties of Pd, Pt, Rh loaded on $Ce_{0.6}Zr_{0.35}Y_{0.05}O_2$. Also, recently, the improvable thermal stability to reduce the particle size of NMs loaded on CeO_2-ZrO_2 or on a Al_2O_3 washcoat have been studied [13-16]. However, catalytic performance in case of lean oxygen has been not reported. Thus, in this chapter, the catalytic performance of the CuO-CeO_2 system is investigated and compared with the CeO_2-ZrO_2 system and the γ-Al_2O_3 system under a simulated automobile exhaust gas. The oxygen release capacity of NMs impregnated on the CuO-CeO_2 system, the CeO_2-ZrO_2 system and the Al_2O_3 system was also investigated, as mean to improve the catalytic performance under lean oxygen condition of simulated automobile exhaust gas.

5.2 Results

5.2.1 The surface characterization of catalysts

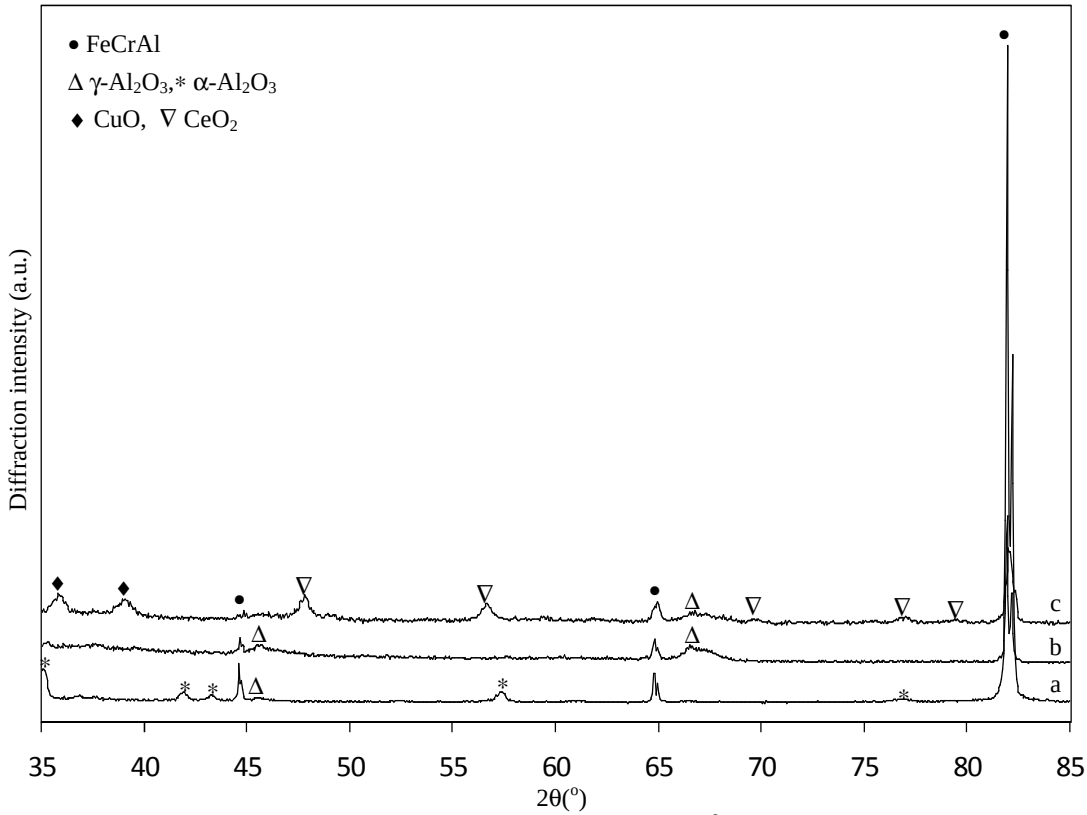

Figure 5-1: XRD patterns of (a) FeCrAl after pre-oxidation at 900 °C for 10h; (b) γ-Al_2O_3 washcoat on FeCrAl substrate; (c) CeO_2-CuO/γ-Al_2O_3 washcoat/FeCrAl substrate

XRD patterns of FeCrAl substrate and γ-Al_2O_3 washcoat layer are shown in Figures 5-1a and 5-1b respectively. The peaks of Fe-Cr-Ni, γ-Al_2O_3 and α-Al_2O_3 are observed (Figure 5-1a) after FeCrAl substrate is pre-oxidized at 900°C for 10h [17], γ-Al_2O_3 peaks become sharper while α-Al_2O_3 peaks and Fe-Cr-Ni peaks decrease after γ-Al_2O_3 washcoat layer was coated on FeCrAl substrate (Figure 5-1b). The XRD patterns of CuO-CeO_2 layer coated on Al_2O_3 washcoat, on FeCrAl substrate can be seen in Figure 5-1c, no phase change of CuO and CeO_2 are observed after sintering at 650°C for 2.5h while the intensive peaks of FeCrAl substrate and γ-Al_2O_3 washcoat become lower. The XRD also shows that, no peaks of NMs or NMs oxides on the CuO-CeO_2 system, the CeO_2-ZrO_2 system and the Al_2O_3 system.

Table 5-1:
The surface areas of noble metals are impregnated on the CuO-CeO_2 system, the CeO_2-ZrO_2 system and the Al_2O_3 system after sintering at 650°C in air for 2.5h.

No	Coating samples	Surface area (cm^2/cm^2 substrate)
1	Pt, Pd, Rh/CuO-CeO_2 system	15-17
2	Pt, Pd, Rh/CeO_2-ZrO_2 system	16-18
3	Pt, Pd, Rh/Al_2O_3 system	11-13

Table 5-1 shows the surface area of the CuO-CeO_2 system, the CeO_2-ZrO_2 system and the Al_2O_3 system after sintering at 650°C for 2.5h. The results show that, the surface area of the CuO-CeO_2 system is in the range of 15 to 17 (cm^2/cm^2-substrate) while the surface area of the CeO_2-ZrO_2 system and the Al_2O_3 system is around 16 to 18 (cm^2/cm^2-substrate) and 11 to 13 (cm^2/cm^2-substrate) respectively, The surface area of the CuO-CeO_2 system proved to be similar with surface area of the CeO_2-ZrO_2 system or the Al_2O_3 system after sintering at 650°C for 2.5h.

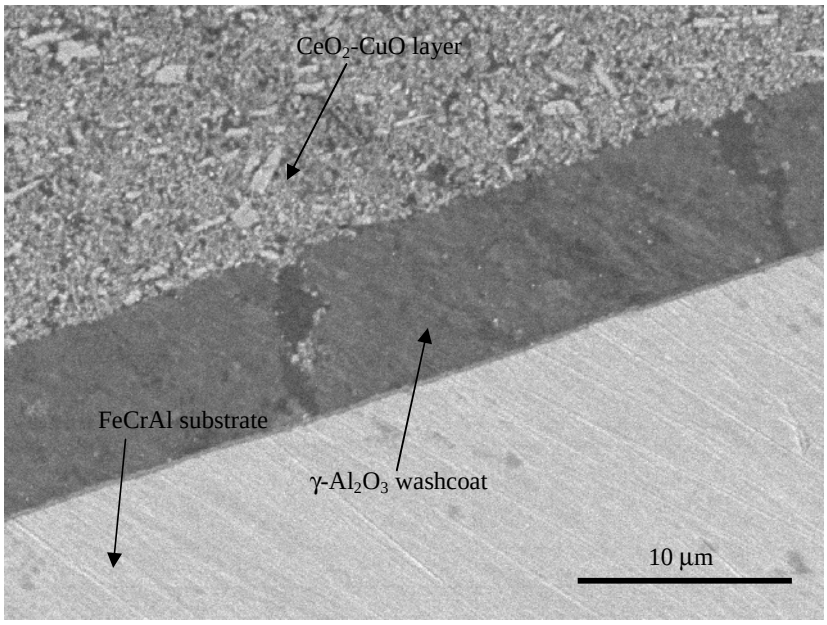

Figure 5-2: SEM photographs of the CeO_2-CuO system after sintering at 650 °C

The Figure 5-2 shows the morphology of the CuO-CeO_2 system. As the results of milling process of the CuO-CeO_2 slurry, the fine agglomerated particles of CuO-CeO_2 after sintering had dimensions of less than 2μm. The contaminations from the milled media (ZrO_2 balls and a steel vial) are also examined by EDX. The results show that, Fe and ZrO_2 contaminations in the CuO-CeO_2 samples are 0.8 wt% and 0.2 wt% after a 48h milling of the CuO-CeO_2 slurry.

5.2.2 Chemical state analysis of noble metals impregnated on CuO-CeO_2/Al_2O_3/FeCrAl substrate

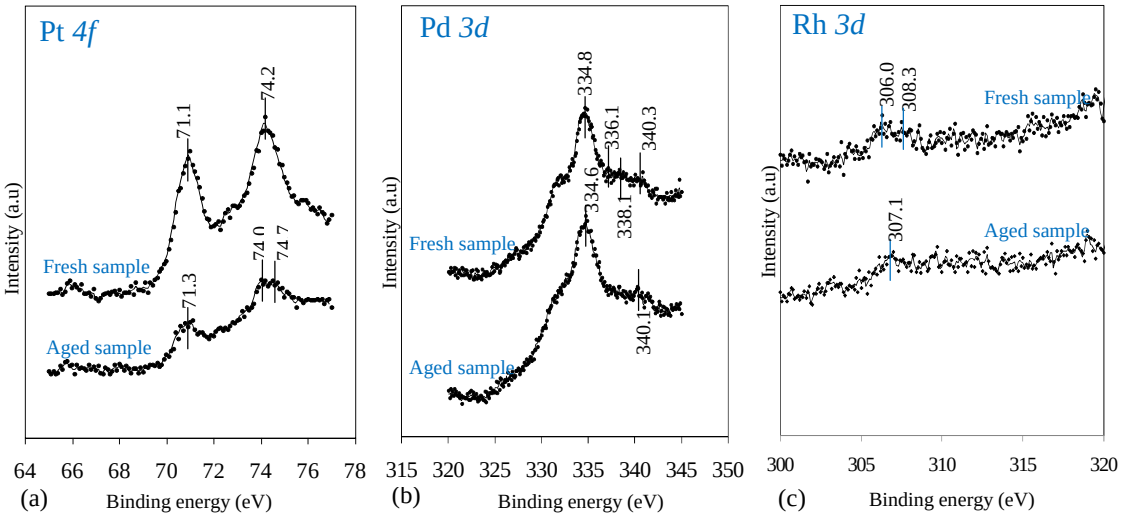

Figure 5-3: Photoelectron spectra of (a) Pt 4f; (b) Pd 3d; (c) Rh 3d impregnated on CuO-CeO_2/Al_2O_3/substrate on region obtained from the fresh samples (dried at 250°C for 2h and sintered at 650°C for 2.5h) and aged samples (heated treatment at 900°C for 10h).

The fresh samples (sintered at 650°C for 2.5h) and aged samples (sintered at 900°C for 10h) of CuO-CeO_2/Al_2O_3/FeCrAl substrate were used for the chemical state analysis of noble metals. The Figure 5-3a shows Pt 4f photoelectron spectra of fresh samples and aged samples, the doublet at 71.1 and 74.3 eV are observed and may be attributed to Pt^0 sites for the fresh samples. After aged at 900°C for 10h, a new peak at 74.7 eV attributes to Pt^{2+} site, the doublet at 71.3 and 74.0 can again be attributed to Pt^0 sites. The Figure 5-3b shows Pd 3d photoelectron spectra, the doublet at 336.1 eV and 338.1.1eV can be attributed for Pd^{2+}

and Pd^{4+} for the fresh samples, while only Pd 3d of Pd^0 is observed at 334.6 eV and 340.1 eV for the aged samples. The Figure 5-3c shows Rh 3d for the fresh and aged sample, the Rh $3p_{5/2}$ peaks are observed at 306.0 eV and 308.3 eV can be attributed for Rh^0 and Rh^{3+} respectively. For aged samples, only Rh $3p_{5/2}$ peaks at 307.1 eV is observed leading to Rh^0. Above, the results show that the chemical state of noble metals impregnated on CuO-CeO_2/Al_2O_3/FeCrAl substrate are determined. Xiaodong Wu et al [11] or S.Suhonen et al [18] reported that those chemical states depend strongly on heated treatment condition, and the formation of noble metals and noble metals oxide are observed the sintering at 650^{o}C for 2.5h, the reason for this may be due to the incomplete decomposition of noble metals salt. H. Shinjoh [12] reported that the platinum reacted with ceria to make the Pt-O-Ce bond after aged at 900^{o}C for 10h, so only state of Pt oxide was observed.

5.2.3 Catalytic performance

The reactions that occur in TWCs are complex mixture of oxidation, reduction, WGS and steam reforming [1]. In this chapter, CO, C_3H_8 and NO conversion ratios (%) were calculated based on the difference between the concentration of CO, C_3H_8 and NO before and after their reaction.

5.2.3.1 Catalytic performance of the CuO-CeO_2 system in case of enough oxygen (λ=1)

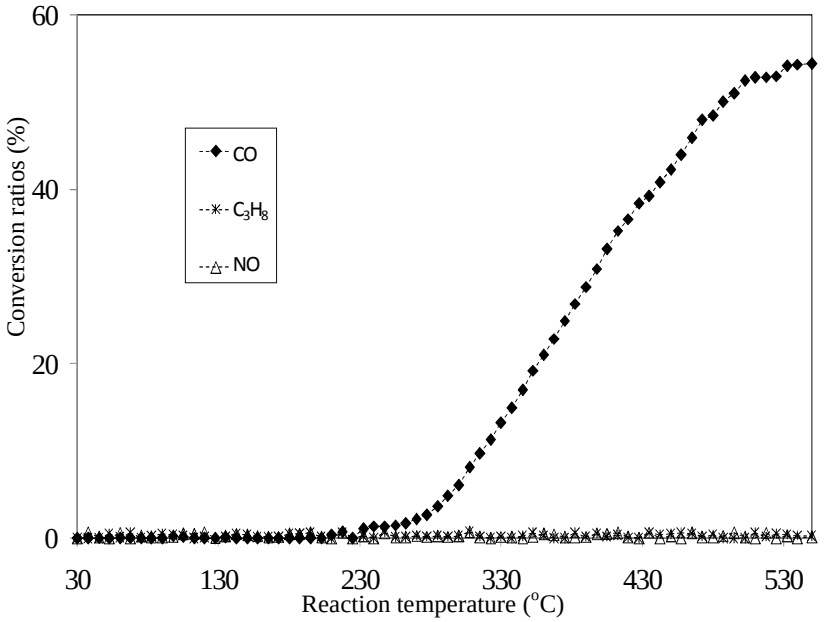

Figure 5-5: CO, C_3H_8, NO conversion performance with the increase of reaction temperature over catalysts of CeO_2-CuO system at λ=1

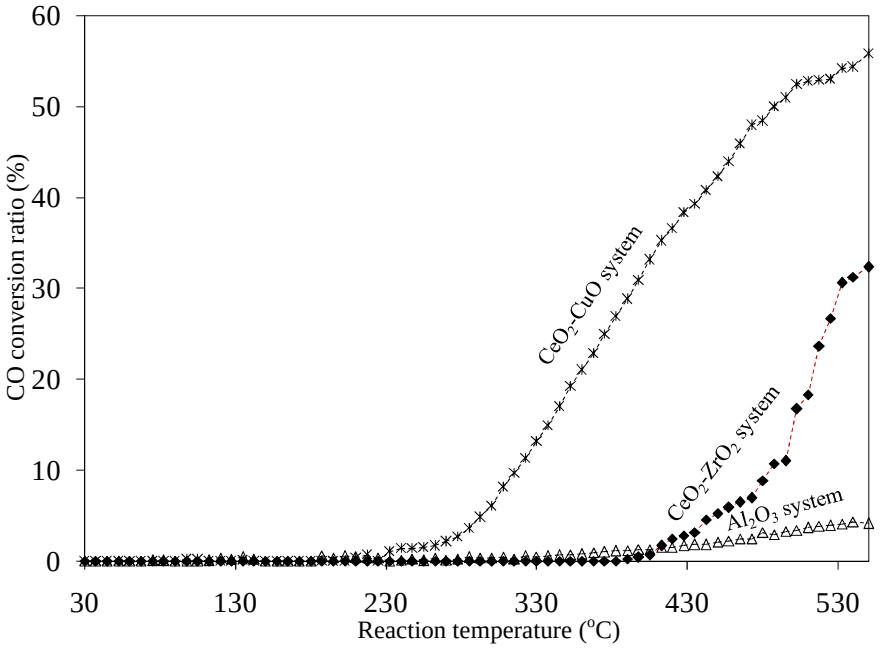

Figure 5-4: CO conversion performance with the increase of reaction temperature over catalysts of the CeO_2-CuO system, the CeO_2-ZrO_2 system and the Al_2O_3 system at λ=1

In case where no NMs impregnated on the CuO-CeO_2 system, CO conversion ratio increased from 0% at 30^0C to 55% at 540^oC. Conversely, no C_3H_8 and NO conversion ratios were observed in the range from 30 to 540^oC (Figure 5-4). Comparing catalytic performances when no NMs are impregnated on the CuO-CeO_2 system, the CeO_2-ZrO_2 system and the γ-Al_2O_3 system, is possible to see that the CO conversion ratio of the CuO-CeO_2 system is higher than the conversion ratio of the CeO_2-ZrO_2 system and the Al_2O_3 system. No C_3H_8 and NO conversion ratios of CeO_2-ZrO_2 system and the Al_2O_3 system were observed (Figure 5-5).

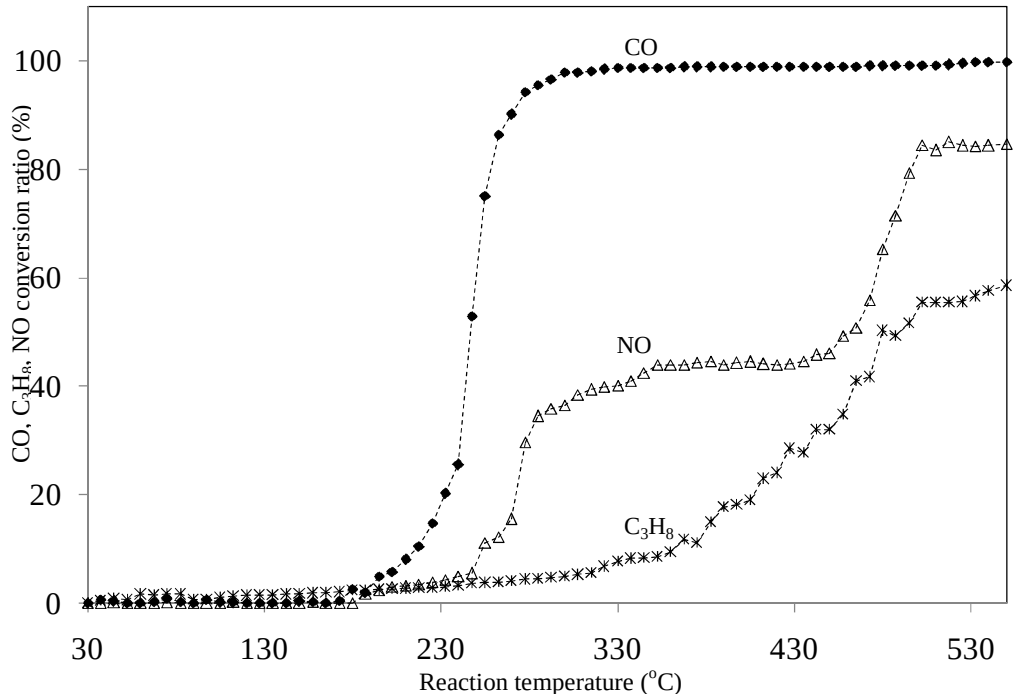

Figure 5-6: CO, C_3H_8, NO conversion performance with the increase of reaction temperature over catalysts of metals impregnated on the CeO_2-CuO system at λ=1

After 4 wt. % of NMs impregnated on the CuO-CeO_2 system, the CO conversion increased in 99%, while the C_3H_8 and NO conversion increased only in 62% and 84.3% respectively, during a temperature increase up to 540^oC (Figure 5-6). Comparing the catalytic performance when NMs impregnated on the CuO-CeO_2 system, the CeO_2-ZrO_2

system and the Al_2O_3 system, Figure 5-7a shows that, CO conversion of the CuO-CeO_2 system is higher than CO conversion of the CeO_2-ZrO_2 system and the γ-Al_2O_3 system due to the increase in the reaction temperature from 30^{o}C to 540^{o}C, the result also shows that, start temperature for CO oxidation of the CuO-CeO_2 system is lower the start temperature for CO oxidation of the CeO_2-ZrO_2 system and the γ-Al_2O_3 system. Similar C_3H_8 and NO conversions ratios are observed due to the increase in the reaction temperature from 30^{o}C to 540^{o}C (Figure. 5-7b, 5-7c). This result coincides with the reports of Meng-Fei Luo et al [19] and G. Avgouropoulos et al [20] who study on CuO-CeO_2 catalytic activity for the oxidation of CO at low temperatures.

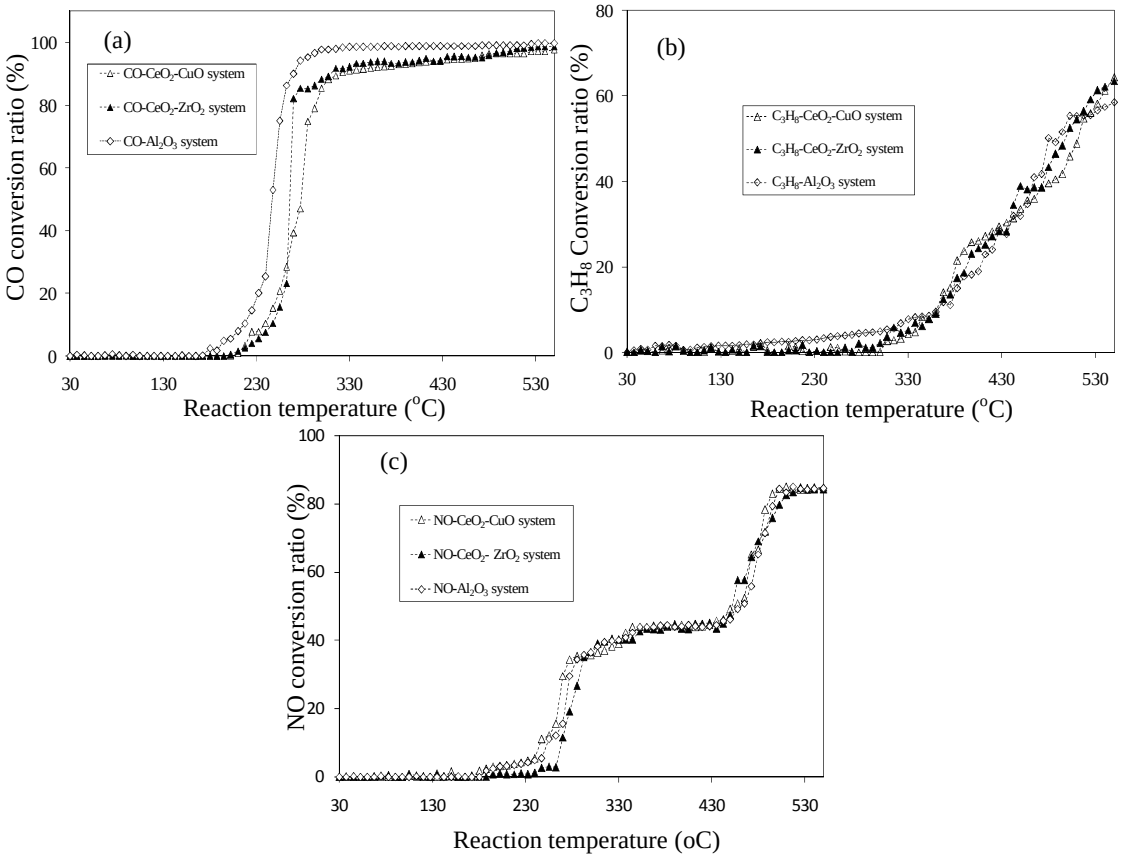

Figure 5-7: (a) CO, (b) C_3H_8, (c) NO conversion performance with the increase of reaction temperature over catalysts of metals impregnated on the CeO_2-CuO system, CeO_2-ZrO_2 system, Al_2O_3 system at λ=1

5.2.3.2 Catalytic performance in case lean and rich oxygen (λ<1 and λ>1)

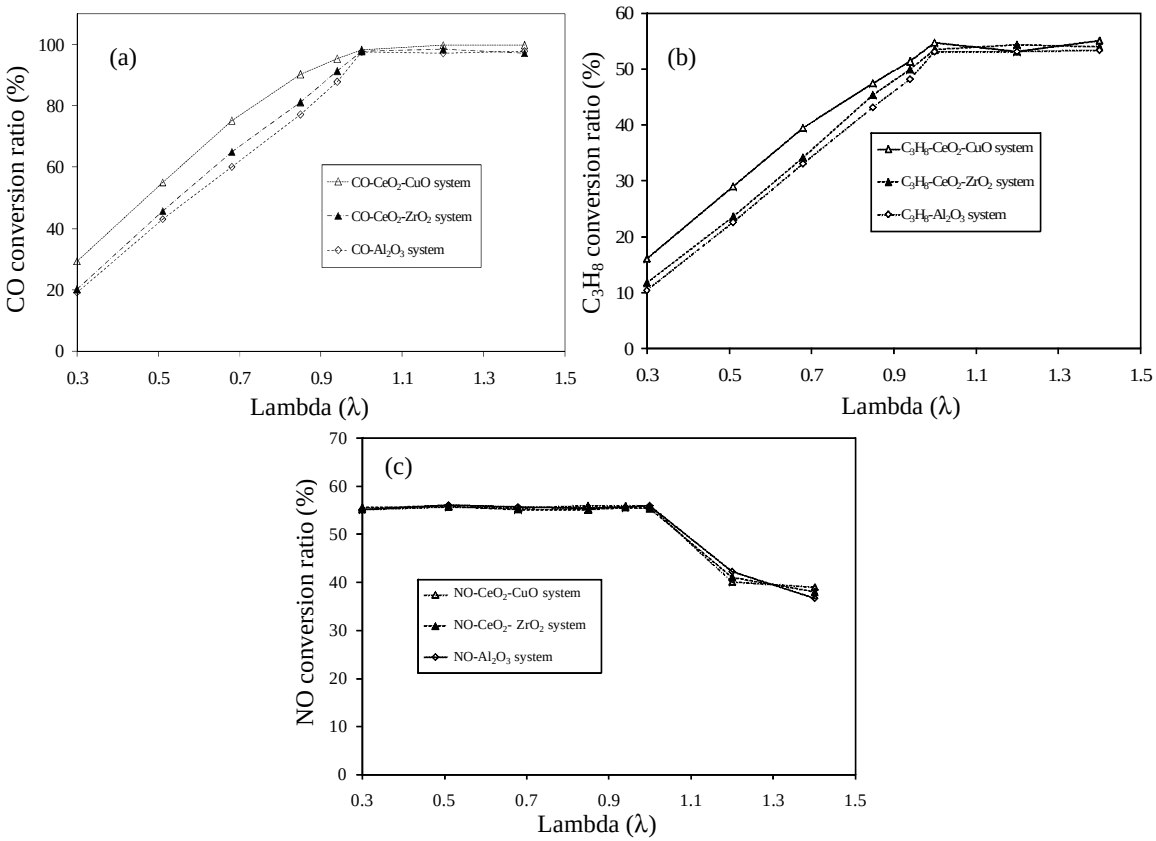

Figure 5-8: (a) CO; (b) C_3H_8, (c) NO conversion performance at 500 ^oC over catalysts of noble metals impregnated on the CeO_2-CuO system, the CeO_2-ZrO_2 system, the Al_2O_3 system at lean and rich oxygen condition (λ<1 and λ>1)

The catalytic performance under lean oxygen conditions was investigated at 500^oC during the decrease of λ from 1 to 0.3. Results showed that, CO and C_3H_8 conversion ratio of NMs impregnated on the CuO-CeO_2 system decreased from 99.1% to 33.3% and from 55.1% to 16.2% as the value of λ decreased from 1 to 0.3 (Figure 5-8a, 5-8b), Conversely, no change in the NO conversion ratio is observed (Figure 5-8c). CO and C_3H_8 conversion ratios of NMs impregnated on ZrO_2-CeO_2 system (or the Al_2O_3 system), also decreased from 98.3% to 20% and from 53.9% to 13%, (or from 98.7% to 15.1% and from 53.3% to 10.3%), respectively (Figure 5-8a, 5-8b). Again, no change of NO conversion ratio is observed when the value of λ varies from 1 to 0.3 (Figure 5-8c). Comparing the catalytic performance when NMs impregnated on the CuO-CeO_2 system, the CeO_2-ZrO_2 system and

the Al_2O_3 system when the value of λ varies from 1 to 0.3, the results show that the decrease of CO and C_3H_8 conversion ratios of the CuO-CeO_2 system (from 99.1% to 33.3% and from 55.1% to 16.2%) is less than the decrease of CO and C_3H_8 conversion ratios of the CeO_2-ZrO_2 system (from 96.3% to 20% and from 53.9% to 13%) and the γ-Al_2O_3 system (from 95.7% to 15.1% and from 53.3% to 10.3%). Similar NO conversion ratio was also observed (Figure 5-8c).

The catalytic performance under rich oxygen condition was investigated at 500^oC for different values of λ from 1 to 1.4. The results show no change in the conversion ratio of CO and C_3H_8 (Figure 5-8a, 5-8b) whereas the conversions ratio of NO decreases from 55.9% to 38.9% (Figure 5-8c). Comparing the catalytic performance with NMs impregnated on the CuO-CeO_2 system, the CeO_2-ZrO_2 system and Al_2O_3 system under rich oxygen condition, shows similar CO, C_3H_8 and NO conversions as λ varies from 1 to 1.4.

5.3 Discussion

This section discusses the role of oxygen storage materials to catalytic performance under lean oxygen condition.

Figure 5-8 shows that, there is no change in the conversion ration of NO when λ decreases from 1 to 0.3. On the contrary, the CO and C_3H_8 conversion ratios of NMs impregnated on the CuO-CeO_2 system are higher than those of NMs impregnated on the CeO_2-ZrO_2 and the Al_2O_3 system. This implies that, the reduction from NO to N_2 does not occur under lean oxygen condition. Consequently, it is reasonable to consider that CO and C_3H_8 conversion ratios under lean oxygen conditions only depend on the effect of CO and C_3H_8 oxidation reactions; thereby, the oxygen that supports the oxidation reactions plays an important role in improving the CO, C_3H_8 conversion ratios. There could be two oxygen sources to support the oxidation reactions under lean oxygen conditions; the first might have been (direct) oxygen from the simulated automobile exhaust gas which was estimated

by subtracting of the amount oxygen in an automobile exhaust gas before passing through the reaction tube, from the amount oxygen after passing reaction tube. The second oxygen source (indirect) might be from oxygen storage materials which were measured by through TG-DTA during the weight change of the sample.

The Figure 5-9 shows the λ property of the simulated automobile exhaust gas after passing an oxygen absorber agent for 15 minutes. The result shows that, λ monotonously decreases from 1 to 0.3 during the decrease of oxygen concentration of the simulated automobile exhaust gas decreases from 1.5% to 0.42%.

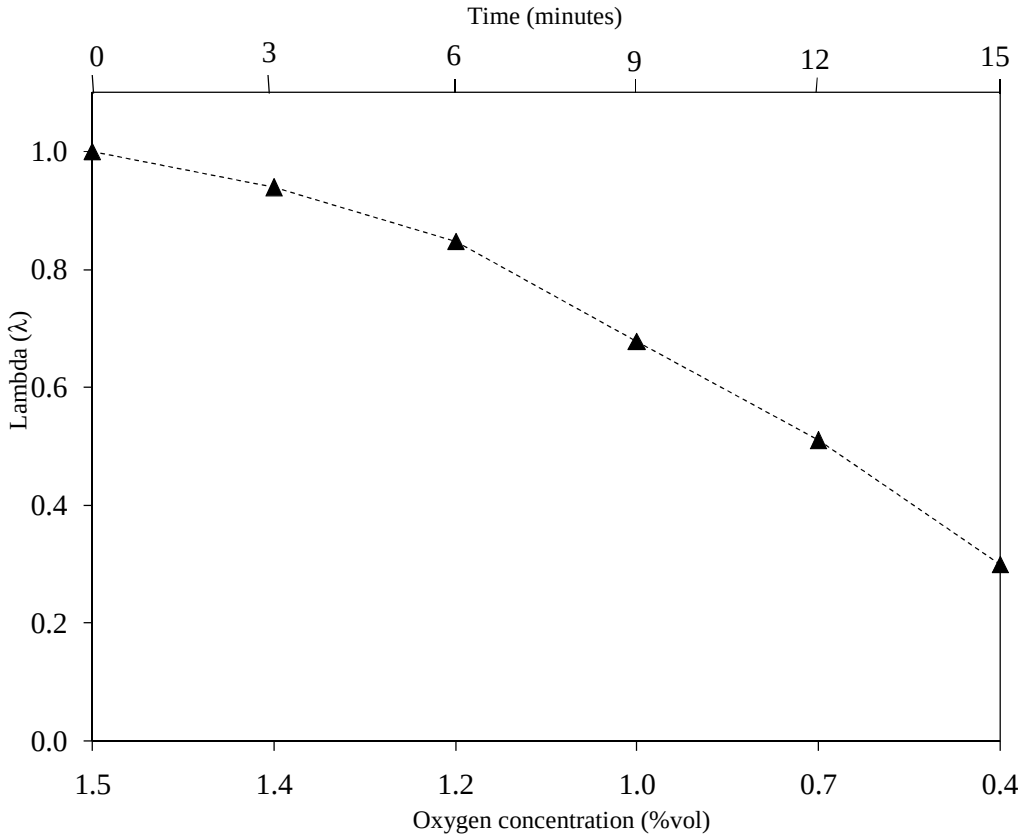

Figure 5-9: Lambda (λ) property of simulated exhaust gas after passing oxygen absorber agent for 15 minutes

Figure 5-10 shows that similar amounts of oxygen, of the simulated automobile exhaust gas, directly supports for the oxidation reaction of CO and C_3H_8 at 500^{o}C, over the

catalysts of NMs impregnated on the CuO-CeO_2 system, the CeO_2-ZrO_2 system and the Al_2O_3 system. It is found that amount of oxygen in the simulated automobile exhaust gas (directly) supported the oxidation reaction of CO and C_3H_8, monotonously decreasing as λ decreases from 1 to 0.3. This decrease in oxygen leads to the decrease of CO and C_3H_8 conversion ratios (Figure 5-7a, 5-7b), during the decrease of λ values.

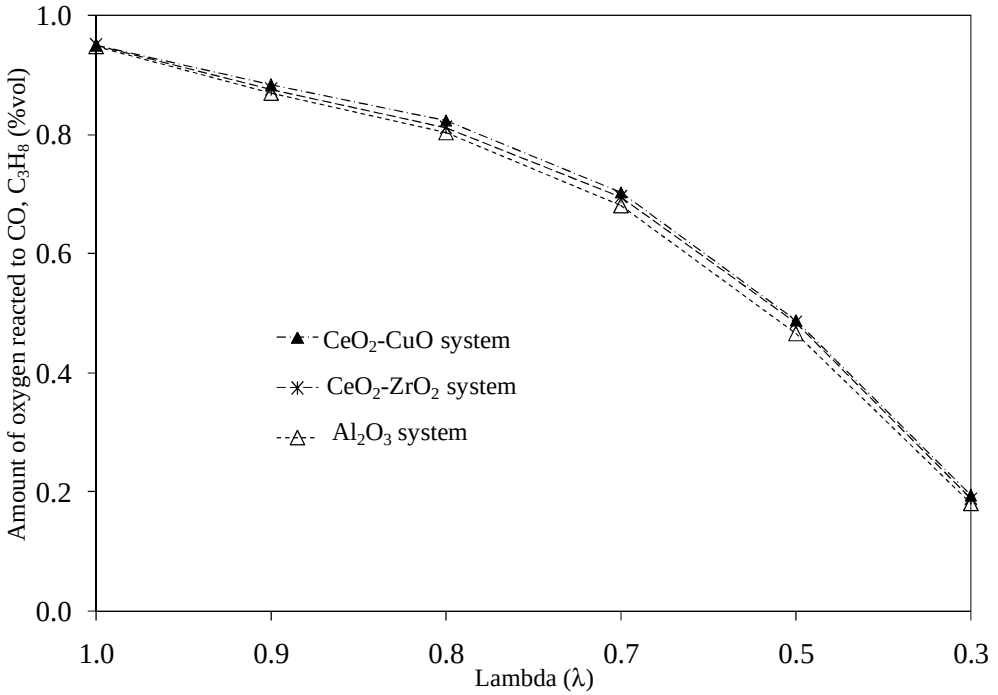

Figure 5-10: Amount of oxygen of simulated automobile exhaust gas reacted to CO and C_3H_8 at 500 ^oC over the catalysts of noble metals impregnated on the CeO_2-CuO system, the CeO_2-ZrO_2 system and the Al_2O_3 system

Figure 5-11 shows the amount of oxygen released from oxygen storage materials to (indirectly) support oxygen for the oxidation reaction of CO and C_3H_8, during the decrease of λ values from 1 to 0.3. The amount of released oxygen from NMs are impregnated on the CuO-CeO_2 system and the CeO_2-ZrO_2 system increases as λ decreases (Figure 5-10a, 5-10b); while other results depict no release of oxygen in the Al_2O_3 system. Comparing the amount of released oxygen of these systems, suggests that the amount of released oxygen from NMs impregnated on the CuO-CeO_2 system is much higher than that of the CeO_2-

ZrO_2 system and the Al_2O_3 system. It has been reported [9] that a ceria-copper oxide compound (CuO-CeO_2) prepared by high energy mechanical milling to significantly promote the OSC during the valence change of Cu^{2+}/Cu and Ce^{4+}/Ce^{3+}. Hence, the OSC of CuO-CeO_2 is much higher than that of CeO_2-ZrO_2, as described by [9]. In this study, the amount of released oxygen from oxygen storage materials was due to the reduction of Cu^{2+} $\rightarrow$ Cu and $Ce^{4+}\rightarrow$ Ce^{3+}. (For details of this reduction see [9]).

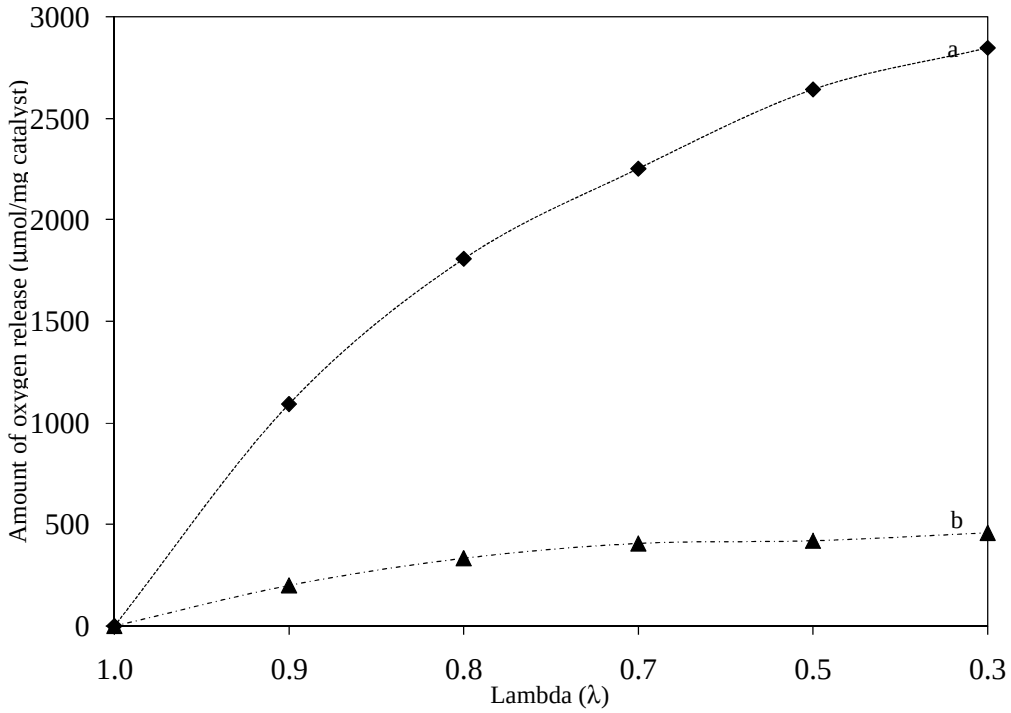

Figure 5-11: Oxygen release capacity at 500°C of (a) Pt, Pd, Rh/CeO_2-CuO/Al_2O_3/substrate and (b) Pt, Pd, Rh/CeO_2-ZrO_2/Al_2O_3/substrate under lean oxygen condition of simulated automobile exhaust gas

It is also quite interesting that the amount of released oxygen from oxygen storage materials is found as λ decreases from 1 to 0.3. It is reasonable to believe that the released oxygen may improve CO and C_3H_8 conversion performance at lean oxygen condition. In synthesis, the decrease in CO and C_3H_8 conversion ratios of NMs impregnated on CuO-CeO_2 system is less than those ratios of on the CeO_2-ZrO_2 system and the Al_2O_3 system

(Figure 5-7a, 5-7b). Thus, this can improve the efficiency of TWCs, at the engine's startup where λ values may range from 0 to 1.

Under an engine real working conditions, the value of λ oscillates at around 1 with a frequency of about 1 Hz [1]. Hence, the efficient conversion of TWCs decreases during the oscillation of λ. The dynamic of released oxygen from oxygen storage materials is therefore an important parameter in the improvement of the TWCs conversion efficiency. In this study, the dynamics of released oxygen was estimated for values of λ from 1 to 0.9 for 3 minutes. Result shows that, the dynamics of released oxygen of NMs impregnated on the CuO-CeO_2 system (6.7 $\mu mol.mg^{-1}.s^{-1}$) is much higher than those on CeO_2-ZrO_2 system (1.1 $\mu mol.mg^{-1}.s^{-1}$).

5.4 Conclusions

The catalytic performance of Pd, Pt and Rh impregnated on the CuO-CeO_2 system was investigated using the automotive exhaust gas simulator comparing with that of noble metals coated on a CeO_2-ZrO_2/Al_2O_3/substrate and Al_2O_3/substrate. The coated samples were characterized by means of XRD, SEM, Brunauer-Emmett-Teller (BET), X-ray photoelectron spectroscopy (XPS) and GC-TCD. The results showed that, when $\lambda=1$, the CO conversion ratio for noble metals coated on CuO-CeO_2 was higher at lower temperatures than that of noble metals coated on CeO_2-ZrO_2 and that of noble metals coated on γ-Al_2O_3. For the case of $\lambda<1$, CO and C_3H_8 conversion ratios of noble metals coated on CuO-CeO_2 were higher than those of noble metals coated on CeO_2-ZrO_2 and on a γ-Al_2O_3 washcoat.

Amount of released oxygen and dynamic release of oxygen from oxygen storage materials of NMs impregnated on the CuO-CeO_2 system are much higher than those on the CeO_2-ZrO_2 system and the Al_2O_3 system due to the λ decreased from 1 to 0.3; thus

suggesting that efficiency of TWCs at initial period of startup engine and the during the oscillation of λ under real work conditions of engine can be improved.

REFERENCES

[1] Jan Kaspar, Paolo Fornasero, Neal Hickey, Catal today 77(2003) 419-449.

[2] Akira Morikawa, Tadashi Suzuki, Takaaki Kanazawa, Koichi Kikuta, Akihiko Suda, Hirofumi Shinjo, Appl, Catal, B 78 (2008).

[3] D. Gamarra, G.Munuera, A. B. Hungria, M. Fernandez-Garcia, J.C. Conesa, P.A. Midgley, X. Q. Wang, J.C.Hanson, J. A. Rodriguez, Martinez-Arias, J. Phys. Chem. C 2007,11026-11038.

[4] R.K. Usmen, G.W. Graham, W.L.H. Watkins, R.W. McCabe, Catal. Lett. 30 (1995) 53.

[5] A. Bensalem, F. Bozon-Verduraz, M. Delamar, G. Bugli, App Catal. A 121 (1995) 81.

[6] M. Ozawa, M. Kimura, H. Sobukawa, K.Yokota, Toyota Tech. Rev. 27 (1992) 43.

[7] S. Matsumoto, N. Miyoshi, T. Kanazawa, M. Kimura, M. Ozawa. Catal. Sci. Technol. 1 (1991) 335.

[8] F. Zamar, A. Trovarelli, C. de Leitenburg, G. Dolcetti, Stud. Surf. Sci. Catal. 101 (1996) 1283.

[9] M.Y. Sinev, G.W. Graham, L.P. Haach, M. Shelef, J. Mater. Res. 11 (1996) 1960.

[10] Nguyen The Luong, Eiji Yamasue, Hideyuki Okumura and Keiichi N. Ishihara, Catalysis Letters (under review).

[11] H. He, H.X.Dai, L.H.Ng, K.W.Wong, C. T. Au, Journal of catalysis 206, 1-13 (2002)

[12] Xiaodong Wu, Luhua Xu, Duan Weng, Applied Surface Science 221 (2004) 375–383

[13] Hirofumi Shinjoh, Catal Surv Asia (2009) 13: 184-190

[14] Takeru Yoshida, Akemi sato, Hiromasa Suzuki SAE 2006-01-1061

[15] Toshitaka Tanabe, Miho Hatanaka and Yasutaka Nagai, SAE 2009-01-1081

[16] Masanori Nakamura, Hironori Wakamatsu, Katsuo Suga, Toru Sekiba, Yoshiaki Hiramoto, Katsuhiro Shibata, SAE 2009-01-1069

[17] K. Nagashima, G. Zhang, T. Hirota, H. Muraki, SAE 2000-01-1954

[18] Nguyen The Luong, Eiji Yamasue, Hideyuki Okumura and Keiichi N. Ishihara (to be appear)

[19] S.Suhonen, M. Valden, M. Hietikko, R. Laitinen, A. Savimaki, M. Haikonen, Applied Catalysis A: General 218 (2001) 151-160.

[20] Meng-Fei Luo, Jing-Meng Ma, Ji-Qing Lu, Yu-Peng Song, Yue-Juan Wang, Journal of Catalysis 246 (2007) 52-59.

[21] G. Avgouropoulos, T. Ioannides, Ch. Papadopoulou, J.Batista, S. Hocevar, H.K. Matralis, Catalysis today 75 (2002) 157-167.

CHAPTER 6

Thermal Stability and Catalytic Performance of Pd, Pt and Rh Loaded on CuO-CeO_2-Al_2O_3 for Three-way Catalysts

6.1 Introduction

TWCs are capable of simultaneously converting CO, HC and NOx into harmless CO_2, H_2O and N_2. In TWCs, NMs, such as platinum, rhodium and palladium act as the active components. OSC is one of the crucial factors for the performance of TWCs, and the higher OSC promotes the better dynamic performance of catalysts in converting CO, HC and NOx under conditions from rich to lean oxygen of air-fuel ratios (A/F) in automobile. CeO_2-ZrO_2 solid solution is well-known as an excellent supporter for OSC [1]. CeO_2 exhibits oxygen storage/release behavior by the redox reaction of Ce ions between Ce^{3+} and Ce^{4+} [2], and the introduction of ZrO_2 into CeO_2 improves the reduction temperature of CeO_2 through

structural modification of CeO_2 [3]. Among many studies on CeO_2 base materials such as CeO_2-Al_2O_3 [4], CeO_2-SiO_2 [5], CeO_2-La_2O_3 [4, 6-7], CeO_2-TbO_x [8], and CeO_2-PrO_x [9] have been reported to improve OSC and increase the thermal stability.

Considering upcoming strict regulation, this is the need of improving the efficiency of TWCs, so that the temperature in a CCCs converter can rise even above 1000°C. In order to adapt to high temperature, many reports based on performance and durability of CeO_2-ZrO_2 were shown [10-13]. Morikawa et al [10] reported a new concept of introducing alumina

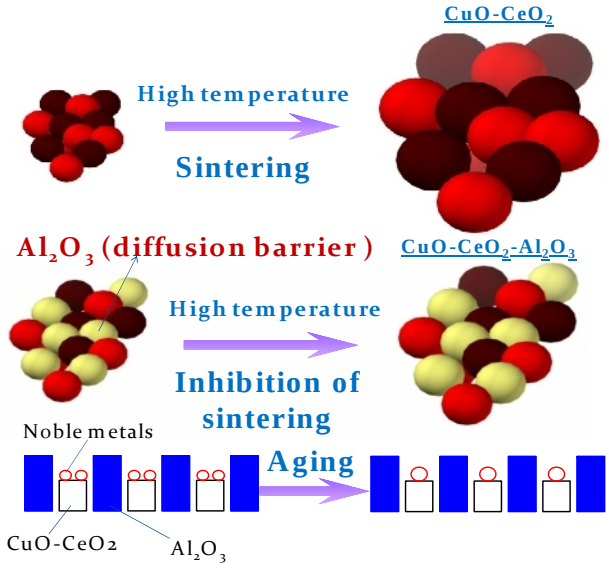

Figure 6-1: Illustration of "diffusion barrier concept"

into ceria-zirconia solid solution (ACZ) which was named the "diffusion barrier concept" to enhance OSC. Nakamura [13] also developed a new concept to prevent the migration of noble metal particles, and thereby to promote the catalytic performance.

Recently, a ceria-copper oxide compound (CuO-CeO_2) prepared by means of high energy mechanical milling has been found to promote OSC by authors [14]. The catalytic performance of Pd, Pt and Rh coated on a CuO-CeO_2/Al_2O_3/FeCrAl substrate could improve CO conversion at lower temperatures and strongly improve oxidation reaction of CO and C_3H_8 in cases of lean oxygen [15].

Nonetheless, it is also extremely important to improve a durability of CuO-CeO_2 to adapt to high temperature. Thus, the aim of this chapter is to develop a "diffusion barrier concept" for the CuO-CeO_2 structure (Figure 6-1). This implies that, Al_2O_3 introduced into CuO-CeO_2 behaves as a diffusion barrier to prevent migration of CuO-CeO_2, thereby suppressing CuO-CeO_2 particle growth (Figure 6-1). The thermal stability and catalytic performance of Pd, Pt and Rh loaded on CuO-CeO_2-Al_2O_3/FeCrAl substrate are also investigated and compared with those NMs loaded on CuO-CeO_2/Al_2O_3/FeCrAl substrate after sintering at 1000^{o}C for 20h.

6.2 Results

6.2.1 The structure characterization of catalysts

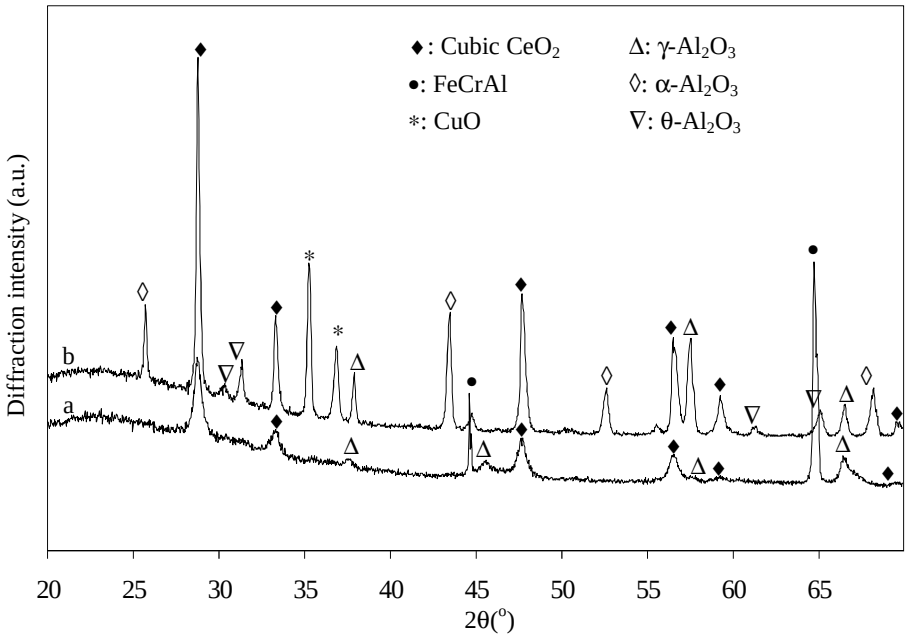

Figure 6-2: XRD patterns of CuO-CeO_2-Al_2O_3 coated on FeCrAl substrate calcined at (a) 650^{o}C and (b) 1000^{o}C for 20h

XRD patterns of CuO-CeO_2-γ-Al_2O_3 layer coated on a FeCrAl substrate calcined at 650^{o}C and 1000^{o}C respectively are shown in Figure 6-2a, 6-2b. The peaks of Fe-Cr-Ni substrate, γ-Al_2O_3, CuO and CeO_2 were observed after sintering at 650^{o}C for 2.5h (Figure

6-2a), the intensity peaks of Fe-Cr-Al, γ-Al_2O_3, CuO and CeO_2 became sharper after aging at 1000^{o}C for 20h. No phase changes of CuO and CeO_2 are observed. On the contrary, the new phases of α-Al_2O_3 and θ-Al_2O_3 are observed after sintering at 1000^{o}C for 20h (Figure 6-2b).

Table 6-1
The surface areas of two and three layers structure after sintering at 650 ^{o}C for 2.5h and at 1000 ^{o}C for 20h

No	Samples	BET (cm^2/cm^2 substrate)
1	$CuO-CeO_2/\gamma-Al_2O_3$/Substrate-650^{o}C for 2.5h	14-16
2	$CuO-CeO_2/\gamma-Al_2O_3$/Substrate-1000^{o}C for 20h	5-7
3	$CuO-CeO_2-\gamma-Al_2O_3$/Substrate-650^{o}C for 2.5h	15-17
4	$CuO-CeO_2-\gamma-Al_2O_3$ Substrate-1000^{o}C for 20h	6-8

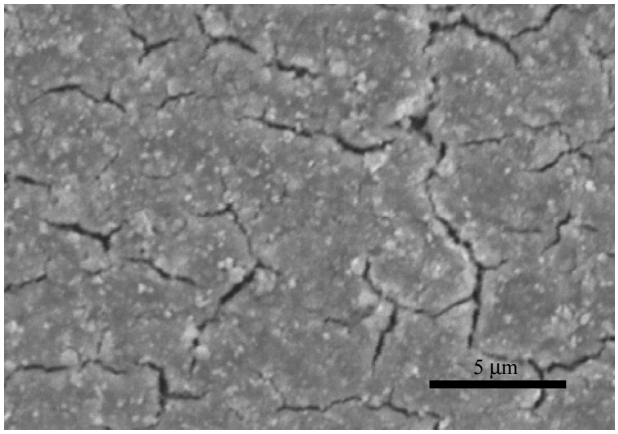

Figure 6-3: SEM photographs of $CuO-CeO_2-\gamma-Al_2O_3$ layer on FeCrAl substrate after sintering at 650^{o}C for 2.5h

Table 6-1 shows that, the surface area of the mixed $CuO-CeO_2-Al_2O_3$ coated on substrate and $CuO-CeO_2$ coated on γ-Al_2O_3 washcoat on substrate decreased after sintering

at 1000°C for 20h. The reason for this, the phase changes of γ-Al_2O_3 to α-Al_2O_3 and θ-Al_2O_3 were observed after sintering at 1000°C for 20h. The surface area of mixed CuO-CeO_2-Al_2O_3 coated on substrate was similar than that of CuO-CeO_2 coated on γ-Al_2O_3 washcoat on substrate after sintering at 650°C for 2.5h and at 1000°C for 20h.

The morphology of CuO-CeO_2-Al_2O_3 layer is shown in Figure 6-3. As the results of milling process of CuO-CeO_2-γ-Al_2O_3 slurry, the fine agglomerate particles of CuO-CeO_2 after sintering at 650°C are observed. The distribution of fine CuO-CeO_2 particles can be seen in the dense microstructure of Al_2O_3 with dimensions less than 2μm. EDX analysis with color mapping of the CuO-CeO_2-Al_3O_3 coating samples is shown in Figure 6-4 which reveals that the contents are limited to Ce, Cu, Al and oxygen. The contaminations from the milled media (ZrO_2 balls and a steel vial) are also examined by EDX, no contamination like Fe, Cr or ZrO_2 was detected while C and Au were observed as pre-treatment step of SEM.

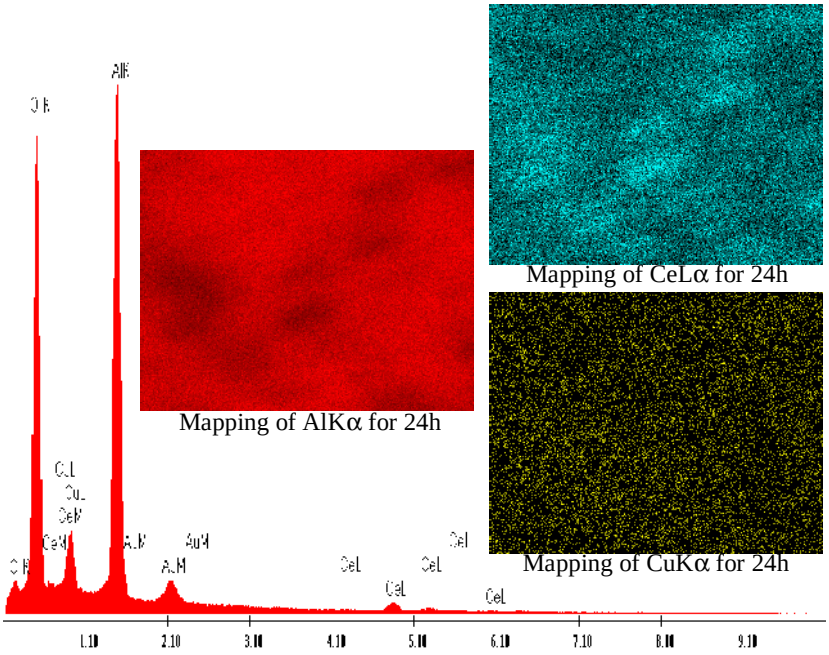

Figure 6-4: Energy dispersive X-ray spectrum of the CuO-CeO_2-Al_2O_3 coating layer after sintering at 650°C, the CuO-CeO_2-Al_2O_3 slurry was milled for 24h, showing the distribution of Cu, Ce, Al on the coating layer

The color mapping of EDX analysis shows homogeneous distributions of CuO, CeO_2 and Al_2O_3.

6.2.2 Catalytic performance

6.2.2.1 Catalytic performance in case λ=1

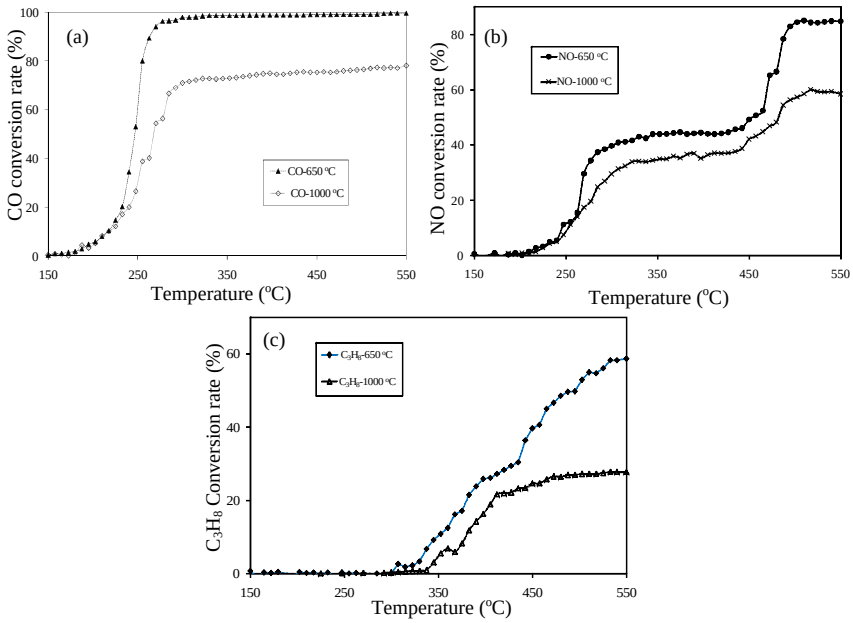

Figure 6-5: (a) CO; (b) C_3H_8, (c) NO conversion performance of noble metals coated on CuO-CeO_2-Al_2O_3/substrate, after sintering at 650°C for 2.5h and sintering at 1000°C for 20h

Figure 6-5 shows the catalytic performance of NMs coated on a CuO-CeO_2-Al_2O_3/substrate after sintering at 650°C for 2.5h and at 1000°C for 20h. when sintering at 650°C for 2.5h, the CO, C_3H_8 and NO conversion ratios increase from 0% to 99%, 62.1% and 84.7%, respectively at a temperature ranging from 30 to 540°C. Additional results, describe similar conversion ratios of CO, C_3H_8 and NO for NMs coated on CuO-CeO_2/Al_2O_3/substrate after sintering at 650°C for 2.5h.

Figure 6-6 shows CO, C_3H_8 and NO conversion ratios at 500°C, under enough oxygen condition (λ=1) and over the catalysts of NMs coated on $CuO-CeO_2-Al_2O_3$/substrate and those NMs coated on $CuO-CeO_2/Al_2O_3$/substrate after sintering at 1000°C for 20h. The results show that CO, C_3H_8 and NO conversion ratios of NMs coated on $CuO-CeO_2-Al_2O_3$/substrate are higher than those on $CuO-CeO_2/Al_2O_3$/substrate after sintering at 1000°C for 20h.

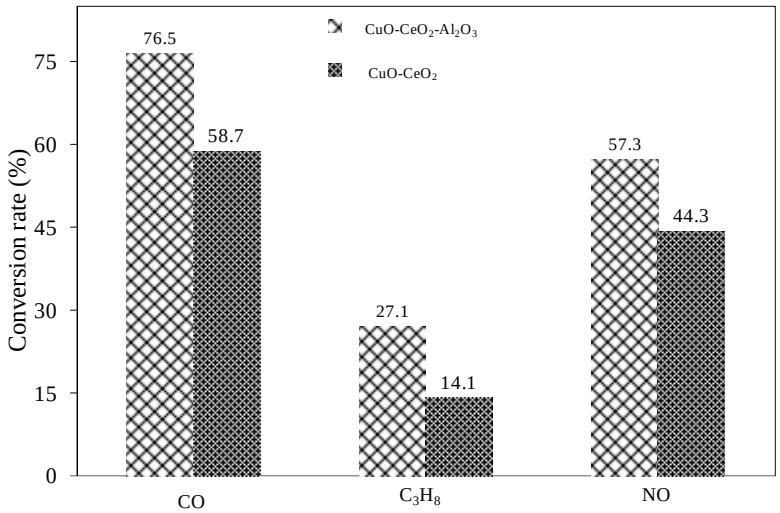

Figure 6-6: CO, C_3H_8 and NO conversion performance at 500 °C of noble metals coated on $CuO-CeO_2-Al_2O_3$/substrate and those noble metals coated on $CuO-CeO_2/Al_2O_3$/substrate after sintering at 1000°C for 20h, λ= 1

6.2.2.2 Catalytic performance in case of lean oxygen (λ<1)

Figure 6-7 shows CO, C_3H_8 and NO conversion ratios at 500°C, under lean oxygen condition (λ<1) and the over catalysts of NMs coated on a $CuO-CeO_2-Al_2O_3$/substrate and those on $CuO-CeO_2/Al_2O_3$/substrate after sintering at 1000°C for 20h. Comparing the catalytic performance when λ =1 and when λ<1 show conversion ratios of CO and C_3H_8 of both two layers and three layers structure when λ <1 are lower than the ratios of those structure when λ=1, while NO conversion ratios was higher.

Comparing the catalytic performance of the two layers structure and three layers structure at 500°C and in case λ<1 (0.85) shows that the conversion ratios of CO and C_3H_8 by NMs coated on CuO-CeO_2-Al_2O_3/substrate are much higher than those on CuO-CeO_2/Al_2O_3/substrate (Figure 6-7).

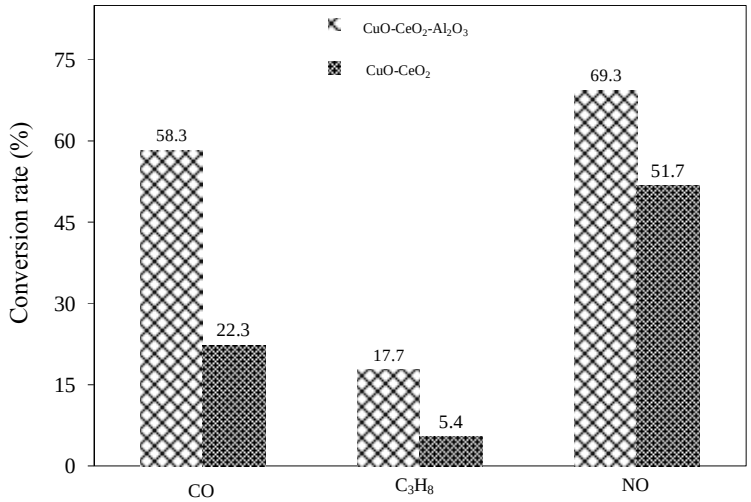

Figure 6-7: CO, C_3H_8 and NO conversion performance at 500°C of noble metals coated on CuO-CeO_2-Al_2O_3/substrate and those noble metals coated on CuO-CeO_2/Al_2O_3/substrate after sintering 1000°C for 20h, in case learn oxygen (λ= 0.85)

6.3 Discussion

In this section, the role of diffusion barrier on structure of CuO-CeO_2-Al_2O_3/substrate will be discussed.

In the order to show the effect of the diffusion barrier, the morphology of $CuO\text{-}CeO_2\text{-}Al_2O_3$ on substrate (two layers) is used to compare with the morphology of $CuO\text{-}CeO_2$ on Al_2O_3 washcoat layer on substrate (three layers). Figure 6-8a, 6-8c shows the similar particle size of $CuO\text{-}CeO_2$ for both two and three layers structure after sintering at 650°C for 2.5h. When sintering at 1000°C for 20h, the particle sizes of $CuO\text{-}CeO_2$ become larger. In case of $CuO\text{-}CeO_2\text{-}Al_2O_3$ coated on substrate, Al_2O_3 introduced into $CuO\text{-}CeO_2$ behaves as a diffusion barrier to prevent the migration of $CuO\text{-}CeO_2$, thereby suppressing $CuO\text{-}CeO_2$ particle growth; hence smaller $CuO\text{-}CeO_2$ particles were observed (Figure 6-8b). In case of $CuO\text{-}CeO_2$ coated on Al_2O_3, $CuO\text{-}CeO_2$ particles were easy to aggregate, thereby the accelerating $CuO\text{-}CeO_2$ particles was larger and appearing space of Al_2O_3 washcoat layer on the surface were observed (Figure 6-8d). It was found that the particle sizes of $CuO\text{-}CeO_2$ are significantly reduced after sintering at 1000°C for 20h for two layers structure.

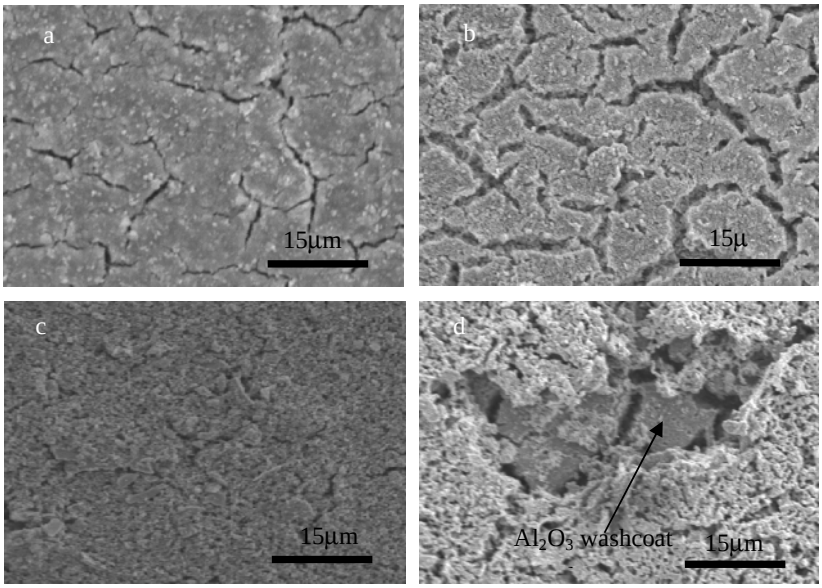

Figure 6-8: Morphology of (a) the $CuO\text{-}CeO_2\text{-}Al_2O_3$ layer coated on FeCrAl substrate after sintering at 650°C for 2.5h and (b) calcined at 1000°C for 20 h; (c) the $CuO\text{-}CeO_2$ coated on Al_2O_3 on FeCrAl substrate sintered at 650°C for 2.5h and (d) calcined at 1000°C for 20 h

It has been previously reported that, CeO_2 has a strong chemical bonding with NMs therefore being used as a material support; while γ-Al_2O_3 has a weak chemical bonding with NMs, thus being used as wall material to inhibit the aggregation of material support particles ($CuO-CeO_2$), since the precious metal particles do not migrate over the wall material. As a result, the precious metal particles are kept in the smaller particles size. Thereby the catalytic performance of a two layers structure is higher than the catalytic performance of a three layers structure after sintering at 1000^{o}C for 20h (Figure 6-6). In case of lean oxygen, the catalytic performance strongly depends on OSC. In two layer structure, Al_2O_3 introduced into $CuO-CeO_2$ behaves as a diffusion barrier to prevent the migration of $CuO-CeO_2$, thereby suppressing $CuO-CeO_2$ particle growth. The OSC of $CuO-CeO_2-Al_2O_3$/substrate improved after sintering at 1000^{o}C for 20h; therefore, the CO and C_3H_8 conversion ratios of two layers structure are higher than those conversion ratios of a three layers structure after sintering at 1000^{o}C for 20h (Figure 6-7).

6.4 Conclusion

The catalytic performance of $CuO-CeO_2-Al_2O_3$ loaded on Pd, Pt and Rh was investigated after sintering at 650^{o}C for 2.5h and 1000^{o}C for 20h.

In $CuO-CeO_2-Al_2O_3$ structure, Al_2O_3 introduced into $CuO-CeO_2$ behaves as wall material to prevent the migration of $CuO-CeO_2$ during sintering at 1000^{o}C for 20h.

As results of this inhibition at high temperature, the structure of $CuO-CeO_2-Al_2O_3$ is more stable than in the $CuO-CeO_2$ layer coated on Al_2O_3. $CuO-CeO_2$ particle sizes and precious metal particle sizes may be kept smaller, so that the CO, C_3H_8, NO conversion ratios of two layers structure is higher than those conversion ratios of three layers structure after sintering at 1000^{o}C for 20h.

REFERENCES

[1] J. Kaspar, P. Fornasero, N. Hickey (2003) Automotive catalytic converters: current status and some perspectives. Catalysis Today 77 419–449.

[2] A. S. Ivanova (2009) Physicochemical and Catalytic Properties of Systems Based on CeO_2. Kinetics and Catalysis,Vol. 50, No. 6, pp. 797–815.

[3] D. Gamarra, G. Munuera, A. B. Hungria, M. Fernandez-Garcia, J.C. Conesa, P.A. Midgley, X. Q. Wang, J.C.Hanson, J. A. Rodriguez, Martinez-Arias (2007) Structure−Activity Relationship in Nanostructured Copper−Ceria-Based Preferential CO Oxidation Catalysts. The Journal of Physical Chemistry C, 111, 11026-11038

[4] R.K. Usmen, G.W. Graham, W.L.H. Watkins, R.W. McCabe (1995) Incorporation of La^{3+} into a Pt/CeO_2 /Al_20_3 catalyst. Catalysis Letters, 30, 53-63

[5] A. Bensalem, F. Bozon-Verduraz, M. Delamar, G. Bugli (1995) Preparation and characterization of highly dispersed silica-supported ceria. Applied Catalysis A: General, 121, 81-93.

[6] T. Miki, T. Ogawa, M. Haneda, N. Kakuta, A. Ueno (1990) Enhanced Oxygen Storage Capacity of Cerium Oxides in CeO2/La2O3/Al2O3 Containing Precious Metals. The Journal of Physical Chemistry 94, 6464-6467.

[7] G. Colón , J. A. Navío , R. Monaci, I. Ferino (2000) CeO_2–La_2O_3 catalytic system Part I. Preparation and characterisation of catalysts. Physical Chemistry Chemical Physics, 2, 4453-4459.

[8] F. Ye, T. Mori, D.R. Ou, J. Zou, J. (2008) Drennan Microstructural characterization of $Ce_{1-x}Tb_xO_{2-\delta}$ (0.60 ≤x ≤0.90) sintered samples. Materials Research Bulletin, 43, 759–764.

[9] M. Yu. Sinev, G. W. Graham, L. P. Haack and M. Shelef (1996) Kinetic and structural studies of oxygen availability of the mixed oxides $Pr_{1-x}M_xO_y$ (M = Ce, Zr). Journal of Materials Research, Volume 11, 1960-1971.

[10] T. Kanazawa, J. Suzuki, T. Takada, T. Suzuki (2003) Development of Three-way Catalyst Using Composite Alumina-Ceria-Zirconia, SAE Technical Paper 2003-01-0811.

[11] A. Morikawa, T. Suzuki, T. Kanazawa, K. Kikuta, A. Suda, H. Shinio (2008) A new concept in high performance ceria-zirconia oxygen storage capacity material with Al_2O_3 as a diffusion barrier. Applied Catalysis B: Environmental, 78, 210-221.

[12] A. Morikawa, K. Kikuta, A. Suda, H. Shinjo (2009) Enhancement of oxygen storage capacity by reductive treatment of Al_2O_3 and CeO_2-ZrO_2 solid solution. Applied Catalysis B: Environmental, 88, 542-549.

M. Nakamura, H. Wakamatsu, K. Suga, T. Sekiba, Y. Hiramoto, K. Shibata (2009) Ultrafine precious catalyst for high conversion efficiency with low precious metal loading. SAE paper No 2009-01-1069.

[13] N.T. Luong, E. Yamasue, H. Okumura, K.N. Ishihara, Structure and catalytic behavior of CuO-CeO_2 prepared by High-Energy Ball Milling, Catalysis Letters (under review).

[14] N.T. Luong, E. Yamasue, H. Okumura, K.N. Ishihara, Investigation on catalytic performance of Pt, Pd and Rh/CuO-CeO_2/Al_2O_3/metallic substrate support for three-way catalysts (to be appeared).

[15] N.T. Luong, E. Yamasue, H. Okumura and K.N. Ishihara, Effect of Mechanical Milling on Adhesion Properties of CuO-CeO_2/γ-Al_2O_3 on metallic substrate support for automotive catalytic converter, Powder Technology (under review).

CHAPTER 7
Conclusions and Recommendations

7.1 Conclusions

OSC property of $CuO\text{-}CeO_2$ prepared mechanical milling has been proposed in this study. The proposal is based that the valence change of Ce^{4+}/Ce^{3+} and/or $Cu^{2+}/Cu^{+}/Cu$ can be improve the OSC property at lower temperatures.

In chapter 3, Mechanical milling was applied to the $CuO\text{-}CeO_2$ system, in order to produce mixed-oxide catalysts. During the milling, structure modifications were observed by XRD and SEM, The dynamic reduction behavior of $CuO\text{-}CeO_2$ was analyzed by the temperature programmed reduction instrument with GC-TCD. The total OSC of the $CuO\text{-}CeO_2$ catalysts system was measured by TG-DTA. The results showed that the CuO reduced Cu when milled $CuO\text{-}CeO_2$ samples were processed in air, three reduction peaks were observed for 0h milling and only one β-peak for various milling times, the valence

change of Cu ions in CuO enhanced the redox activity. The total OSC of the $CuO\text{-}CeO_2$ system was much greater than $CeO_2\text{-}ZrO_2$ traditional catalysts system: at 300^oC the OSC of $CuO\text{-}CeO_2$ was 97.5%, which is higher than that of $CeO_2\text{-}ZrO_2$.

In order to apply new catalysts to the TWCs system, the chapter 4 presented the coating characteristics of $CuO\text{-}CeO_2/\gamma\text{-}Al_2O_3$ layers on FeCrAl metallic substrate. The adhesiveness between the developed material and the washcoat was one of these important factors. The adhesion property of $CuO\text{-}CeO_2/\gamma\text{-}Al_2O_3$ on metallic substrate was investigated focusing on the particle size, which secure the durability of $\gamma\text{-}Al_2O_3$ and $CuO\text{-}CeO_2$ on the metallic substrate. The milled powder of $CuO\text{-}CeO_2$ always agglomerates, with the particle size of about few micrometers, and exhibits poor adhesion. The reduction of the agglomerates' size was realized by wet milling. The results showed that, when it was coated on $\gamma\text{-}Al_2O_3$ layer, the weight loss reduces from 100% to 25% after 48h wet milling. As the increase of milling time to 72h, the so-called "over-milling" phenomenon was also found, where the elongated large particles were observed after sintering of the longer-milled powders, leading to the lowered adhesion quality.

In chapter 5, the catalytic performance of Pd, Pt and Rh impregnated on the $CuO\text{-}CeO_2$ system was investigated using the automotive exhaust gas simulator comparing with that of noble metals coated on a $CeO_2\text{-}ZrO_2/Al_2O_3$/substrate and Al_2O_3/substrate. The coated samples were characterized by means of XRD, SEM, Brunauer-Emmett-Teller (BET), X-ray photoelectron spectroscopy (XPS) and GC-TCD. The results showed that, when λ=1, the CO conversion ratio for noble metals coated on $CuO\text{-}CeO_2$ was higher at lower temperatures than that of noble metals coated on $CeO_2\text{-}ZrO_2$ and that of noble metals coated on $\gamma\text{-}Al_2O_3$.

For the case of λ<1, CO and C_3H_8 conversion ratios of noble metals coated on $CuO\text{-}CeO_2$ were higher than those of noble metals coated on $CeO_2\text{-}ZrO_2$ and on a $\gamma\text{-}Al_2O_3$ washcoat. Amount of released oxygen and dynamic release of oxygen from oxygen storage materials of NMs impregnated on the $CuO\text{-}CeO_2$ system are much higher than those on the

CeO_2-ZrO_2 system and the Al_2O_3 system; thus suggesting that efficiency of TWCs at initial period of startup engine and due to the oscillation of λ under real work conditions of engine can be improved.

Finally, in order to improve the thermal stability and catalytic performance of Pd, Pt and Rh loaded on CuO-CeO_2/Al_2O_3 at high temperature, the chapter 6 presented the mixture of Al_2O_3 with CuO-CeO_2. The mixture of CuO-CeO_2 was firstly produced using high energy vibratory ball milling for 18h and then the milled powders of CuO-CeO_2 (40 wt.%) and γ-Al_2O_3 (60 wt.%) were further milled with water and a small amount of $Al(NO_3)_3$ as the binder for 24h. The results showed a good distribution of Al_2O_3 into CuO-CeO_2, rather small particles of CuO-CeO_2 were determined at high temperature. The phase change from γ-Al_2O_3 to α-Al_2O_3 at 1000^{o}C was observed. After being heated at 1000^{o}C for 20h, the CO, C_3H_8, NO conversion ratios of two layers structure was better than those of three layers structure.

7.2 Recommendations

After the present work, there are several important issues that remain unresolved. The following recommendations are proposed in order to direct further research in TWCs.

1. OSC property of milled CuO-CeO_2 was investigated; future study should be compared to OSC property of mixed CuO-CeO_2 prepared by other preparation methods.

2. The sulfur in gasoline fuel is one of the components that deactivate TWCs, because the Cu and CuO are sensitive to sulfur. Hence, the deactivation of CuO-CeO_2 by sulfur must be further studied.

3. The increase in use of Pt, Pd, Rh for TWCs technology is leading to an increase in NM's market prices. In order to decrease the price of the NMs, the possible

replacement of Pt, Pd by Cu and/or CuO, for the conversion of CO and HC, need to be further studied.

4. Future work should also focus on distribution of NM particles on the $CuO\text{-}CeO_2$ catalytic layer, for this may influence the catalytic performance of TWCs.

5. Finally, future study should also be directed to the one-way catalysis required to oxidize CO in a diesel engine, namely, investigating the effect of using CuO or mixed $CuO\text{-}CeO_2$ on this catalysis, since it has been shown that these two compounds promote CO oxidation.

Appendix A

Temperature property of Furnace and Temperature calibration

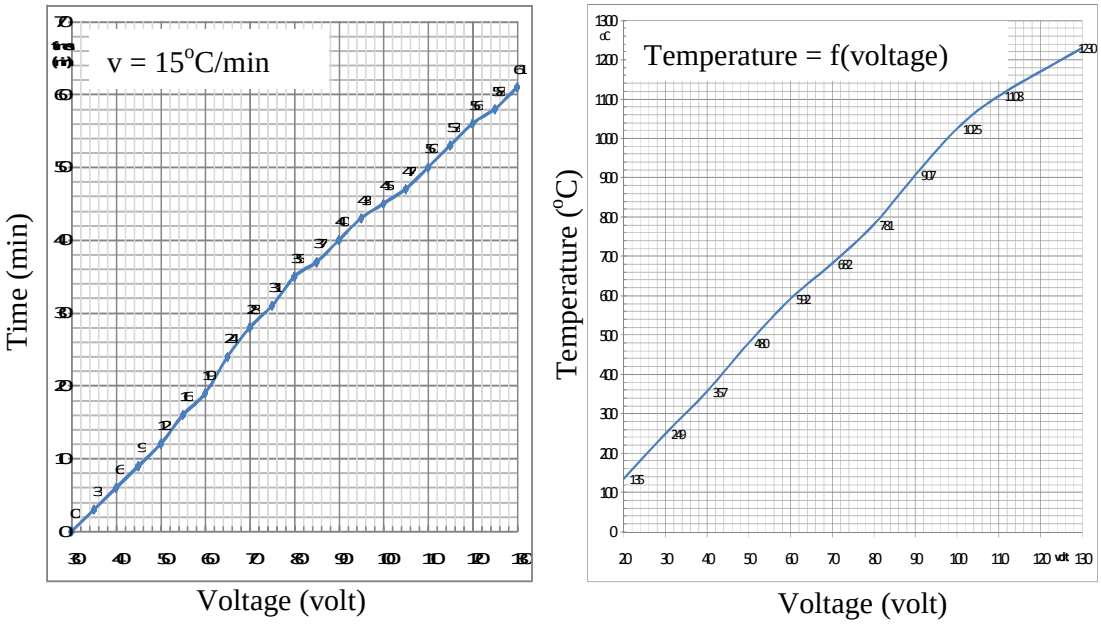

Figure A1: The increasing temperature of furnace depend on the increasing voltage, v = 15°C/min

Furnace is an equipment used to heat treatment of coating layers and to measure TPR and OSC property. The temperature of furnace was controlled with the increase of temperature as 15^{o}C/min in case of TPR measurement, the power of furnace was controlled by voltage. The temperature properties of furnace depended on voltage were investigated (figure A1).

The dynamic reduction of CuO-CeO_2 was measured by temperature-programmed reduction (TPR), where the milled sample (about 50 mg) was put in a quartz reactor and heated with 15^{o}C/min in the temperature range of 35^{o}C-1000^{o}C. However, the temperature at the sample location was different with the temperature of furnace, so the temperature at the sample location has to adjust according to the temperature of furnace; temperature sensor of furnace was calibrated with standard temperature sensor. Figure A2 showed the temperature property at the sample location was adjusted due to the increasing temperature of furnace from 20^{o}C to 1010^{o}C.

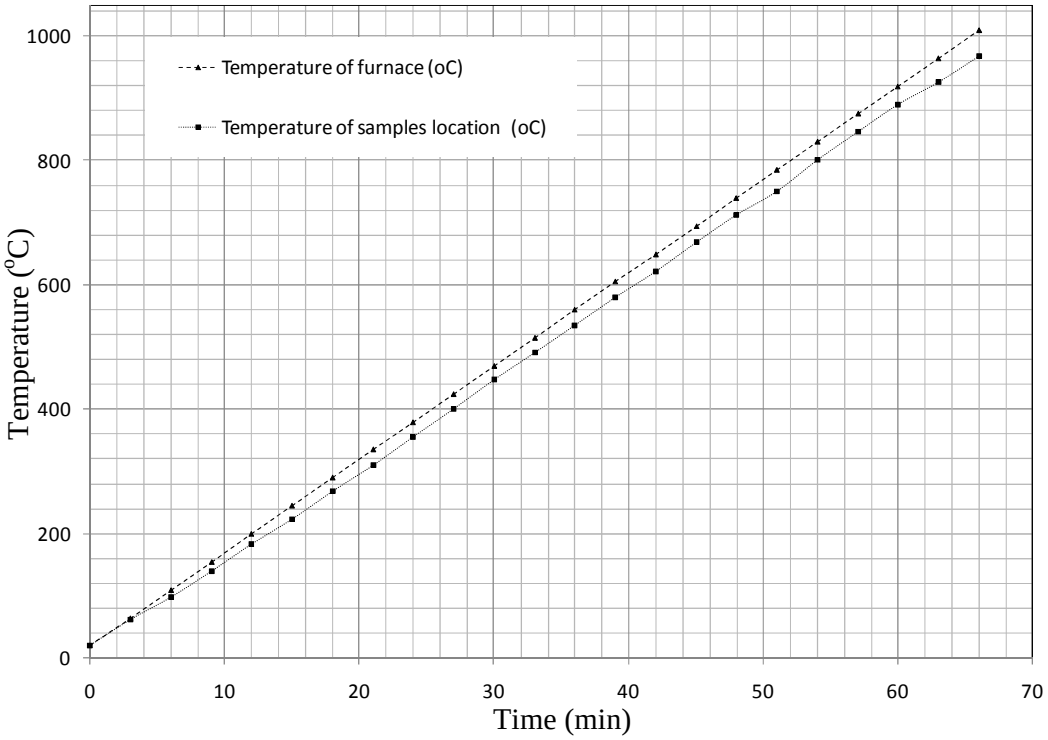

Figure A2: The temperature property of sample location depend on temperature of furnace

Appendix B
Lattice parameter and crystallite size calculation

X-ray diffraction is a convenient method for determining the mean size of nano crystallites in nano crystalline bulk materials. The first scientist, Paul Scherrer, published his results in a paper that included what became known as the Scherrer equation in 1981 [1].

This can be attributed to the fact that “crystallite size” is not synonymous with “particle size”, while X-Ray diffraction is sensitive to the crystallite size inside the particles. From the well-known Scherrer formula the average crystallite size, *L*, is:

$$L = \frac{K\lambda}{\beta.\cos\phi}$$

where λ is the X-ray wavelength in nanometer (nm), β is the peak width of the diffraction peak profile at half maximum height resulting from small crystallite size in radians and *K* is

a constant related to crystallite shape, normally taken as 0.9. The value of β in 2θ axis of diffraction profile must be in radians. The θ can be in degrees or radians.

In this study, β was determined by using OriginPro 7.5 software (figure B1), λ is the x-ray wavelength: $\lambda = 1.54\ A^0$ (Cu).

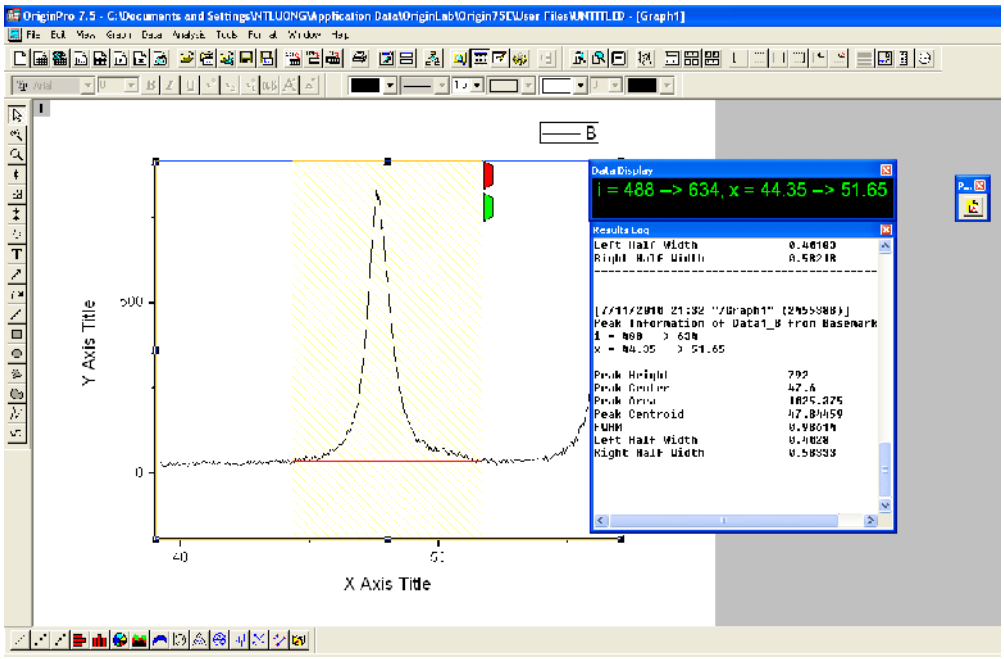

Figure B1: Peak width (β) was determined by OriginPro 7.5 software

Lattice parameter of cubic CeO_2 was calculated as following:

$$d = \frac{a}{\sqrt{h^2 + k^2 + l^2}}$$

d: is the spacing of parallel plane

h,l,k: is the Miller indices

a: lattice parameter

The peak [220] of CeO_2 was used to calculate lattice parameter, so $a = d.\sqrt{3}$.

Appendix C

List of gases and quality

No	Component	Content	Quality
$C_3H_8/O_2/CO/H_2/CO_2/N_2$	C_3H_8	0.1%	± 0.001
	O_2	0.5%	± 0.01
	H_2	1.5%	± 0.05
	CO_2	12.0%	± 0.05
	N_2	Balance	
NO/N_2	NO	190 ppm	± 0.05
	N_2	Balance	
H_2/Ar	H_2	5%	± 0.05
	Ar	Balance	

Appendix D

The formation of metallic copper upon milling was checked by NMR method

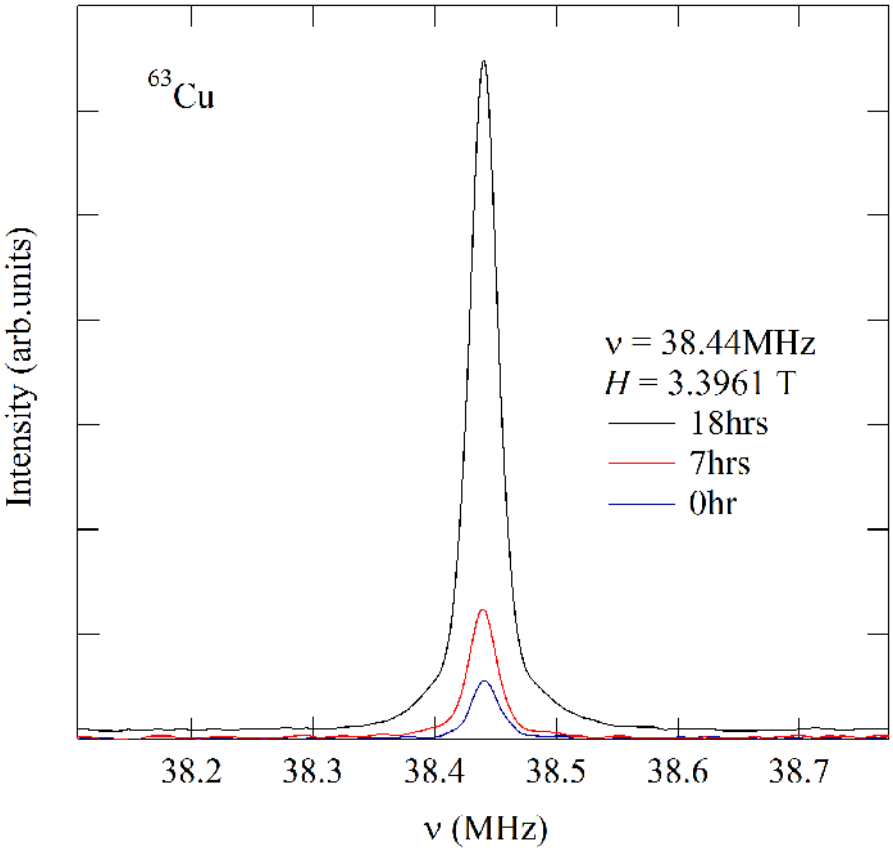

List of publications

Original Paper

1. Nguyen The Luong, Eiji Yamasue, Hideyuki Okumura, and Keiichi N. Ishihara, Thermal Stability and Catalytic Performance of Pd, Pt and Rh Loaded on $CuO–CeO_2–Al_2O_3$ Support for Three-Way Catalysts, In Takeshi Yao (editor) Zero-Carbon Energy Kyoto 2012, Green Energy and Technology, DOI 10.1007/978-4-431-54264-3_19.
2. Nguyen The Luong, Eiji Yamasue, Hideyuki Okumura, and Keiichi N. Ishihara, Adhesion Properties of milled $CuO\text{-}CeO_2/\gamma\text{-}Al_2O_3$ on Metallic Substrate for Automotive Catalytic Converter, Particulate Science and Technology, (Accepted).
3. Nguyen The Luong, Eiji Yamasue, Hideyuki Okumura, and Keiichi N. Ishihara, Structure and catalytic behavior of $CuO\text{-}CeO_2$ prepared by High-Energy Ball Milling, Catalysis letters (Under review).
4. Nguyen The Luong, Eiji Yamasue, Hideyuki Okumura, and Keiichi N. Ishihara, Investigation on Catalytic Performance of Pt, Pd and $Rh/CuO\text{-}CeO_2/Al_2O_3$ on Metallic Substrate for Advanced Three-Way Catalysts (Preparing).

Abstracts and Proceedings of the International Conferences

1. Nguyen The Luong, Eiji Yamasue, Hideyuki Okumura, and Keiichi N. Ishihara, Structure and Catalytic Behavior of $CuO\text{-}CeO_2$ Prepared by High-Energy Ball Milling, Abstract of Presentation and poster of KU – HU International Symposium on Education and Research in Environmental Management of 3rd Symposium of EML project, March 5, 2011, Hue, Vietnam.
2. Nguyen The Luong, Eiji Yamasue, Hideyuki Okumura and Keiichi N. Ishihara, ”The adhesion characteristics of $\gamma\text{-}Al_2O_3$, $CuO\text{-}CeO_2$ on metallic substrate prepare by hybrid suspension”, Abstract of Presentation of The 3rd International Symposium of Kyoto University G-COE of Energy Science, "Zero-Carbon Energy Kyoto 2011", August 19-20, 2011, Suwon, Korea.
3. Nguyen The Luong, Eiji Yamasue, Hideyuki Okumura and Keiichi N. Ishihara, ” The thermal stability and catalytic performance of Pd, Pt and Rh loaded on $CuO\text{-}CeO_2\text{-}Al_2O_3$ support for three-way catalysts”, Abstract of Poster of The 4th International Symposium of Kyoto University G-COE of Energy Science, "Zero-Carbon Energy Kyoto 2012", 22 – 23 May 2012, Bangkok, Thailand.
4. Nguyen The Luong, Eiji Yamasue, Hideyuki Okumura, Keiichi N. Ishihara, "Catalytic Performance of Pd, Pt and Rh loaded on $CuO\text{-}CeO_2$ Washcoat", Abstract of Poster of 15th International Congress on Catalysis 2012. International Congress Center Munich, Munich, Germany, 1-6 July, 2012.
5. Nguyen The Luong, Eiji Yamasue, Hideyuki Okumura and Keiichi N. Ishihara, ”The catalytic performance of Pd, Pt and Rh loaded on $CuO\text{-}CeO_2\text{-}Al_2O_3$ Washcoat”, Abstract of Presentation of Ajou-KIT-Kyoto University Joint International Symposium, January 31-Febuary 1, 2012, Kyoto, Japan.

Curriculum Vitae

Personal Information

Name: Nguyen The Luong
Birthdate: Oct. 23, 1979
Birthplace: Bacninh, Vietnam

Education

1998-2003 Bachelor of Internal combustion engine, School of Transportation Engineering, Hanoi University of Science and Technology, Hanoi, Vietnam

2005-2007 Master of Internal combustion engine, School of Transportation Engineering, Hanoi University of Science and Technology, Hanoi, Vietnam

2009-2013 Ph.D. Thesis under the supervision of Prof. Keiichi N. Ishihara at Graduate school of Energy Science, Kyoto University, Kyoto, Japan